

4-2018

Geochemical and Radiological Baseline Studies and Environmental Impact of the Area Surrounding Barakah Nuclear Power Plant, UAE

Mouza Rashed Mohamed Al Rashdi

Follow this and additional works at: https://scholarworks.uaeu.ac.ae/all_dissertations

Part of the [Environmental Sciences Commons](#)

Recommended Citation

Mohamed Al Rashdi, Mouza Rashed, "Geochemical and Radiological Baseline Studies and Environmental Impact of the Area Surrounding Barakah Nuclear Power Plant, UAE" (2018). *Dissertations*. 78.
https://scholarworks.uaeu.ac.ae/all_dissertations/78

This Dissertation is brought to you for free and open access by the Electronic Theses and Dissertations at Scholarworks@UAEU. It has been accepted for inclusion in Dissertations by an authorized administrator of Scholarworks@UAEU. For more information, please contact fadl.musa@uaeu.ac.ae.

UAEU



جامعة الإمارات العربية المتحدة
United Arab Emirates University

United Arab Emirates University

College of Science

GEOCHEMICAL AND RADIOLOGICAL BASELINE STUDIES AND
ENVIRONMENTAL IMPACT OF THE AREA SURROUNDING
BARAKAH NUCLEAR POWER PLANT, UAE

Mouza Rashed Mohamed Al Rashdi

This dissertation is submitted in partial fulfilment of the requirements for the degree
of Doctor of Philosophy

Under the Supervision of Dr. Sulaiman Ali Alaabed Alkaabi

April 2018

Declaration of Original Work

I, Mouza Rashid Mohamed Al Rashdi, the undersigned, a graduate student at the United Arab Emirates University (UAEU), and the author of this dissertation entitled "*Geochemical and Radiological Baseline studies and Environmental Impact of the Area Surrounding Barakah Nuclear Power Plant, UAE*", hereby, solemnly declare that this dissertation is my own original research work that has been done and prepared by me under the supervision of Dr. Sulaiman Ali Alaabed Alkaabi, in the College of Science at UAEU. This work has not previously been presented or published, or formed the basis for the award of any academic degree, diploma or a similar title at this or any other university. Any materials borrowed from other sources (whether published or unpublished) and relied upon or included in my dissertation have been properly cited and acknowledged in accordance with appropriate academic conventions. I further declare that there is no potential conflict of interest with respect to the research, data collection, authorship, presentation and/or publication of this dissertation.

Student's Signature: _____

Date: 13-5-18

Copyright © 2018 Mouza Rashid Mohamed Al Rashdi
All Rights Reserved

Advisory Committee

1) Advisor: Sulaiman Ali Alaabed Alkaabi

Title: Associate Professor

Department of Geology

College of Science

2) Co-advisor: Mohamed El Tokhi

Title: Associate Professor

Department of Geology

College of Science

3) Member: Walid El Mowafi

Title: Sr. Specialist, Emergency Preparedness & Response

Federal Authority of Nuclear Regulation, UAE

Approval of the Doctorate Dissertation

This Doctorate Dissertation is approved by the following Examining Committee Members:

- 1) Advisor (Committee Chair): Sulaiman Ali Alaabed Alkaabi

Title: Associate Professor

Department of Geology

College of Science

Signature  _____

Date April 18 2018

- 2) Member: Ala Aldahan

Title: Professor

Department of Geology

College of Science

Signature  _____

Date 2018-04-18

- 1) Member: Mohammed A Almeetani

Title: Associate Professor

Department of Chemistry

College of Science

Signature  _____

Date 18/04/2018

- 4) Member (External Examiner): Xiaolin Hou

Title: Professor

Department of Center for Nuclear Technologies, DTU Nutech

Institution: [Technical University of Denmark (DTU Nutech), Denmark]

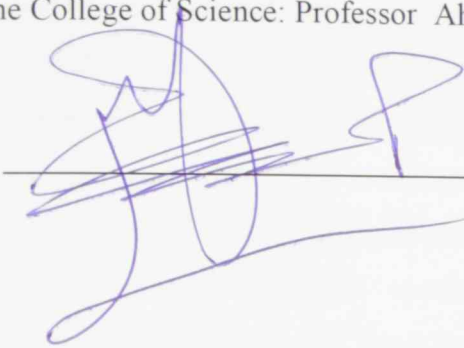
Signature  _____

Date 18/4-2018

This Doctorate Dissertation is accepted by:

Dean of the College of Science: Professor Ahmed Murad

Signature



Date

13/5/2018

Dean of the College of Graduate Studies: Professor Nagi T. Wakim

Signature



Date

13/5/2018

Copy 12 of 14

Abstract

Geochemical, mineralogical and natural radiation analysis techniques were used for establishment of geochemical and radiological baseline around Barakah Nuclear Power Plant, UAE. The natural radioactivity concentrations of ^{238}U (^{226}Ra), ^{232}Th and ^{40}K were measured for soil, shore and bottom sediment samples, using gamma spectrometry equipped with HPGe detector. In addition, alpha spectrometry was used to measure $^{234}\text{U}/^{238}\text{U}$ ratio for some selected samples. Furthermore, inductively coupled plasma atomic emission spectroscopy was used to measure the concentrations of heavy metals and Rare Earth Elements (REE). The grain size of the samples ranged from fine to coarse sand. The inverse relationship between grain size and heavy metal contaminations was validated. The results indicated the mean concentrations of heavy metals and REE are much higher in soil samples compared to bottom sediments, which in turn relatively higher than shore samples. All heavy metals concentrations were significantly below the UAE soil contamination safe limits. The levels of heavy metals and REE reported in the UAE were lower than the levels reported in the soil, shore and bottom sediments of several countries around the world. Enrichment factor calculated for heavy metals shows no to moderate enrichment (As and Cd), while the contamination factor (CF) was $\text{CF} < 1$ which indicates low contamination factor. Geoaccumulation results suggest uncontaminated area. Furthermore, the pollution load index, > 1 , indicates no pollution in the area. With exception of La in shore samples, all the REE show no enrichment. Contamination factor for REE indicates a low contamination factor and geoaccumulation results indicate that the studied area was uncontaminated. Moreover, the pollution load index indicates no pollution in the area.

The measured gamma activity concentrations in shore-sediment samples are much lower comparing to those concentrations in soil and bottom sediments. The average activity concentrations of ^{238}U (^{226}Ra) are 15.68 ± 0.56 , 4.43 ± 0.39 and 4.73 ± 0.47 Bq/kg, for ^{232}Th are 8.3 ± 0.23 , 1.68 ± 0.17 and 1.83 ± 0.24 Bq/kg and for ^{40}K , are 349.72 ± 11.76 , 106.3 ± 7.27 and 105.23 ± 10.03 Bq/kg in soil, shore and bottom sediment samples, respectively. Anthropogenic radionuclide ^{137}Cs is low than the detection limit in the studied area. The $^{234}\text{U}/^{238}\text{U}$ activity ratios show wide range

from 0.59 to 2.24 indicating effects of sources and in situ processes. In addition, the hazard parameters such as Radium equivalent and absorption dose were estimated and all are below the world average. The spatial distribution for heavy metals, REE and natural radionuclides was generally more compact in the south compared to the north, with less severe contaminations in the east and west. Relationships between heavy metals, REE and natural radioactivity concentrations were investigated and varied between soil, shore and bottom sediment samples. The previous relationships may indicate that uranium and thorium have detrital sources possibly associated with silicate minerals.

Keywords: UAE, radiological baseline, Barakah Nuclear Power Plant, heavy metal, gamma spectrometry, geoaccumulation index, pollution load index, enrichment factor, and spatial distribution.

Title and Abstract (in Arabic)

دراسة جيوكيميائية وإشعاعية وبيئية للمنطقة المحيطة بمحطة براكا للطاقة النووية في دولة الإمارات العربية المتحدة

المخلص

يهدف هذا البحث إلى عمل دراسة متكاملة وإنشاء قاعدة بيانات للمنطقة المحيطة بمحطة براكا للطاقة النووية في دولة الإمارات. وقد تم استخدام التحاليل الجيوكيميائية المختلفة للعناصر الثقيلة والعناصر الأرضية النادرة والإشعاع النووي الطبيعي. وقد تم قياس النشاط الإشعاعي لليورانيوم 238 (الراديوم 226) والثوريوم 232 والپوتاسيوم 40 في عينات من التربة البرية (200 متر من الشاطئ) والتربة الشاطئية والرواسب القاعية باستخدام مطياف الجرمانيوم عالي النقاوة. وتم أيضا استخدام مطياف ألفا لقياس نسبة نظائر اليورانيوم (234 و 238) لبعض العينات. أما بالنسبة لتراكيز العناصر الثقيلة والعناصر الأرضية النادرة فتم استخدام مقياس الانبعاثات بمطياف البلازما. وبالنسبة للتحليل الحجمي لحبيبات التربة فتراوحت بين الرمل الناعم والخشن. وأوضحت العلاقة بين تراكيز العناصر الثقيلة وحجم الحبيبات وجود علاقة عكسية حيث تزداد تراكيز تلك العناصر مع انخفاض حجم الحبيبات. أظهرت النتائج أن متوسط تراكيز العناصر الثقيلة والعناصر الأرضية النادرة أعلى في عينات التربة البرية مقارنة بعينات الرواسب القاعية والتربة الشاطئية حيث أن الأخيرة هي الأقل تركيزاً. أما بالنسبة لتراكيز العناصر الثقيلة في فهي أقل من الحدود المسموح بها في دولة الإمارات وتعتبر هذه التراكيز وتراكيز العناصر الأرضية النادرة قليلة جداً مقارنة بالقيم المسجلة في بعض دول العالم. ويشير معامل الإثراء للعناصر الثقيلة إلى الحالة الثانية وهي حالة عدم إثراء معتدل (الزرنخ والكادميوم)، في حين أن عامل التلوث المقدر للمعادن الثقيلة هو >1 يشير إلى حالة تلوث منخفض. من جهة أخرى تشير نتائج التراكم الجغرافي إلى منطقة غير ملوثة ويدعم ذلك مؤشر تحمل التلوث حيث يشير إلى عدم وجود تلوث في المنطقة. أما بالنسبة للعناصر الأرضية النادرة فقد أظهرت النتائج أن جميع العناصر باستثناء عنصر اللانثينيوم (في عينات التربة الشاطئية) تشير إلى معامل إثراء من الدرجة الأولى وهي معدومة. ويشير عامل التلوث للعناصر الأرضية النادرة إلى وجود عامل تلوث منخفض وأما بالنسبة لكل من نتائج التراكم الجغرافي ومؤشر تحمل التلوث فهما يشيران معاً إلى أن المنطقة المدروسة غير ملوثة.

أظهرت النتائج أن تراكيز النشاط الإشعاعي المقاسة في عينات الرواسب الشاطئية أقل بكثير مقارنة بنتائج التركيزات في التربة البرية والرواسب القاعية ويبلغ متوسط تركيز النشاط الإشعاعي لعنصر اليورانيوم 238 5.56 ± 1.57 ، 3.88 ± 0.44 و 4.65 ± 0.47 بيكريل / كيلوغرام، أما بالنسبة لعنصر الثوريوم 232 فمتوسط تركيز النشاط الإشعاعي هو 2.29 ± 0.83 ، 1.71 ± 0.17 و 2.41 ± 0.18 بيكريل / كيلوغرام وبالنسبة للبتاسيوم 40 فتراكيذه هي 11.76 ± 349.72 ، 7.27 ± 106.3 و 10.03 ± 105.23 بيكريل / كيلوغرام في عينات التربة البرية والتربة الشاطئية و الرواسب القاعية على التوالي. لم يتم تسجيل أي تراكيز ملحوظة لعنصر السيزيوم 137 في المنطقة المدروسة. أظهرت نتائج مطياف ألفا لقياس نسبة نظائر اليورانيوم (234 و 238) تفاوتت النسبة من 0.59 إلى 2.24 وهو مدى واسع مما يشير إلى وجود عدة مؤثرات مثل اختلاف مصادر التربة والعمليات الداخلية المرتبطة بها. بالإضافة إلى قياس تراكيز النشاط الإشعاعي، تم قياس مؤشرات الخطر الإشعاعي مثل مكافئ الراديوم وجرعة الامتصاص وقد أشارت النتائج إلى أن كل القيم المقاسة أقل من المتوسط العالمي.

أوضحت خرائط التوزيع المكاني لكل من المعادن الثقيلة والعناصر الأرضية النادرة والعناصر المشعة الطبيعية تراكيزاً أعلى في جنوب منطقة الدراسة مقارنة مع شمالها، وظهرت أيضاً تلوث أقل حدة في شرق وغرب الخريطة. وتمت دراسة العلاقة بين العناصر الثقيلة والعناصر الأرضية النادرة وتراكيز النشاط الإشعاعي الطبيعي وتفاوتت طبيعة وشدة العلاقات بين عينات التربة القارية والتربة الشاطئية و الرواسب القاعية وقد أشارت العلاقات المدروسة إلى مصادر فتاتية لليورانيوم والثوريوم ربما تكون مرتبطة مع معادن السيليكا.

مفاهيم البحث الرئيسية: دولة الإمارات العربية المتحدة، قاعدة بيانات النشاط الإشعاعي، محطة براكاة للطاقة النووية، العناصر الثقيلة، مطياف جاما، مؤشر التراكم الجغرافي، مؤشر تحمل التلوث ، معامل الإثراء والتوزيع المكاني.

Acknowledgements

First and above all, I praise God, the almighty for providing me this opportunity and granting me the capability to proceed successfully.

I would like to extend my sincere thanks and gratitude to the UAE University, Geology department, Environment Agency-Abu Dhabi and Colleague of graduate studies for giving the chance and offering many facilities to achieve this work.

I would like to thank Dr. Sulaiman Alaabed (Associate Professor, Department of Geology) and Prof. Mohamed El Tokhi (Professor, Department of Geology) for supervising this work. I greatly appreciate the freedom you have given me to find my own path and providing me with an excellent atmosphere for doing this research. I am indebted to them for their supervision, patience, encouragement and continuous advice during the progress of this work.

I am grateful to my supervisor Dr. Walid El Mowafi from Federal Authority of Nuclear Regulation for his help and advice. I am also grateful to the head (Dr. Khalid AlBloushi) and faculty members from Geology department, especially Dr. Osman Abdelghany for their continuous support.

Special thanks to Prof. Ala Aldahan who was always willing to help and give his best suggestions and for the assistance he provided at all levels of the project.

Appreciation is extended to Dr. Bahaa Eddin Mahmoud for his continuous help from the first stages of this project and for both of Mr. Wajeeh Kettaneh and Mr. Salah Alasar for their efforts in offering many lab facilities.

I would never forget to thank my master thesis supervisors Dr. Amr El-Sammak and Dr. Mohamed Gameil for their encouragement. I would like also to

extend my deep thank and gratitude to my mentors Mark Turner and Richard Hipwood from RTI in North Carolina for their encouragement to join the PhD program and all the kind support they offered.

My thanks are due also to the UAEU library for providing me with all the scientific data and related research paper. I would also extend my thanks to the Egyptian Nuclear and Radiological Regulatory Authority for welcoming me into their laboratory and training me on their various spectroscopic instruments where a unique part of this thesis have been carried out.

Words are insufficient to express my gratefulness and indebtedness to Dr. Alya Arabi, Assistant Professor in College of Natural and Health Sciences, Zayed University, who truly made a difference in my life. I want to thank you for your enormous support and encouragements during my work. You illuminated my mind and showed me the way through countless discussions.

I express my heartfelt thanks to each of Dr. Dalal Alshamsi, Dr. Shaikha AlNeyadi and Ashwaq Alkorbi for providing me with the motivation and continuous help.

A special thanks to my parents and siblings. Words cannot express how grateful I am to you all for being a member of such a great family. Special thanks to Dr. Saeed who highlighted the study area in the thesis proposal stage. I extend my gratitude and heartfelt thanks to my husband and my four precious sons: Mohamed, Hamed, Ghanem and Zayed for adding joy and happiness in my life.

Finally, I thank everyone who has played a vital or small role either directly or indirectly for preparation of this work.

Dedication

To my beloved parents, siblings, husband and sons

Table of Contents

Title	i
Declaration of Original Work	ii
Copyright	iii
Advisory Committee	iv
Approval of the Doctorate Dissertation	v
Abstract	vii
Title and Abstract (in Arabic)	ix
Acknowledgements	xi
Dedication	xiii
Table of Contents	xiv
List of Tables.....	xvii
List of Figures	xx
List of Abbreviations.....	xxii
Chapter 1: Introduction	1
1.1 Research Focus.....	1
1.2 Background	2
1.3 Study Area.....	5
1.4 Geological Setting.....	7
1.4.1 UAE General Geology	7
1.4.2 Abu Dhabi Geology	8
1.4.3 Barakah Area Setting	10
1.4.4 Coastal Environment	13
1.5 Literature Review	14
1.6 Research Objectives and Aim	23
Chapter 2: Methodology	24
2.1 Field Work and Sampling	24
2.2 Data Management	26
2.3 Analytical Techniques.....	27
2.3.1 Inductively Coupled Plasma (ICP) Analysis.....	27
2.3.2 X-Ray Diffraction (XRD) Spectrometry Analysis.....	28
2.3.3 Grain Size Analysis	29
2.3.4 Carbonate Content Analysis.....	30
2.3.5 High Pure Germanium Gamma Analysis.....	30
2.3.6 Alpha Spectrometry.....	39

Chapter 3: Results	42
3.1 Grain-Size Analysis	42
3.1.1 Mean Size (Mz)	42
3.1.2 Inclusive Standard Deviation (σI)	43
3.1.3 Skewness (SKI)	43
3.1.4 Kurtosis (KG)	43
3.1.5 Determination of the Mechanical and Environments of Deposition	48
3.2 Mineralogy	50
3.2.1 Soil Samples Mineralogy	50
3.2.2 Shore Samples Mineralogy	50
3.2.3 Bottom Sediment Samples Mineralogy	51
3.3 Carbonate Content	54
3.4 Major Oxides	56
3.5 Heavy Metal	61
3.6 Rare Earth Elements	66
3.7 Radionuclide Activity Concentrations	74
3.8 Radium Equivalent Activity Concentrations and Absorbed Dose Rates	78
3.9 Alpha Spectrometry	78
3.10 Relationship between Heavy Metals, REE and Natural Radioactivity Concentrations	80
Chapter 4: Discussion	81
4.1 Grain Size Analysis	81
4.1.1 Grain Size Parameters	81
4.1.2 Mechanical and Environments of Deposition	85
4.1.3 Grain Size vs. Heavy Metals in the Bottom Sediment Samples	85
4.1.4 Grain Size vs. Carbonate Content in Soil, Shore and Bottom Sediment Samples	87
4.2 Geochemistry	90
4.2.1 Major Oxides Indication	90
4.2.2 Heavy Metals Concentration	91
4.2.3 Spatial Distribution of Heavy Metals	94
4.2.4 Regional and International Comparison of Heavy Metal Average Concentrations	100
4.2.5 Heavy Metal Contamination Assessment	106
4.2.6 REE Concentration and Normalization	110
4.2.7 Spatial Distribution of REE	120
4.2.8 Regional and International Comparison of REE Average Concentrations	124
4.2.9 REE Contamination Assessment	126
4.3 Radiology	129

4.3.1 Radionuclide Gamma and Alpha Activity	129
4.3.2 Spatial Distribution of Radionuclide Activity Concentrations.....	134
4.3.3 Regional and World Average Comparison of Radionuclide Activity Concentrations	136
4.4 Relationships between Heavy Metals, Rare Earth Elements (REE) and Natural Radioactivity Concentrations	138
4.4.1 Pearson Correlation Coefficient	138
4.4.2 Cluster Analysis of Soil, Shore and Bottom Sediment Samples	149
Chapter 5: Conclusion and Recommendation.....	152
5.1 Concluding Summary	152
References	155
List of Publications	170

List of Tables

Table 2.1: List of samples collected with their label, coordinates and location	25
Table 2.2: Radionuclides present in the standard source	33
Table 2.3: Energy lines and their associated radionuclides efficiency and emission probability	36
Table 3.1: Values of statistical parameters and Phi percentiles for the analyzed soil samples	44
Table 3.2: Values of statistical parameters and Phi percentiles for the analyzed shore samples	45
Table 3.3: Values of statistical parameters and Phi percentiles for the analyzed bottom sediments.....	46
Table 3.4: Statistical summary of grain size parameters in studied samples	47
Table 3.5: discriminate function of grain size parameters in soil and shore samples	49
Table 3.6: Mineralogical composition of soil samples	51
Table 3.7: Mineralogical composition of shore samples	52
Table 3.8: Mineralogical composition of bottom sediment samples	53
Table 3.9: Carbonate content (%) of soil, shore and bottom sediment samples	55
Table 3.10: Major oxides Wt.% of soil samples (analytical error is <0.01)	58
Table 3.11: Major oxides Wt.% of shore samples (analytical error is <0.01)	59
Table 3.12: Major oxides Wt.% of bottom samples (analytical error is <0.01).....	60
Table 3.13: Heavy metal concentrations (in ppm) for the soil samples (analytical error is <0.01)	63
Table 3.14: Heavy metal concentrations (in ppm) for the shore samples.....	64
Table 3.15: Heavy metal concentrations (in ppm) in bottom sediment samples (analytical error is <0.01). The grain size notations “C”, “M” and “F” stand for coarse, medium and fine	64
Table 3.16: REE and Al concentrations (in ppm) in soil samples (analytical error is <0.01)	68
Table 3.17: REE and Al concentrations (in ppm) in shore samples (analytical error is <0.01)	70
Table 3.18: REE and Al concentrations (in ppm) in bottom sediment samples (analytical error is <0.01)	71
Table 3.19: Radionuclides Activity concentrations and radium equivalent in (Bq/kg) and absorbed dose (nGy/hr) in soil samples	75
Table 3.20: Radionuclides Activity concentrations and radium equivalent in (Bq/kg) and absorbed dose (nGy/hr) in shore samples	76

Table 3.21: Radionuclides Activity concentrations and radium equivalent in (Bq/kg) and absorbed dose (nGy/hr) in bottom sediment samples	77
Table 3.22: ^{234}U and ^{238}U activity ratios for selected samples.....	79
Table 4.1: Characteristics samples location with the maximum heavy metal concentrations (in ppm) in shore, soil and bottom sediment	93
Table 4.2: Heavy metal contaminations (in ppm) in BNPP (for shore, soil and bottom samples) in comparison with other studies in the UAE and with Dutch guidelines (Lijzen et al., 2001).....	101
Table 4.3: Heavy metal concentrations (in ppm) in soil samples from BNPP in comparison with other international studies	101
Table 4.4: Heavy metal concentrations (in ppm) in shore samples from BNPP in comparison with other international studies. BDL stands for below detection limit	103
Table 4.5: Heavy metal concentrations (in ppm) in bottom sediments of BNPP in comparison with other international studies	105
Table 4.6: The average background values, enrichments factors (EF), contamination factor (CF) and geoaccumulation indices (I-geo) for the soil, shore, bottom areas and overall average.....	109
Table 4.7: REE average concentrations in soil, shore and bottom sediments compared to average background values and chondrite value.....	112
Table 4.8: Basic statistics of REE normalized to the concentrations in chondrite normalized in soil, shore and bottom sediments	116
Table 4.9: REE distribution (ppm) in soil, shore and bottom sediments of BNPP in comparison with other international studies	125
Table 4.10: Average enrichment factors (EF), contamination factors (CF) and geoaccumulation indices (I-geo) for the soil, shore and bottom areas and for all samples together (overall average).....	128
Table 4.11: International and regional comparison of radionuclide activity concentrations (in Bq/kg).....	137
Table 4.12: Pearson correlation coefficients between major oxides (%) and heavy metals (ppm) in soil samples (red values indicate significant correlation at 0.01 level).....	142
Table 4.13: Pearson correlation coefficients between ^{238}U , ^{232}Th , ^{40}K (Bq/kg) and major oxides (%) in soil samples (red values indicate significant correlation at 0.01 level).....	143
Table 4.14: Pearson correlation coefficients between major oxides (%) and heavy metals (ppm) in shore samples (red values indicate significant correlation at 0.01 level).....	144
Table 4.15: Pearson correlation coefficients between ^{238}U , ^{232}Th , ^{40}K (Bq/kg) and major oxides (%) in shore samples (red values indicate significant correlation at 0.01 level).....	145

Table 4.16: Pearson correlation coefficients between ^{238}U , ^{232}Th , ^{40}K (Bq/kg) and major oxides (%) in bottom sediments (red values indicate significant correlation at 0.01 level).....	147
Table 4.17: Pearson correlation coefficients between the activity concentrations of ^{238}U , ^{232}Th , ^{40}K (Bq/kg) and the REE (in ppm) in soil samples (red values indicate significant correlation at 0.01 level).....	148
Table 4.18: Pearson correlation coefficients between the activity concentrations of ^{238}U , ^{232}Th , ^{40}K (Bq/kg) and the REE (in ppm) in shore samples (red values indicate significant correlation at 0.01 level).....	148
Table 4.19: Pearson correlation coefficients between the activity concentrations of ^{238}U , ^{232}Th , ^{40}K (Bq/kg) and the REE (in ppm) in bottom sediment samples (red values indicate significant correlation at 0.01 level)	148

List of Figures

Figure 1.1: Location map of the study area (Barakah area).....	6
Figure 1.2: Surface geology of the United Arab Emirates (Modified after the Ministry of Energy, Petroleum and Minerals sector, 2006).....	8
Figure 1.3: Geological map of the surroundings of Abu Dhabi emirate (Simplified from EAD, 2012)	10
Figure 1.4: Schematic interrelationships between principal stratigraphic formations, UAE related to Miocene age (After Steve and Richard, 2012).....	12
Figure 1.5: Sedimentary facies distribution of Sabkha Matti in western United Arab Emirates (modified from Hunting Geology and Geophysics, 1979; Alsharhan and Kendall, 2002	13
Figure 2.1: Locality map showing the location of sampling sites.....	26
Figure 2.2: Flow chart showing how a standard spectrum was obtained.....	33
Figure 2.3: Gamma emission spectrum of soil sample (S11) showing the lines used.....	37
Figure 2.4: Flow chart showing how a standard spectrum was obtained.....	38
Figure 2.5: Source efficiency as a function of energy	38
Figure 2.6: An alpha spectrum showing the energy lines of U isotopes, the horizontal axis is the energy in Mev while the vertical axis is the counts/channel.....	40
Figure 2.7: Schematic procedure of soil digestion and Uranium separation and measurement.....	41
Figure 3.1: Location of the samples with maximum heavy metal concentrations (in ppm) in shore, soil and bottom sediment	66
Figure 3.2: Concentrations of heavy metals, total REE and radium equivalent in S14, B4 and M17, in addition to their average values in soil, shore and bottom sediments.....	80
Figure 4.1: Mean size distribution for all 58 samples in mm. All the samples, grouped in soil, shore and bottom, are shown in this plot.....	82
Figure 4.2: Stacked column showing the percent by weight of the grains in the different size ranges	83
Figure 4.3: Graphical plot of Y1 against Y2.....	84
Figure 4.4: Graphical plot of Y2 against Y3.....	84

Figure 4.5: Average concentrations (in ppm) of various heavy metals for each of the coarse, medium and fine grains of the bottom samples	86
Figure 4.6: Comparison between mean grain size and carbonate percentage in soil, shore and bottom sediment samples	88
Figure 4.7: Correlation between mean grain size and carbonate percentage in soil, shore and bottom sediment samples	89
Figure 4.8: CaO, SiO ₂ and Al ₂ O ₃ ternary plot for shore, soil and bottom sediments of study area.....	90
Figure 4.9: Average concentrations (in ppm) of the heavy metals and their standard deviations in the shore, soil and bottom samples.....	92
Figure 4.10: Spatial distribution maps showing the heavy metal distributions across all 58 sampling sites, which are represented by dots.....	96
Figure 4.11: REE average concentrations in soil, shore and bottom sediments compared to average background values and chondrite value	111
Figure 4.12: Average concentrations of REE in soil, shore and bottom sediments	111
Figure 4.13: Concentrations of REE: LREE (La, Pr, Nd,Sm and Eu) and HREE (Gd, Tb, Dy, Ho, Er, Tm, Yb and Lu) normalized to the concentrations in chondrite in Average of soil, shore and bottom sediments	115
Figure 4.14: Concentrations of REE: LREE(La, Pr, Nd,Sm and Eu) and HREE (Gd, Tb, Dy, Ho, Er, Tm, Yb and Lu) normalized to the concentrations in chondrite for all soil samples	115
Figure 4.15: Average REE distribution pattern normalized to the concentrations in chondrite in different fraction (C coarse, M medium and F fine) of bottom sediments.....	117
Figure 4.16: Scatter diagram of Al ₂ O ₃ (%) contents against REE concentration in ppm for bottom sediment.....	118
Figure 4.17: The distribution pattern of REE in the studied area	121
Figure 4.18: Average values of the radiological activities and radium equivalent in (Bq/kg) and absorbed dose (nGy/hr)	131
Figure 4.19: Correlation between ²³⁸ U (²²⁶ Ra), ²³² Th and ⁴⁰ K in different environments (shore, soil and bottom)	133
Figure 4.20: Spatial Distribution pattern of radionuclides activities, Rad _{eq} and abs. dose in the studied area.....	135
Figure 4.21: Dendrogram for soil samples using centroid method.....	150
Figure 4.22: Dendrogram for shore samples using centroid method.....	150
Figure 4.23: Dendrogram for bottom sediment samples using centroid method	151

List of Abbreviations

Abs dose	Absorbed dose
ASTM	American Society for Testing and Materials
Ave.	Average
BNPP	Barakah Nuclear Power Plant
Bq/k	Becquerel per kilogram
Br	Branching ratio
BVML	Bureau Veritas Minerals Laboratories
CF	Contamination Factor
EF	Enrichment Factor
ENEC	Emirates Nuclear Energy Corporation
FANR	Federal Agency for Nuclear Regulation
HPGe	High Pure Germanium
HREE	Heavy Rare Earth Element
IAEA	International Atomic Energy Agency
ICP	Inductively Coupled Plasma
keV	Kilo electron Volt
St. Dev.	Standard Deviation
LOI	Lost of Ignition
LREE	Light Rare Earth Element
M	Mass
Mz	Mean size
nGy/h	Nano Gray per hour
NP	Net Peak
Ppm	Part per million

QA/AC	Quality Assurance / Quality Control
Rad eq	Radium equivalent
REE	Rare Earth Element
S	Sample
SKI	Skewness
UAE	United Arab Emirates
UNSCEAR	United Nations Scientific Committee on the Effect of Atomic Radiation
WHO	World Health Organization
XRD	X-Ray Diffraction

Chapter 1: Introduction

1.1 Research Focus

United Arab Emirates (UAE) is embarking a nuclear power program for the peaceful uses through constructing four units of Nuclear Power Plant (NPP) in Barakah area at the western region of the Arabian Gulf, with the highest standard of safety and performance, which meet the UAE 2020 vision. Switching to alternative energies other than oil is supported and managed by the government and the leadership of the United Arab Emirates. The construction of the NPPs is directed by Emirates Nuclear Energy Corporation (ENEC) to supply the growing of UAE electricity demands. This project and other relevant projects in some countries such as Saudi Arabia and Kuwait are likely to influence the radionuclide levels in the Gulf water (Huber, 2007). As the first NPP will be operated in 2018, the routine operation of the nuclear facilities may have some release of radioactive materials to the environment. It is mandatory by UAE standards and environmental laws to establish a geochemical and radiological baseline before the operation of the NPPs and investigate the environmental impact in case of emergency especially that some nuclear activities have been established in near surrounding of the UAE. This study aims to determine the activity concentrations of natural uranium, thorium and potassium, hazard parameters such as radium equivalent and absorption dose, the $^{234}\text{U}/^{238}\text{U}$ activity ratios, anthropogenic radioactive isotopes and the level of heavy metals around Barakah area before the operation of the nuclear power plant. These radiological measurements and geochemical investigation will establish a documented geochemical and radiological reference data for Barakah area “pre-

operation of Barakah NPP” which can be used later to assess any changes in the radioactive background level or heavy metal concentration.

The average concentrations for the measured elements (radionuclides and heavy metals) will be also compared with the environmental guideline and geochemical baseline values to evaluate and indicate any significant radiological risk or heavy metal contamination related to human activities in the area.

The proceeding sections will discuss and outline the introduction, study area background information, literature and methods employed in the thesis, results, their detailed explanation, and the conclusions and recommendations arrived at from the results.

1.2 Background

Nuclear energy is a much cleaner source to generate electricity than traditional forms like oil and coal because it saves millions of tons of CO₂ from being released into the atmosphere. Moreover, nuclear reactors produce a huge amount of electricity from a very small volume of fuel. As of 1 July 2016, the world had 444 operable grid-electric nuclear power reactors with 62 others under construction (WNA, 2017). About 11.7% of the world’s electricity demand in 2011 is produced by nuclear power (IEA, 2013). Simply, nuclear energy is generated by splitting atoms, through a heat releasing process called fission. These atoms are radionuclides producing radioactive energy. Radioactivity is around us and simply refers to the particles that are emitted from nuclei as a result of nuclear instability. Alpha, beta, and gamma radiation are the most common types of ionized radiation (Faure and Mensing, 2005). Natural occurring radioactive materials (NORM) are present in our environment and bodies through atmosphere and Earth ‘crust. Rocks and minerals

provide a constant natural background of low level radioactivity (Baiulescu, et al., 1991). Generally, NORM includes long-lived radioactive elements such as uranium, thorium and potassium and their decay products, such as radium and radon. Based on their distribution in the environment, natural radioactive substances are often classified into two groups: (1) naturally occurring radioactive materials (NORM), and (2) technologically enhanced NORM. Fertilizer production and fossil fuel combustion are examples of the second group, which contain elevated concentrations of radioactive elements as a result of technological transformations of various natures (Chau et al., 2011).

Uranium has an increasing importance as the main source in generating energy in nuclear power plant. There are three long lived naturally occurring isotopes of uranium: ^{234}U ($T_{1/2} = 2.45 \times 10^5$ years), ^{235}U ($T_{1/2} = 7.04 \times 10^8$ years) and ^{238}U ($T_{1/2} = 4.47 \times 10^9$ years). The natural abundances of the isotopes ^{238}U , ^{235}U and ^{234}U are 99.27%, 0.72% and 0.005%; respectively. Combining these mass percentages with the unique half-life of each isotope converts mass into radioactivity units and shows that crustal uranium contains 48.7% ^{234}U , 2.27% ^{235}U , and 49.0% ^{238}U by radioactivity, and has a very low specific activity (activity per quantity) of $0.69 \mu\text{Ci/g}$ based on data compiled by the National Nuclear Data Center (NNDC 2011). Only one of these isotopes is used in nuclear power plant, which is enriched ^{235}U . In closed system (undisturbed minerals), both ^{234}U and ^{238}U are in secular equilibrium, which mean the alpha decay rates of both isotopes are equal (Paces et al., 2001). Under these conditions, the $^{234}\text{U}/^{238}\text{U}$ activity ratio equal 1.

Radionuclides spread through the environment along the same pathways as other materials. They travel through the air, water, and food chain. Radionuclides may enter the human body by eating, drinking, inhalation or absorption through the

skin (WHO, 2011). Radionuclides can be hazardous to living tissue because of the radiation energy emitted when a radionuclide decays. The more common the radionuclide is, the more important to be investigated. Examples of more common radionuclides are uranium, thorium and potassium; all are widespread in most rocks and soils. Radium (^{226}Ra) is a decay product of ^{238}U series, which in turn decay to radon (^{222}Rn), an inert gas with half life ($T_{1/2} = 3.68$ days). Another hazardous short-lived radon isotope is ^{220}Rn which is result from thorium series with half-life ($T_{1/2} = 44$ second). Because of short half-life, exposure to radon is a problem in certain mining activities and the use of self-protection equipment is essential.

Environment contamination by heavy metals have gained a lot of interest by ecologist and public health specialist in recent years. Human exposure to heavy metals has risen dramatically due to the increasing usage in many industrial, agricultural, domestic and technological applications (Bradl, 2002). Heavy metals are naturally occurring elements that have a high atomic weight. They are widely distributed in the environment that raises concerns over their potential effects on human health and the environment. Their toxicity depends on several factors including the dose, route of exposure, and chemical species, as well as the age, gender, genetics, and nutritional status of exposed individuals. Arsenic, cadmium, chromium, lead, and mercury have high degree of toxicity and consider the most significant in public health (Tchounwou et al., 2012).

Anthropogenic activities such as construction, mining, transportation, power plants, sewage treatment plants, industrial activities, urban waste and agricultural runoff have significantly affected the distribution and the level of contamination of radionuclides and heavy metals in marine, soil and sediments. The purpose of

measuring the radioactivity and heavy metals concentrations in soil is to assess their level of concentration and evaluate any associated environmental impact.

1.3 Study Area

The United Arab Emirates (UAE), a federation of seven independent states since 1971, is located in the southeastern corner of the Arabian Peninsula and lies between latitudes 22° 50' and 26° North and longitudes 51° and 56° 25 ' East (Figure 1.1). It is bordered by the Arabian Gulf to the north, Saudi Arabia to the south and west, and Oman and the Gulf of Oman to the east; it is in a strategic location along northern approach to the Strait of Hormuz, a vital transit point for world crude oil. The Northern coast of the United Arab Emirates forms the southern margin of the Arabian Gulf, a NW–SE trending sea that is approximately 900 km long and up to 350 km wide. It covers approximately 226,000 km², and has an average depth of 35 m and a maximum depth of 100 m at the Strait of Hormuz (Purser and Seibold, 1973).

Barakah area is located to the west of the Abu Dhabi Emirate, the capital of the UAE. Abu Dhabi is geographically divided into four distinct regions as (1) Abu Dhabi Island, (2) Eastern Region, (3) the Gulf Islands and (4) Western Region (where the study area located). Barakah area is about 224 km west-southwest of Abu Dhabi City and about 75 km from the Saudi Border. UAE government's decision of constructing four units of Nuclear Power Plant (NPP) in Barakah area on the western Region of the Arabian Gulf is to supply the growing electricity requirements of the UAE.



Figure 1.1: Location map of the study area (Barakah area)

The Barakah NPP site selection and evaluation process was based on a guidance from FANR (Federal Regulation of Nuclear Regulatory), the US Electric Power Research Institute, the US Nuclear Regulatory Commission, and the IAEA (WNA, 2017). The construction of the non-nuclear structures commenced in Sep 2010 and the propose date for the partially operation of the nuclear plant will be 2018 while the full operation of the four unit nuclear power plant will be by 2020. Switching to alternative energies other than oil is supported and managed by the government and the leadership of the United Arab Emirates. Although the nuclear energy is not renewable since it relies on nuclear fuel that must be mined out of the earth, much like coal, it may be considered a green energy because it does not

produce carbon dioxide so help to reduce climate change. At the same time, the nuclear energy produces nuclear waste, which is difficult to dispose safely.

1.4 Geological Setting

1.4.1 UAE General Geology

The UAE lies at the northeastern part of the Arabian Peninsula. This peninsula is limited by four major tectonic features: (1) the Red Sea and Dead Sea rift system at the west and northwest, (2) the Thrust zone from the Alpine Orogeny at the north, (3) the mobile belt of Zagros and Oman Mountains at the east and southeast and (4) the wrench fault associated with Owen Fracture zone at the south (Powers et al., 1966 and Jamali, et al., 2006). The Arabian Peninsula can be divided into three main divisions: shield, shelf and mountains. The Arabian Shield lies to the west of the Peninsula occupying about one third of its area and composed largely of Precambrian Igneous and metamorphic rocks while the Arabian platform (Shelf) lies to the east of the Arabian shield and contain Paleozoic, Mesozoic and Lower Tertiary rocks crop. The third part of the Arabian Peninsula is the Oman and Zagros Mountains (Powers et al., 1966 and Alsharhan et al., 2001).

The UAE has a diverse landscape as a result of the geologic processes that have occurred during earth's history. The surface area of UAE is 83600 km² and is located within the arid climate zone. Figure 1.2 shows the UAE surface geology with some dominant geologic features such as dunes, wadis, mountains and sabkhas. Sand dunes and wadis alluvial of Quaternary ages cover most of the UAE surface geology and mountains are represented by the eastern mountains and Jebel Hafit. Sabkha, Arabic term for coastal and inland saline flats (Powers et al., 1966), is also

very common. Generally, Holocene carbonates and evaporate complex dominate the northern coast of the UAE while terrigenous clastic sediments with a range of mountains cover the eastern coast (Al Rashdi, 2004; Basaham & El-Sayed, 1998).

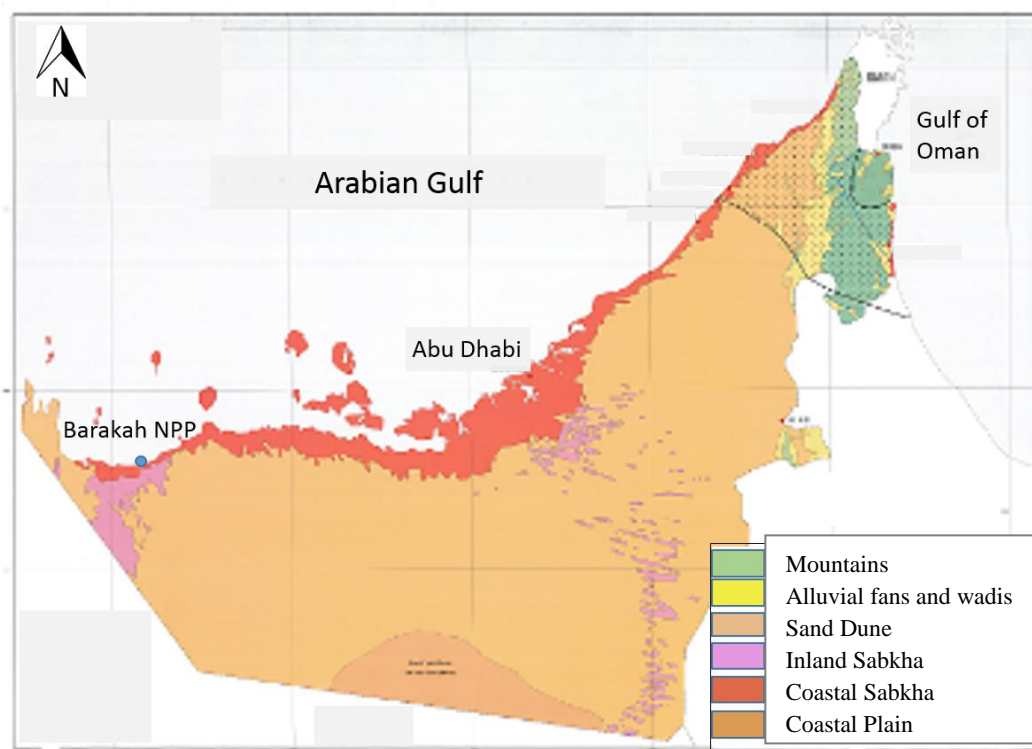


Figure 1.2: Surface geology of the United Arab Emirates (Modified after the Ministry of Energy, Petroleum and Minerals sector, 2006)

1.4.2 Abu Dhabi Geology

According to a recent soil survey done by the Environment Agency- Abu Dhabi for identification and mapping the soil of Abu Dhabi Emirate, the soil in the UAE is sandy, infertile and dominated by minerals such as quartz and carbonates (EAD, 2012). The Western area of the Abu Dhabi emirate contains terrestrial sediments related to the Miocene period. The Miocene period extended from approximately 23 to 5 million years Before Present. The substrate of this Miocene is consisting of a sequence of marls, sandstone, limestone and evaporates occurred

southward and gently dipping (AlSharhan and Kendall, 2003).

According to Alsharhan and Kendall (2003), coral reefs and coralgall sand is common to the west of Abu Dhabi Island while to the east oolites accumulate on the tidal deltas of channels located between barrier islands. Figure 1.3 shows the geological features of Abu Dhabi. Among others, sabkha and sand dunes are dominant geological features. Inland sabkhas consist of calcareous and gypsiferous silt and sand while near the coast the composition is mostly haliferous (coastal Sabkha). The mode of sabkhas formation in Abu Dhabi is explained by Alsharhan and Kendall (2003) in their discussion of carbonate and evaporates of the area. Although the coastal plains are dominated by sabkhas, unfortunately, these coastal sabkhas in Abu Dhabi emirates had decreased to only 54 km due to land development activities (Lokier, 2013). Graham et al. (2002) studied the Quaternary outcrop in Marawah islands near the coast of Abu Dhabi. He found that the Pleistocene deposits accumulated partly in a shallow-marine environment and partly under aeolian conditions. The Marawah sections have revealed that there were periods when sea level was close to present-day levels and other times when it was approximately 4 to 5 m higher than today. In general, Abu Dhabi emirate has numbers of barrier island which spread at the southwest along the coast of the UAE. These islands, which is located to the east of the study area include Abu Dhabi, Al Saadiyat, Al Qanatir, Abu Al Abyad and Marawwah. The absence of offshore barriers (as is the case of the study area) means that the deep waters impinge directly onto the shore causing a region of maximum water agitation (Purser and Seibold, 1973).

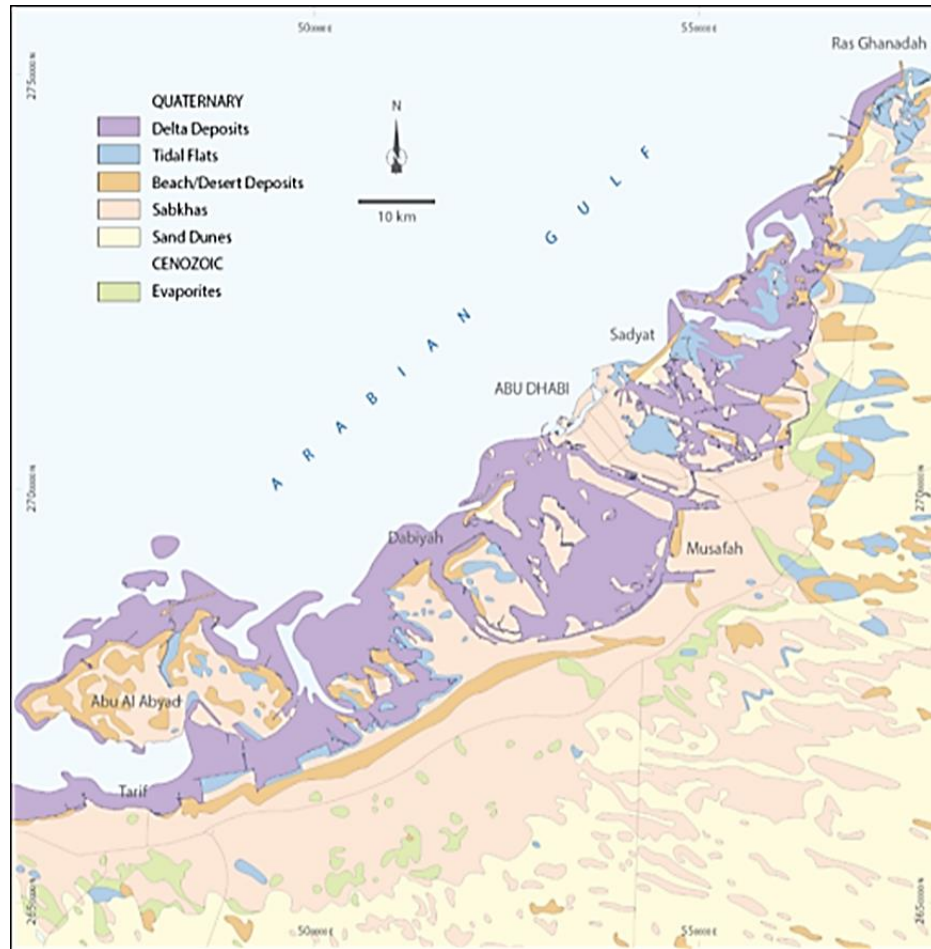


Figure 1.3: Geological map of the surroundings of Abu Dhabi emirate (Simplified from EAD, 2012)

1.4.3 Barakah Area Setting

The Barakah area is undeveloped and has limited dwellings or infrastructure along the coast. There are no commercial, industrial, institutional or recreational structures exist in the area. There are also no dominant land uses within 20 km of the site other than few houses and small-scale commercial fishing for local consumption. The nearest large settlements to the studied area is Ruwais, 53 km to the northeast and Sila, 48 km to the northwest. The Barakah area is a flat area at the sea level with elevations estimated to be 3 to 4 m. The coastal area of the site consists of carbonate sands, interspersed dunes and beach ridges next to the shoreline. The Inland area of

the western area of UAE is dominated by calcareous and gypsiferous silt and sand (Alsharhan & Kendall, 2003).

The Jebel Dhannah region, also included in this study, is located to the west of Abu Dhabi city and it is about 45 km away from the Barakah NPP. Whybrow and Hill (1999) studied the geological setting of Jebel Dhannah including the upper Dam formation to the west of Abu Dhabi. They described the formation of the lower Shuweihat and the upper Baynunah. Figure 1.4 shows a schematic interrelationships between principal stratigraphic formations related to Miocene age in UAE area (Dam formation is appear to the west of Abu Dhabi). The lower Shuweihat is mainly composed of sedimentary rocks with pink to red cross-bedded layers of quartz sands from salt flats, fluvial and aeolian origins (Bristow, 1999). On the other hand, Baynunah Formation is composed mainly of sandstones and mudstones from fluvial settings with fossil accumulation at various levels. This formation is exposed along more than 200 km of the Abu Dhabi coast in the western Al Gharbia region, and extends more than 30 km inland (Whybrow, 1989). The findings of Whybrow *et. al.* (1999) suggest the presence of a (currently disappearing) large river system in the Baynunah area as evident by the abundance of reptiles and fish remains (Whybrow *et al.*, 1999 and Friend, 1999).

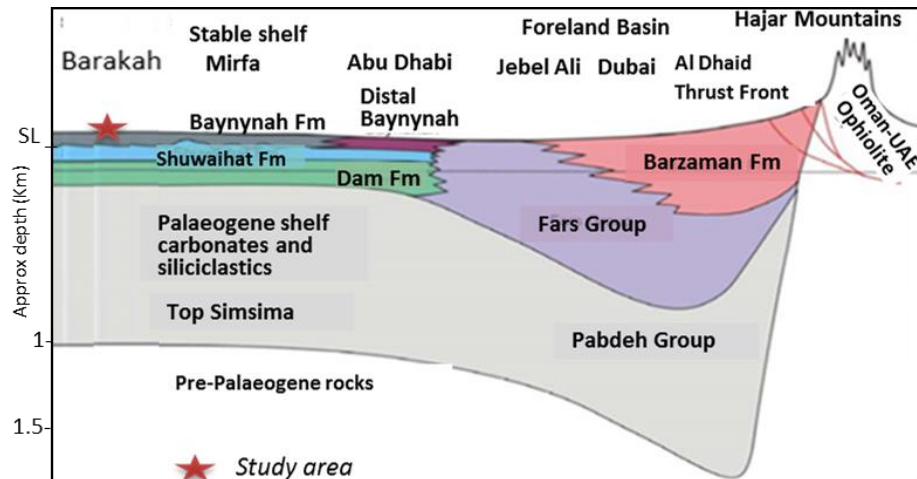


Figure 1.4: Schematic interrelationships between principal stratigraphic formations, UAE related to Miocene age (After Steve and Richard, 2012)

Sedimentary facies distribution from Jebel Barakah to Sila were studied by Alsharhan and Kendall (2002). They mentioned that the area is extending from Jebel Barakah (west of Jebel Dhannah) to Sila embraces the massive, 6000 years old, inland sabkha, the “Sabkha Matti” (Figure 1.5). Sabkha Matti extends 150 km southward from the coast and is characterized by a narrow strip of supratidal carbonate sands and evaporates near the coast, while southward it grades into an area of inland siliciclastic sabkha.

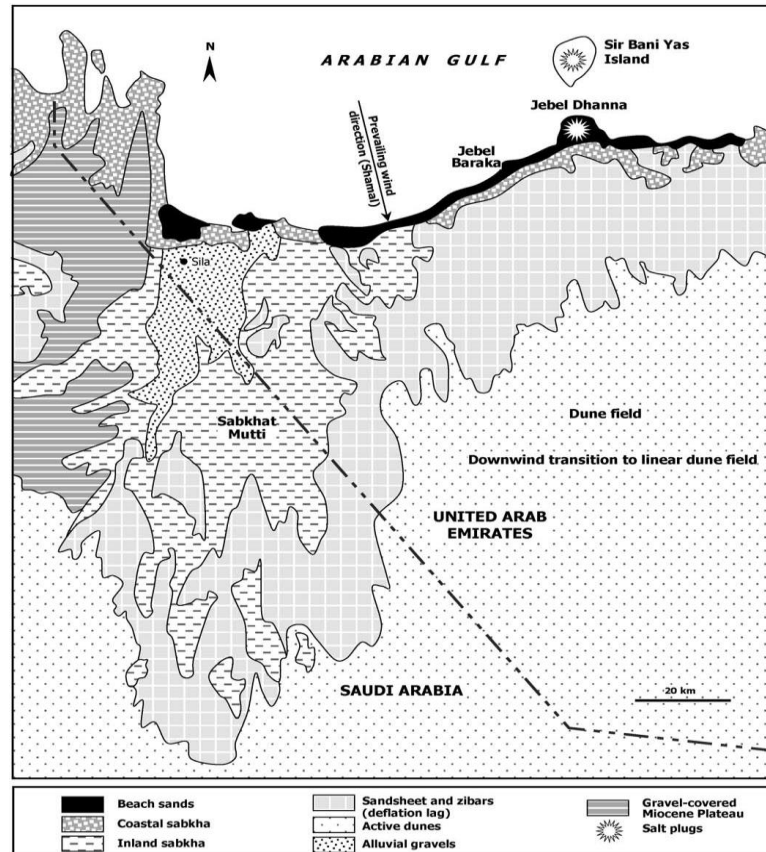


Figure 1.5: Sedimentary facies distribution of Sabkha Matti in western United Arab Emirates (modified from Hunting Geology and Geophysics, 1979; Alsharhan and Kendall, 2002)

1.4.4 Coastal Environment

Calcium carbonate is secreted by many invertebrate organisms, most common of which are the molluscan animal. Abbot (1976) identified mollusks as soft-bodied animal that usually produce an external shell composed of a limy material called calcium carbonate secreted by fleshy organ called mantle. In the present study, two major classes were found along the coast of the Barakah area; Gastropods and Bivalves as well as some coral species. No species taxonomy was done in the present study, however some previous taxonomy were conducted in the Northern and Eastern coast of UAE (Al Rashdi, 2004). Bosch et al. (1995) published

a book on the seashell of the Eastern Arabia. They identified 1273 species from different classes such as Scaphopods, Gastropods, Bivalves and Cephalopods.

The UAE has an arid, sub-tropical continental climate because the Arabian Gulf is surrounded by land and exhibits extreme seasonal fluctuations (Purser and Seibold, 1973). Strait of Hormuz passes the marine water to the Arabian Gulf and travels by density currents in a broadly counter clockwise direction around the basin (Sheppard et al., 1992). UAE coast has extensive shallow regions, <20 m deep, and also characterized with the densest water in the Arabian Gulf forms during winter resulted from atmospheric cooling of extremely saline water masses in shallow water (Kampf and Sadrinasab, 2006). There are two types of tides in the Arabian Gulf, semidiurnal to diurnal (Reynolds, 1993). The diurnal tides are predominately along the western coast of Abu Dhabi emirate, whilst semi-diurnal tides occur mostly along the eastern shores of the coastline (Sheppard et al., 1992). The UAE coastlines are affected by Shamal winds, which are associated with surface currents and waves (Alsharhan and Kendall, 2003).

1.5 Literature Review

The coastal region of the United Arab Emirates (UAE) consists of the Arabian Gulf Coastal and the Eastern Coast regions. A comprehensive review that summarizes the findings of publications over the past three decades about heavy metal contamination and hydrocarbon pollution in the Arabian Gulf is prepared by Freiji (2015). Among others, Abaychi and Douabul (1986), Fowler et al. (1993), Al-Arfaj and Alam (1993), Al-Abdali et al. (1996) and Basaham and El-Sayed (1998) studied the heavy metal distribution in the Arabian Gulf. Abyachi and Douabul (1986) investigated the trace element geochemical associations in the Arabian Gulf.

They determined the geochemical fraction of Cd, Cr, Cu, Fe, Mn, Ni, V and Zn in sediments from the northwestern part of the Arabian Gulf. They found that in the non-lithogenous fraction, the easily or freely leachable and exchangeable fraction is not geochemically significant while the carbonates and Fe-Mn oxides and hydroxides fractions appear in the most dominant phases. Fowler et al. (1993) studied the distribution of petroleum hydrocarbons, trace metals and biota in the Arabian Gulf sediments, near the shore, before and after the 1991 Gulf war. They concluded that the highest concentrations were found along the northern coast of Saudi Arabia as evident from the elevated concentrations of hydrocarbon compounds in the subtidal sediments. Al-Arfaj & Alam (1993) studied the chemical characterization of sediments from the Arabian Gulf after the 1991 oil spill. Al-Abdali et al. (1996) found chronic contamination of iron, vanadium, copper, nickel and lead in the northern, central and eastern areas of the Arabian Gulf. They also found that the contamination of trace metals in the western area, known for its pollution by the Kuwait oil slick, does not exceed the permissible natural background levels. Basaham and El-Sayed (1998) investigated the distribution and phase association of some major and trace elements in the Arabian Gulf sediments. They observed two major sediment types: (1) a terrigenous, fine-grained and Al-rich type predominating along the Iranian side; and (2) a coarse grained and carbonate-rich type predominating along the Arabian side of the Gulf. On the other hand, Shriadah (1998a) studied the impacts of an oil spill on the marine environment of the UAE along the Gulf of Oman. He concluded that the oil spill resulted in a temporary elevation of contamination levels, which were rapidly reduced, and the oil pollution levels have returned to prevailing background levels. Schnetger et al. (1999) carried out a high-resolution study on geochemical characteristics of deep-sea sediments

from the Arabian Gulf. They sampled five deep-sea cores at high resolution and analyzed major and trace elements. They observed that Ba/Al ratios, used as a productivity proxy, were variable but high in all deep-sea cores of the Arabian Sea which indicate that a basin-wide influence of nutrient-rich water masses. They also observed that the Mn distribution in a core from the Western Arabia Sea showed enrichments during interglacial periods and may indicate Mn export owing to the presence of a strong oxygen-minimum zone. Shriadah (1999) studied oil contamination along oil tanker routes of the UAE in the Arabian Gulf and Gulf of Oman. He aimed to examine the current state of oil contamination at offshore areas. He found that the pattern of distribution of petroleum hydrocarbons in marine sediments from the study areas resembled to some extent the distributions of organic carbon in marine sediments. This observation led him to conclude that the increase in petroleum hydrocarbons contamination from oil tankers traffic and oil terminals would result in an increase in organic carbon contents. De Mora et al. (2004) assessed the heavy metal contamination in marine sediment in the Arabian Gulf. They named two hotspots of heavy metals in Bahrain and on the eastern coast of the UAE. Elevated levels of heavy metals of Cu, Hg, Pb and Zn were recorded off the oil refinery in Bahrain. Higher concentrations of heavy metals Co, Cr and Ni were reported at Akkah beach on the eastern coast of the UAE with a maximum concentrations of 45, 303 and 1010 $\mu\text{g/g}$ dry weight, respectively and attributed to the metal-rich mineralogy of the region. El Tokhi et al. (2015a) studied the distribution of heavy metals in bottom sediments of the Arabian Gulf near the UAE coast (Dubai, Sharjah, Ajman, and Ras Al-Khaimah) indicated that the concentration of Cu, Zn, Pb, Fe, Mn, Ni, Cd and V do not exceed the safe limits suggesting no pollution around the studied area. A recent study by El Tokhi et al. (2016) on the

distribution of heavy metals in bottom sediments near Abu Dhabi's coast, they found that the average concentrations of copper, zinc, lead, iron, manganese nickel, cadmium and vanadium are 4.65, 11.94, 1.91, 2800, 92.26, 10.55, 0.082 and 11.43 $\mu\text{g/g}$ respectively and all are within the permissible levels.

Juma (1995), Shriadah (1998b), El-Sammak (2001) and Alsharhan and El-Sammak (2004) studied the heavy metal distribution along the coast of UAE. Juma (1995) studied the heavy metals and minerals concentrations in the sediments of the eastern coast of the UAE. Shriadah (1998b) carried out a study for heavy metals in mangrove sediments of the UAE shoreline. By correlations between some heavy metals and grain particles, he suggested that the mangrove sediments might inevitable become enriched in heavy metals in a source is available. He investigated eight heavy metals, which are Cd, Co, Cr, Cu, Mn, Ni, Pb and Zn and observed the concentrations of Mn, Ni and Pb were significantly higher than the other metals. The high concentration of Mn and Ni were due to non-anthropogenic sources such as the geologic nature formations and the presence of high mountains of basic igneous rocks, where the high levels of Pb were due to inputs from spills and discarded solid wastes. El-Sammak (2001) investigated the heavy metal pollution in bottom sediments of Dubai, UAE. He quantified the metal pollution using statistical methods and simple quantification methods. He observed that most of the stations reflect natural background composition of different metals. On the other hand, few samples reflect the man-made impact on the metals contents in the investigated area. Al-Sharhan and El-Sammak (2004) investigated grain size analysis and characterization of sedimentary environments of the UAE coastal areas. Their results revealed that the Arabian Gulf coast could be divided into three provinces: a) Abu Dhabi/Dubai province, b) Sharjah/Ajman/Um Al-Quwain province and c) Ras

Al-Khaimah province. They suggested that the variations among the studied sites might be due to either to the diversity of sediment sources, or to the geomorphology of the coastal areas. A recent study by Al Rashdi et al. (2015) investigated the concentrations of heavy metals along the coastal area of Abu Dhabi. It was found that the contamination of heavy metals including antimony, arsenic, cadmium, cobalt, copper, mercury, lead, molybdenum, nickel and zinc has increased in the coastal area of Abu Dhabi from 2004 to 2014. Heavy metal concentrations in the UAE are generally within the natural background levels (Al Rashdi et al., 2015; El Tokhi et al., 2016). However, elevated levels of heavy metals may be associated with anthropogenic activities such as oil refiners, desalination plants and power plants. However, there is paucity of data on geochemical distribution.

Several researchers studied radioactivity around the world. Among others, Kannan et al. (2002), Lu & Zhang (2008), Nenadovic et al. (2012) and Arnedo et al. (2013) studied the natural radioactivity in India, China, Serbia and Spain; respectively. Kannan et al. (2002) studied the distribution of ^{238}U , ^{232}Th and ^{40}K in soil samples of Kalpakkam in India which known with the presence of pockets of monazite mineral in their beach sands. He found that the concentrations of ^{238}U , ^{232}Th and ^{40}K varied in the range of 36-258, 352-3872 and 324-405 Bq/kg dry, respectively. The total absorbed gamma dose rates in air due to the presence of ^{238}U , ^{232}Th and ^{40}K in Kalpakkam soil samples varied between 24 and 556nGyh⁻¹ with a mean of 103nGyh⁻¹. The presence of ^{232}Th in beach sand contributed maximum (94.0%) to the total absorbed gamma dose rates in air. Lu & Zhang (2008) measured natural activity concentrations in China beach sand ranges from 7.6 to 17.2, 7.8 to 25.1 and 883.4 to 1313.6 Bq/kg for ^{226}Ra , ^{232}Th and ^{40}K with mean values of 12.0, 15.2 and 1079.2 Bq/kg, respectively. The activity concentrations of ^{226}Ra and ^{232}Th

in beach sands are lower, while ^{40}K is higher than the world average. Nenadovic et al. (2012) measured the vertical distribution of ^{238}U , ^{232}Th and ^{40}K in soil samples from the cultivated and undisturbed areas in Rudovci, municipality of Lazarevac, Serbia. The specific activity concentrations of ^{238}U , ^{232}Th and ^{40}K in soil and sediment samples was determined by gamma spectrometry using the HPGe semiconductor detector. Obtained activity concentrations ranged from 28.0 to 44.0 Bq/kg for ^{238}U , from 59.4 to 71.4 Bq/kg for ^{232}Th and from 335.0 to 517.0 Bq/kg for ^{40}K . While, Arnedo et al. (2013) measured the activity concentrations of ^{226}Ra , ^{232}Th and ^{40}K and found out that the activity concentrations are higher at a depth than at the surface. The average values of the activity concentrations of ^{226}Ra and ^{232}Th are lower than the world's mean values. However, the average values of the activity concentrations of ^{40}K are observed to be higher than worldwide.

Since Iran is relative to the regional studied area, relevant studies and their remarks are discussed. Abdi et al. (2009) determined the activity concentrations of the radioactive elements ^{238}U , ^{232}Th , ^{40}K and ^{137}Cs in the southern coast of the Caspian Sea in Iran. While Tari et al. (2013) used high pure germanium detectors to measure gamma emitting radionuclides in beach sand cores of coastal regions of Ramsar in Iran. He measured the average specific activities of natural radionuclides ^{226}Ra , ^{235}U , ^{232}Th , ^{40}K and ^{137}Cs , he concluded that none of the studied beaches was consider as radiological risk. On the Gulf of Aqaba of Jordan, Ahmad et al. (1997) investigated the radium equivalent activities in sand samples collected from different areas in Jordan. The radium equivalent activities calculated from measurements of ^{226}Ra , ^{232}Th and ^{40}K activities by gamma ray spectroscopy technique. The average value of the radium equivalent activities were calculated whereas the lowest average value were 41.06 Bq/kg measured in Adasiah and the highest average value were

85.536 Bq/kg in Ghor As-Safi. A study done on Gulf of Aqaba by Ababneh et al. (2010) using a core sediment from five locations, one of them is the phosphate loading berth which showed a higher activity concentrations of ^{238}U , ^{235}U and ^{226}Ra that other location and more than twice as high as the worldwide average. Another study by Al-Trabulsy et al. (2011) who measured the activity concentrations of ^{238}U , ^{232}Th , ^{226}Ra , ^{40}K and ^{137}Cs in coast of the Gulf of Aqaba by using gamma-ray spectrometry. They concluded that the average specific activities for ^{226}Ra , ^{232}Th , ^{40}K and ^{137}Cs were found to be 11.4, 22.5, 641.1 and 3.5 Bq/Kg, respectively. Which mean that the average activity concentrations of ^{226}Ra and ^{232}Th are lower than that of the world average of 25 Bq/Kg for both of them, whereas the mean value of ^{40}K is about double the world average of 370 Bq/Kg. While Abd El-Mageed et al. (2011) studied the radio activities of ^{232}Th , ^{226}Ra , ^{40}K and ^{137}Cs in soil in Juban town in Yemen by gamma-ray spectrometry. They concluded that the activity concentrations of ^{232}Th and ^{226}Ra agree with the world wide average concentrations of these radionuclides except ^{40}K . Farid et al. (2013) assessed natural radioactivity in some local cement type in Yemen using gamma-ray spectrometry. They found that the average values obtained for ^{226}Ra , ^{232}Th and ^{40}K activity concentrations in different types of cement are lower than the corresponding global values reported in United Nation Scientific Committee on the Effect of Atomic Radiation publications.

Some studies were conducted in the Arabian Gulf region by some researchers; Saad and Al Azmi (2002), Al-Zahrany et al. (2012), Al-Sulaiti, et al. (2012), Saleh (2012), Saif Uddin et al. (2012), Jallad (2014) and Bajoga et al. (2015). Saad and Al Azmi (2002) used Gamma-ray spectrometric measurements to study the concentration of ^{238}U , ^{232}Th , ^{226}Ra , ^{40}K and ^{137}Cs in both northern and southern coast of Kuwait. They concluded that the radioactivity in southern areas

reaches about one-half of the values commonly assigned as the world average. In northern areas, higher radioactivity concentrations are found but are still below the international levels. Al-Zahrany et al. (2012) measured the marine radioactivity near the Saudi Arabian coasts of the Red Sea and Arabian Gulf. The purpose of that study was to establish a marine radioactivity database, which includes necessary information on the background levels of both naturally occurring and man-made radionuclides in the marine environment. On the other hand, determination of the natural radioactivity levels in Qatar coast was done by Al-Sulaiti, et al. (2012). They concluded that activity concentrations of ^{232}Th and ^{40}K were found to be within the worldwide average values. They focused on inshore oil field area, and they found that the weighted mean value of the activity concentrations of ^{226}Ra in one of the samples was found to be around a factor of 10 higher than the accepted worldwide average value of 35 Bq/kg. On the other hand, the weighted mean values of the activity concentrations of ^{232}Th and ^{40}K were found to be within the worldwide average values of 30 and 400 Bq/kg. Similar study was done by Saleh, (2012) where he assessed the radioactivity of ^{238}U , ^{232}Th , ^{40}K , and ^{137}Cs and assessment of depleted uranium in soil of the Musandam Peninsula, Sultanate of Oman. He concluded that depleted uranium concentration matches its range in natural uranium. His results showed that the levels of ^{238}U , ^{232}Th and ^{40}K are relatively low. ^{137}Cs levels showed wide variability (0.11-61.40 Bq/kg) in the studied locations and this reveals a great diversity in the properties and textures of tested soil. The total annual external effective radiation dose from the measured radionuclides is 25.4 μSv . The contributions of radionuclides in the total annual effective dose are 30% from ^{238}U , 32% from ^{232}Th and 32% from ^{40}K while the contribution of ^{137}Cs is 6%. The obtained results revealed that the mean of isotopic abundance of ^{235}U is 0.66%;

therefore, the uranium detected in the investigated soil is almost of the natural type. The concentration of tritium, polonium, strontium and cesium in Kuwait territorial water are low and are comparable to most oceanic waters (Saif Uddin et al. 2012). Jallad (2014) studied the activity concentrations of ^{238}U , ^{232}Th , ^{226}Ra , ^{40}K and ^{137}Cs in sand of Failka Island and compared the absorbed dose and the effective dose rates with international values. Anthropogenic radionuclide ^{137}Cs were studied by Bajoga et al. (2015) by using a high-resolution gamma-ray spectroscopy and found that ^{137}Cs was not observed above the minimum detectable activity in that study.

There is paucity of data on radioactivity levels in United Arab Emirates. AlShamsi et al. (2013) and Murad et al. (2014) studied radioactivity levels in groundwater in UAE and Oman by using ICP-MS in carbonate aquifer and alluvial aquifer, respectively. AlShamsi et al. (2013) concluded that the uranium concentration in groundwater of the carbonate aquifers are below the higher permissible WHO limit for drinking water. On the other hand, Murad et al. (2014) concluded that the measured groundwater radioactivity including ^{323}Th , ^{238}U , ^{235}U , ^{226}Ra , ^{222}Rn , gross- α and gross- β , indicates values below the WHO permissible limits for drinking water. They also conclude a large difference in radioactivity fingerprints, in particular for ^{226}Ra and ^{222}Rn within the investigated aquifers. Al Rashdi and Siad (2015) concluded that there is no uranium or thorium contamination in the coast of Abu Dhabi. Although there is enrichment of uranium for some samples in comparison to average earth crust. The result U is mainly associated with CaO and Lost of Ignition (LOI) indicating the source of the U is mainly marine while Th is associated with terrigenous elements like Al_2O_3 indicating the source of the Th is originating from possible felsic rocks. Uranium (1.3-4.6 ppm, average 2.3 ppm),

exceeding the value in average upper continental crust, rather than Thorium (0.2-2.5; average 1.4 ppm).

1.6 Research Objectives and Aim

The aim of this research is to establish a documented geochemical and radiological reference data for Barakah area before operation of NPP. This will enable the assessment of any revealing radioactive contamination and evaluate any associated environmental impact, after the nuclear power plant commences. The main objectives of this research are to:

1. Prepare a geochemical data about Barakah NPP's area including both heavy metals and rare earth elements concentrations.
2. Assessment of heavy metals and rare earth elements concentrations by ICP-AES and evaluate their anthropogenic influences on environment.
3. Measure the level of natural and anthropogenic radionuclides at Barakah NPP area.
4. Estimate the hazard parameters such as radium equivalent and absorption dose.
5. Measure of the U isotopes and estimate the $^{234}\text{U}/^{238}\text{U}$ activity ratio.
6. Identify any geochemical and/or radiological anomalies in the area.
7. Mapping the spatial distribution of heavy metals, rare earth elements and activity radioactive concentrations and its related hazard parameters.
8. Establish a radiological baseline as a reference for Barakah NPP to assess the potential environmental impact that might be arisen from operation of NPP.

Chapter 2: Methodology

2.1 Field Work and Sampling

The materials used in the present study are depositional bottom sediment (from the surface to 0.3 m depth) and friable soil (from the surface to 0.5 m depth) samples collected from the bottom of the Arabian Gulf and coastal line and onshore area of Barakah. Fifty eight representative samples were collected in November 2014 (soil and shore samples) and May 2015 (bottom sediments). The six months difference in sampling were due to sea conditions and other arrangements. Going from west to east, the samples were collected from the Sila, Barakah and Jebel Dhannah areas. The collected samples were classified in three categories (as listed in Table 2.1): sediments along the shoreline (intertidal zone) of the Barakah area (B1-B16) referred to as “shore” samples; soil at 2000 meters inland in the Barakah area (S1-S24) referred to as “soil” samples and marine sediments at a distance of 500 to 7000 meters from the shore of Arabian Gulf and at a depth of 4 to 7 meters (M1-M18) referred to as marine “bottom” sediments samples. The bottom samples were collected also from Sila and Jebel Dhannah in addition to Barakah (Figure 2.1) and (Table 2.1).

A total of 58 samples had been collected for this study. 25 x 25 x 5 cm stainless steel box was used, for collecting 16 shore and 24 soil samples, and a grab sampler with expert divers were used for collecting 18 bottom sediments samples. The sediment samples were dried in oven at a temperature of 60°C and kept in labeled plastic bags for further use.

Table 2.1: List of samples collected with their label, coordinates and location

	Label	Coordinates		Label	Coordinates		Label	Coordinates
Shore Samples (sediments in Barakah)	B1	N 23 57 33.2 E 52 08 54.2	Soil Samples (soil in Barakah)	S1	N 23 56 22.1 E 52 08 54.0	Bottom samples (marine sediments M1-M5 in Sila, M6-M10 in Barakah and M11-M18 in Jebel Dhannah)	M1	N 24 04 12.7 E 51 47 37.2
	B2	N 23 57 38.9 E 52 10 10.2		S2	N 23 56 35.6 E 52 10 13.2		M2	N 24 00 41.6 E 51 53 22.2
	B3	N 23 57 41.2 E 52 11 19.1		S3	N 23 56 51.2 E 52 11 10.6		M3	N 24 03 06.5 E 51 56 37.8
	B4	N 23 57 43.7 E 52 11 46.1		S4	N 23 56 36.8 E 52 11 51.5		M4	N 24 02 46.8 E 52 01 08.0
	B5	N 23 58 50.5 E 52 16 0.5		S5	N 23 56 51.5 E 52 12 03.4		M5	N 24 01 47.5 E 52 04 42.4
	B6	N 23 58 55.2 E 52 16 27.8		S6	N 23 57 06.2 E 52 13 55.0		M6	N 23 58 36.9 E 52 09 22.1
	B7	N 23 59 05.7 E 52 17 03.6		S7	N 23 57 33.8 E 52 14 26.9		M7	N 23 58 12.3 E 52 11 22.3
	B8	N 23 59 35.7 E 52 18 17.5		S8	N 23 57 55.6 E 52 15 10.6		M8	N 23 58 19.9 E 52 12 32.5
	B9	N 24 00 01.4 E 52 19 13.7		S9	N 23 57 57.2 E 52 15 33.0		M9	N 23 59 09.5 E 52 15 40.5
	B10	N 24 00 48.9 E 52 19 52.8		S10	N 23 57 11.9 E 52 15 17.7		M10	N 24 01 06.4 E 52 18 23.8
	B11	N 24 01 23.6 E 52 20 54.1		S11	N 23 58 01.5 E 52 16 23.7		M11	N 24 02 59.3 E 52 20 37.8
	B12	N 24 02 04.1 E 52 22 02.3		S12	N 23 58 19.0 E 52 16 39.5		M12	N 24 03 38.0 E 52 23 35.9
	B13	N 24 02 20.4 E 52 22 34.5		S13	N 23 58 32.2 E 52 17 45.1		M13	N 24 06 20.1 E 52 25 44.9
	B14	N 24 02 41.5 E 52 23 33.3		S14	N 23 58 43.6 E 52 17 46.3		M14	N 24 08 41.2 E 52 27 34.2
	B15	N 24 02 54.2 E 52 24 29.4		S15	N 23 59 15.3 E 52 18 45.0		M15	N 24 08 00.9 E 52 30 55.9
	B16	N 24 03 16.3 E 52 25 24.6		S16	N 23 59 25.5 E 52 19 25.5		M16	N 24 09 25.9 E 52 32 55.6
		S17	N 23 59 45.8 E 52 19 41.3	M17	N 24 10 49.2 E 52 33 46.9			
		S18	N 23 59 08.5 E 52 12 24.6	M18	N 24 12 21.7 E 52 34 33.9			
		S19	N 24 00 21.0 E 52 20 39.7					
		S20	N 24 00 55.5 E 52 21 40.4					
		S21	N 24 01 11.0 E 52 22 46.8					
		S22	N 24 01 19.5 E 52 23 58.1					
		S23	N 24 01 37.4 E 52 25 06.4					

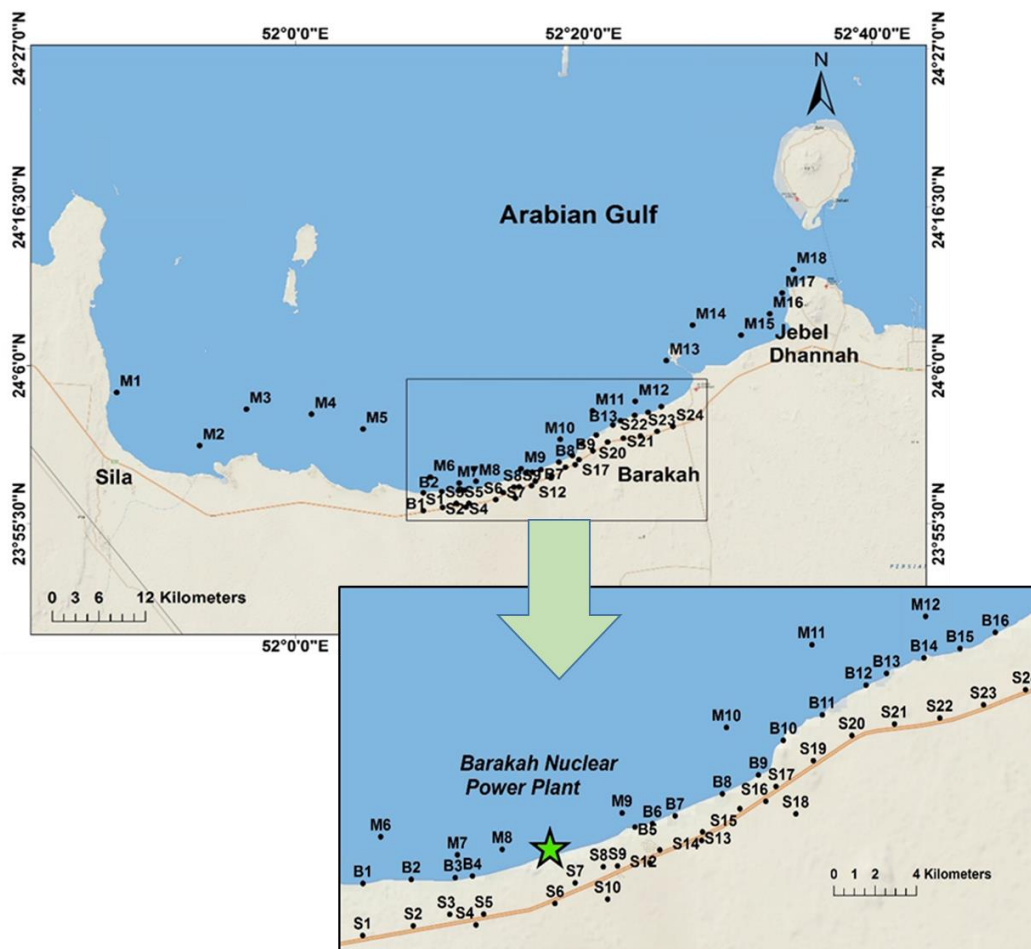


Figure 2.1: Locality map showing the location of sampling sites

2.2 Data Management

Data were organized in excel sheets and SPSS 13.0. A global positioning system (GPS) was used to record the locations of the samples. ArcGIS (version 10.1) was used to produce spatial distribution maps by interpolation method (kernel smoothing). Mapping was also performed to present a comprehensive spatial distribution illustration of all heavy metals, rare earth elements concentrations as well as radionuclides activities and hazard parameters over the studied area. In this study, maps will represent the 58 sampling locations and summarizes the distribution of the measured parameters. Such maps are helpful to build up and interpret the variability in concentrations in terms of geographical location (covering east and

west sides of the study area) and the different in depositional environments (onshore, coastal line and offshore).

2.3 Analytical Techniques

There are several methods and analytical techniques used in this study. Geochemical and mineralogical analysis techniques were used for the chemistry and mineralogy analyses of the samples, whereas, radiation methods were used for the radiological analysis. Analyses described and discussed in this section include:

- Inductively Coupled Plasma (ICP-AES) analysis.
- X-Ray Diffraction (XRD) spectrometry analysis.
- Sieve analysis and soil type diagram classification.
- Carbonate content analysis.
- High pure Germanium Gamma analysis.
- Alpha spectrometry analysis.

2.3.1 Inductively Coupled Plasma (ICP) Analysis

The inductively coupled plasma atomic emission spectroscopy (ICP-AES) analysis, for the determination of the heavy metals and REE content, was done in Bureau Veritas Minerals Laboratories (BVML) in Ankara, Turkey. Samples were prepared according to BVML guideline. Soil samples were dried and pulverize to $\geq 85\%$ passing $75 \mu\text{m}$. For the Rare Earth Elements and heavy metals, 0.5 g of soil samples is digested with a modified Aqua Regia solution using concentrated nitric acid and hydrochloric acid at a 1:3 ratio to extract the elements into solution. After

digestion, REE and heavy metals were measured by (ICP-AES) after fusion with lithium borate ($\text{LiBO}_2/\text{Li}_2\text{B}_4\text{O}_7$ flux). Crucibles are fused in a furnace. The cooled bead is dissolved in ACS grade nitric acid and analyzed by ICP-AES. Lost on ignition (LOI) is determined by igniting a sample split then measuring the weight loss. The instrumentation used for this analysis are Spectro Ciros Vision and/or Spectro Arcos and for AQ250 the instrumentation used is Perkin Elmer ELAN 9000. The error of analysis for both heavy metal and REE is <0.01 . Bureau Veritas Minerals Laboratories (BVML) QA/QC protocol includes a sample-prep blank carried through all stages of analysis as the first sample, a certified reference materials (STD DS10), a pulp duplicate to monitor analytical precision and two reagent blanks to measure background. More information about BVML guidelines for preparing and analyzing samples are available on the website www.bureauveritas.com.

Measurements of the rare earth elements and heavy metals concentrations by ICP analysis were carried out for the 40 soil samples (16 shore and 24 soil samples). The 18 bottom sediments were split into three sizes for each: coarse > 0.5 mm, medium > 0.25 mm and fine > 0.125 mm (Udden, 1914). Concentrations of rare earth elements and heavy metals were conducted for all three fractions of each of the 18 sample. This allow studying the relationship between the grain size and the concentrations of REE and heavy metals.

2.3.2 X-Ray Diffraction (XRD) Spectrometry Analysis

All the collected samples (58 samples) were prepared for XRD analysis in order to determine qualitatively the mineral composition of the collected sediments and soils. This analysis was carried out in Egypt in the Central Egyptian Labs. A

Philips X-ray diffractometer model PW/1840 was used. Samples were grinded to fine powder then pressed into steel rings to get a mechanical stable sample and finally processed by the X-ray diffractometer.

2.3.3 Grain Size Analysis

The main purpose of the Sieve analysis of beach soil is to determine and understand their granulometric characteristics and textural properties. There are several techniques for the size analysis of soil. The most widely used is the sieve analysis, which is mostly used for sands and gravels. All 58 samples were analyzed for sieve analysis using the American Society for Testing and Materials (ASTM) Sieves, part of the samples were dried using dry oven while others used as reference samples. 200 g representing the original dry sample was taken using john splitter and poured in a set of sieves arranged from coarse to fine as follow (4,2,1,0.5,0.25,0.125,0.062 mm and pan). The set of sieves were fixed on a mechanical shaker and were shacked for about 15 minutes. The device used is Fritsch mechanical shaker with ASTM Sieves. The weight of each retained fraction was recorded in a form sheet used for this purpose using a sensitive balance. The weight percentages and cumulative weight percentages were calculated for all samples. All samples were analyzed at the Geology Department of UAE University.

The weight percentages and cumulative weight percentages were calculated for each sieve using the following equation:

$$Weight \% = \frac{\frac{W. retained}{W. total}}{2} * 100$$

Where the w. retained is the sample weight recorded for each sieves while w. total is the total initial weight (200g). The Cumulative weight % for the 1st =1st Wt. %, 2ndWt. % = the 1st + 2nd, 3rd Wt. % =Sum. of 1st + 2nd + 3rdetc.

2.3.4 Carbonate Content Analysis

Measuring the carbonate content of the collected samples were carried at the UAEU Geology lab. For the carbonate content analysis, 10% hydrochloric acid (HCl) is added to a known weight of sediment in glass beaker. The beaker should be placed on a hot plate and heated to 80°C until effervescence stops and a ph of 3.5 to 4 is reached, a ph paper can be used as indicator that changes from yellow in a neutral solution to orange at ph 3.1 to 4.4 and red below ph 3.1. Decantation for the solution should be done and this step can be repeated three times until the residual sand is properly washed. A known weighted filter paper is used to hold the residue the weight of the dried filter paper is used to calculate the carbonate content by using the difference between the initial and final sample weight divided by the initial sample weight times 100%.

2.3.5 High Pure Germanium Gamma Analysis

2.3.5.1 Sample Preparation

All collected samples were prepared for Non-Destructive analysis using High-pure Germanium Detector (HPGe). Sample preparation started with drying the sediments and soil in drying oven at 60°C until the moisture is completely removed. The sample were homogenized and sieved using 2 mm sieve (IAEA, 1989). Marinilli beakers of a volume of one liter were used to hold the samples, density of the samples were measured. Marinilli beakers were sealed with adhesive tape and left

for at least 4 weeks to achieve secular equilibrium between ^{226}Ra (daughter of ^{238}U) and their corresponding daughter (NEA-OECD, 1979). HPGe detector was used since it is a sensitive and efficient device as well as it has been widely used in determining activity of radionuclides. This analysis was performed at the UAEU in department of physics with a relative efficiency 40%.

2.3.5.2 High Pure Germanium detector

2.3.5.2.1 Description of the system

Gamma-ray spectrometry is one of the most accepted and widely used techniques for the detection and analysis of radioactive isotopes. It is a popular technique being used for low-background radio analysis. Three types of gamma ray detectors can be used for gamma analysis: thallium doped sodium iodide crystal NaI(Tl) scintillation detector, lithium drifted crystal of purified germanium detector, and High-Pur Germanium (HPGe) detector (Hansen, 1971). A typical HPGe gamma-ray spectrometry system is composed of: a detector (Ge) with a lead shielding, to reduce the background, high voltage power supply, electronics for signal processing (preamplifier, amplifier, multichannel analyzer), computer and dedicated software. The spectrometric system records, stores and processes the gamma-ray spectrum of the analyzed sample, using validated computer software packages (Ortec gammavision).

2.3.5.2.2 Energy calibration

The main principle of calibrating a gamma spectrometer is to relate the total number of counts in the full energy peak to the gamma ray intensity or the activity concentrations of source. The calibration of a spectrometric gamma system involves three main aspects (Figure 2.2): (i) The energy as a function of the number of the

channels; (ii) FWHM (Full Width of Half Maximum) as a function of the number of the channels; (iii) The efficiency as a function of the energy correlated with the acquisition geometry of the radiation spectrum. Energy calibration is in simple words, setting up a relation between the gamma ray energy and the analyzer channel number. X-axis (channels) of the spectrum will be calibrated in units of energy such as keV. It will ensure peaks in the spectrum appear at the correct energies. Energy calibration is done by using the known spectra generated by what is called standard source that have isolated peaks. In the present study, a mixed of 12 radionuclides as shown in Table 2.2, was used for energy calibration. There were also considered as the energetic lines for ^{137}Cs of 661.6 keV and ^{60}Co of 1173 and 1332 keV for a more accurate energy calibration in the work energy interval. The program that is used in the present study (Ortec) calibrate the peak width which is called full width at half maximum (FWHM) as part of the energy calibration (channel to energy calibration).

2.3.5.2.3 Efficiency calibration

After matching the gamma ray energies with the analyzer channel number, the activity concentrations of the radionuclides should be quantified. This is done by efficiency calibration, which calculates the detection efficiency of HPGe detector system as function of energy. The detector was calibrated for absolute efficiency using radioactive standard sources with gamma-ray emissions covering a wide energy range (Table 2.2).

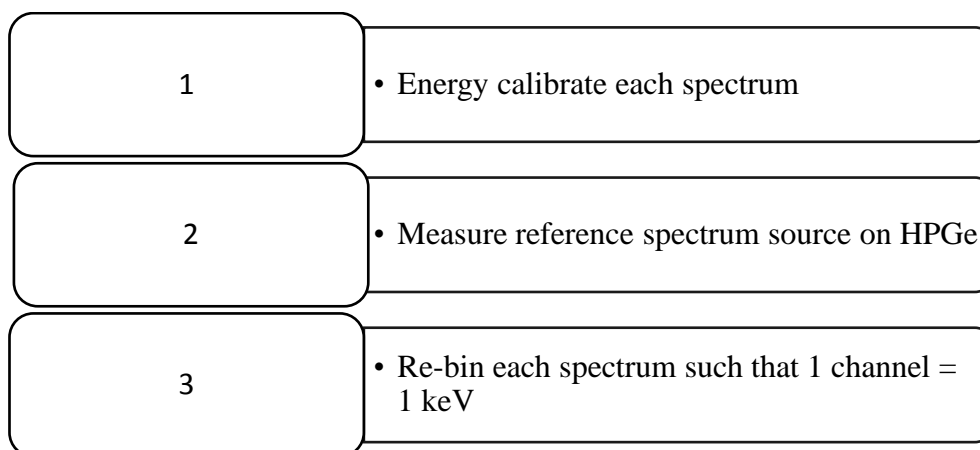


Figure 2.2: Flow chart showing how a standard spectrum was obtained

Table 2.2: Radionuclides present in the standard source

Radionuclides	Energy lines (keV)	Activity (Bq/Kg) as in certificate	Net count rate (cps)	live time	Half life days
²⁴¹ Am	59.54	4.331	73.95	83628.86	157800
¹⁰⁹ Cd	88.03	13.62	15.54	83628.86	462.6
⁵⁷ Co	122.07	1.094	17	83628.86	271.26
⁵⁷ Co	136.47	1.094	2.08	83628.86	271.26
¹³⁹ Ce	165.85	1.314	5.59	83628.86	137.5
²⁰³ Hg	279.17	2.242	0.11	83628.86	46.72
¹¹³ Sn	391.69	3.677	4.54	83628.86	115.1
⁸⁵ Sr	514	4.402	1.04	83628.86	64.78
¹³⁷ Cs	661.66	2.483	36.28	83628.86	11019
⁶⁰ Co	1173.24	2.497	23.48	83628.86	1925.4
⁶⁰ Co	1332.4	2.497	21.45	83628.86	1925.4
⁸⁸ Y	1836.01	4.916	2.2	83628.86	106.6

Background gamma ray measurement were conducted using empty Marinilli beaker by acquiring spectra for 24 hours. The need for measuring the background gamma ray is because in most locations there is a considerable gamma ray flux from natural background (NORM) and cosmic nuclides, which can mask the material of the interest (Keyser and Twomey, 2008). All of these contribute to change the detector total count rates unrelated to the nuclides of interest and can hide considerable quantities of material. Thus, background gamma ray measurement was done and the spectrum were corrected to the background.

2.3.5.2.4 Calculation of radionuclides activity concentrations

Count rates for selected energy lines (Table 2.3 and Figure 2.3) are used to estimate the activity concentrations of U^{238} (^{226}Ra), ^{232}Th and ^{40}K . ^{238}U can be determined by gamma spectrometry via its gamma emitting daughter ^{226}Ra in assumptions that secular equilibrium between ^{226}Ra (daughter of ^{238}U) and its corresponding daughter is achieved. As shown in Table 2.3 the energy lines 352, 609, 1120 and 1764 keV were used to estimate the activity concentration of ^{226}Ra , while ^{232}Th is estimated through its gamma emitting daughter using each of 238, 583 and 911 keV energy lines (EML, 1979). Furthermore lines overlapping with others were not used such as 186 keV line (doublet due to lines $^{238}U/^{235}U$). There was no peak in the energy line associated for ^{137}Cs in all samples (example is Figure 2.3), thus no calculation was done for this anthropogenic radionuclide. The activity concentrations of both U^{238} (^{226}Ra) and ^{232}Th are derived from the spectrum (using daughter's energy lines) through calculation based on that the radioactive equilibrium is exists. Since ^{40}K is a direct gamma ray emitter, its energy line can be

measured directly. Table 2.3 shows the energy lines of selected radionuclides and daughters.

The Activity concentrations of radionuclides are estimated through the following equation (Beretka and Mathew, 1985) and (El Assaly, 1981):

$$A = \frac{NP}{t * Br * \varepsilon(E) * M}$$

A is activity concentration in Bq/kg, NP is the net peak, Br is the emission probability of the gamma ray produced at the full energy peak, t is the counting time in second, ε is the full energy peak efficiency and M is the sample mass.

The method for determining the efficiency for the radionuclides of interest (Table 2.3) involves three steps as shown in Figure 2.4. The first step involves the measurement of the experimental efficiency using standard radionuclide source with standardized activity concentrations (Table 2.2) using the above mentioned equation. The second step entails constructing the efficiency fitting curve (Figure 2.5) for the given set of experimental data (energy, efficiency). Finally, deriving the curve equation to estimate the efficiency ε for the different radionuclides. Estimated efficiency ε is presented in Table 2.3 along with the emission probability of each radionuclide.

Table 2.3: Energy lines and their associated radionuclides efficiency and emission probability

Nuclides	Energy lines KeV	Efficiency	Emission probabilities
----------	---------------------	------------	------------------------

U^{238} (^{226}Ra)
series

Pb^{214}	351	0.02847	0.353
Bi^{214}	609	0.01881	0.452
Bi^{214}	1120	0.01152	0.148
Bi^{214}	1764	0.00813	0.152

Th^{232}
series

Pb^{212}	238	0.03768	0.436
Tl^{208}	583	0.01946	0.306
Ac^{228}	911	0.01364	0.266

K^{40}

K^{40}	1460	0.00932	0.1066
----------	------	---------	--------

Cs^{137}

Cs^{137}	661.1	0.01764	0.8499
------------	-------	---------	--------

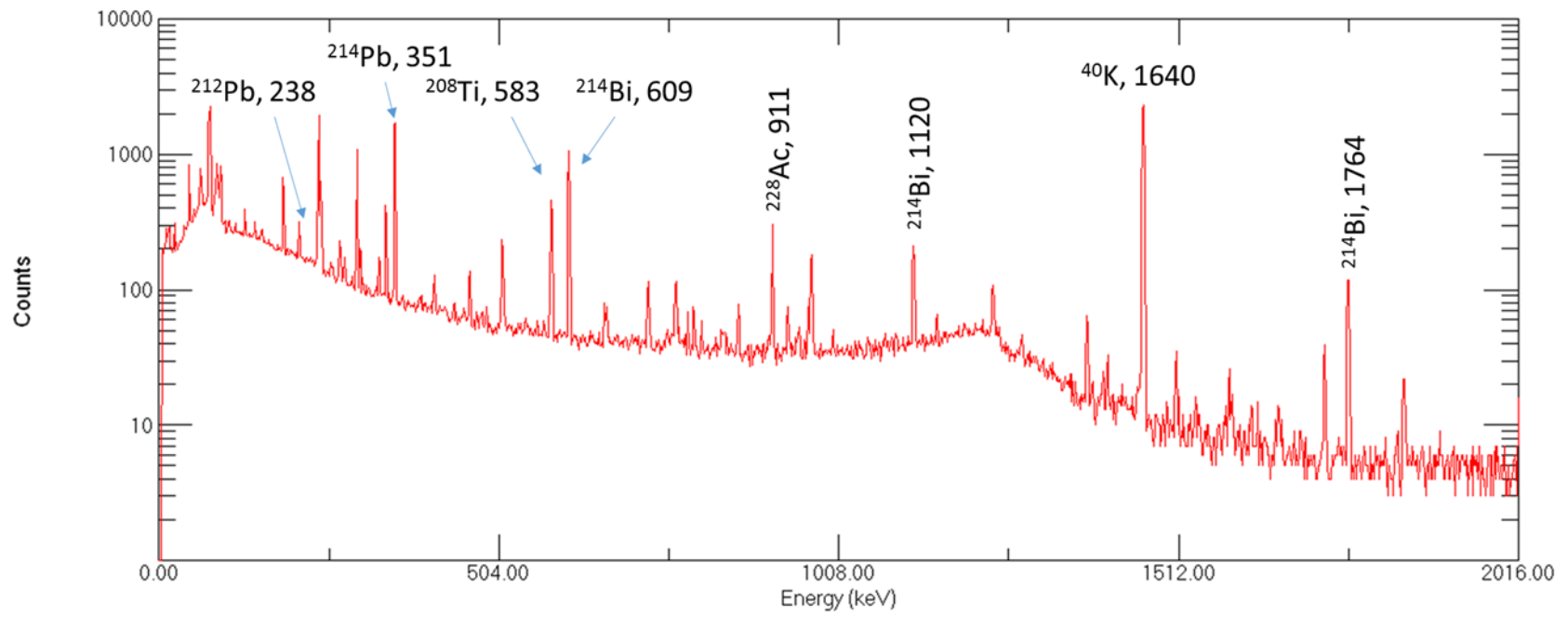


Figure 2.3: Gamma emission spectrum of soil sample (S11) showing the lines used

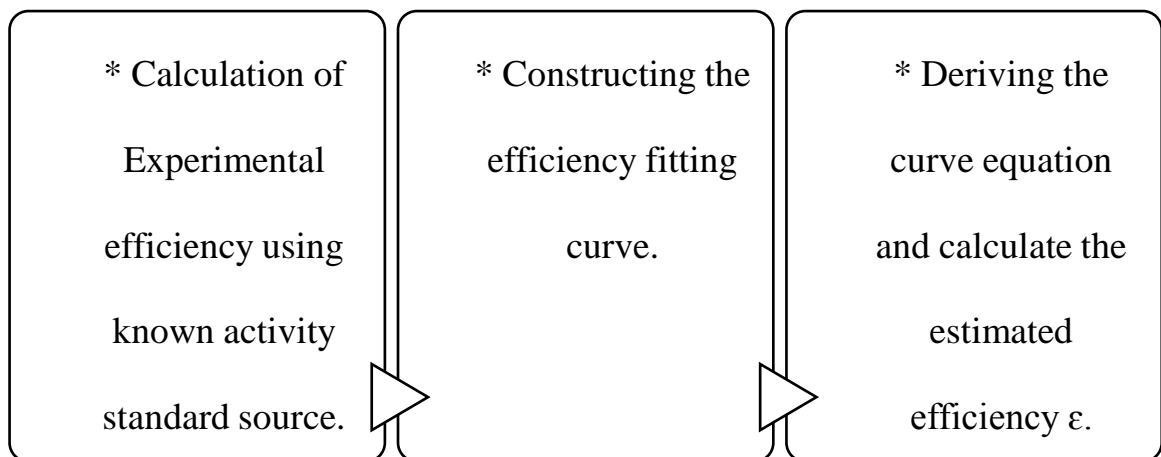


Figure 2.4: Flow chart showing how a standard spectrum was obtained

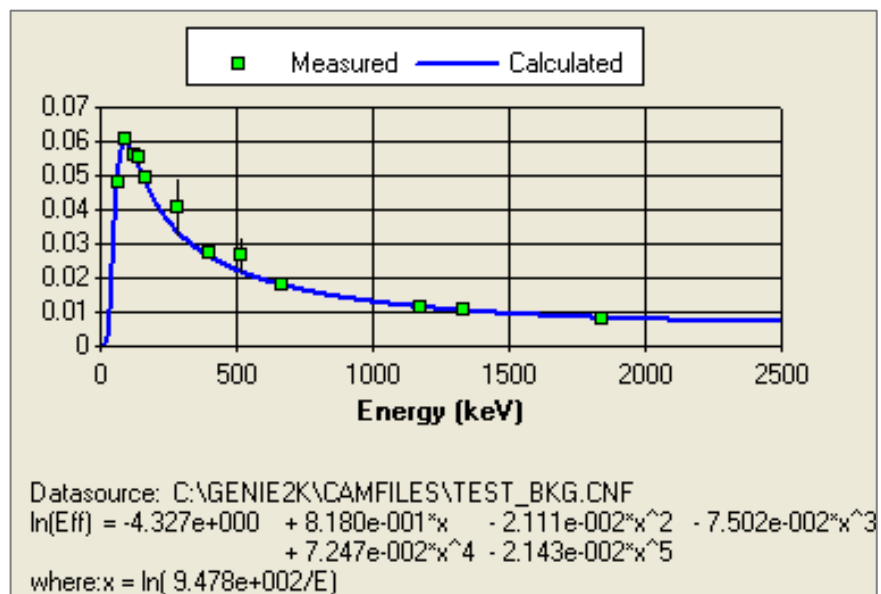


Figure 2.5: Source efficiency as a function of energy

2.3.5.2.5 The Radium Equivalent activity concentrations and Absorbed Dose Rates

Radium equivalent activity is used to assess the hazards associated with materials that contain U^{238} (^{226}Ra), ^{232}Th and ^{40}K in Bq/kg and is mathematically defined by (Beretka and Mathew, 1985) and (Mujahid et al., 2008).

$$\text{Rad eq} \left(\frac{\text{Bq}}{\text{kg}} \right) = A(\text{Ra}) + 1.43 A(\text{Th}) + 0.077A(\text{K})$$

Where A is the activity concentrations.

Since radioactivity from radionuclides is not uniform and varies from place to another, radioactivity has been defined worldwide in terms of radium equivalent activity in Bq/kg (Al Jundi, 2002) which allows comparing different places with the world allowed value for radium equivalent activity which is 370 Bq/kg. United Nations Scientific Committee on the Effect of Atomic Radiation (UNSCEAR) (2000) provided guidelines to measure the absorbed dose rates (D) which are measured by nGy.h^{-1} due to gamma radiations in air at 1m above the ground surface for the uniform distribution of the naturally occurring radionuclides (U^{238} (^{226}Ra), ^{232}Th and ^{40}K). The previous guidelines (UNSCEAR, 2000) were used to estimate the absorbed dose rates.

$$\text{Abs. Dose (nGy/h)} = 0.604 A(\text{Th}) + 0.462 A(\text{U}) + 0.0417 A(\text{K})$$

2.3.6 Alpha Spectrometry

Ten sediment samples were analyzed using alpha spectrometry in nuclear and radiological regulatory authority in Cairo, Egypt. Generally, Uranium is separated by Eichrom UTEVA resin prior to elector deposition on stainless steel disc then

measurement by alpha spectrometry as shown by a standard alpha spectrum in Figure 2.6. A detailed analytical procedure by Eichrom is available in http://www.eichrom.com/docs/methods/pdf/acs07-15_u-soil.pdf. Figure 2.7 shows a schematic diagram of the radiochemical separation procedure of Uranium. Uranium isotopes (^{234}U , ^{235}U and ^{238}U) were extracted from the soil digestion solution by coprecipitation with calcium phosphate, separated from other actinides and purified using extraction chromatography followed by the electrodeposition on a stainless steel disc and counted using alpha spectrometry.

To minimize the experimental error, quality assurance were achieved by analyzing a known activity samples from the international Atomic Agency and by using a DDW (Distilled and Deionized Water) with a known activity of ^{232}U and then calculate the theoretical count rate of ^{232}U .

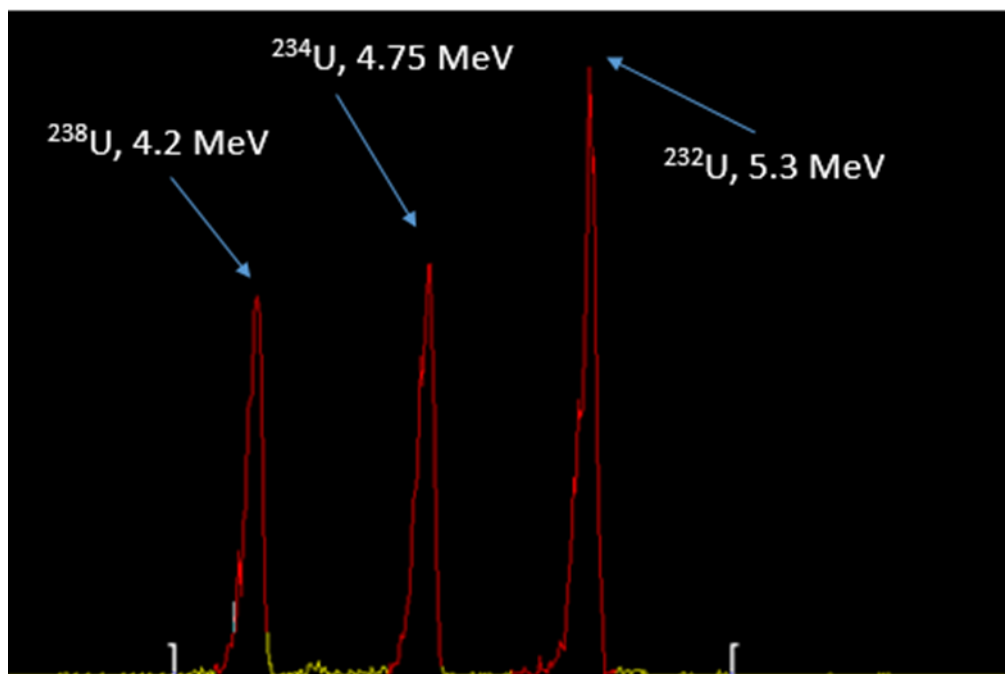


Figure 2.6: An alpha spectrum showing the energy lines of U isotopes, the horizontal axis is the energy in Mev while the vertical axis is the counts/channel

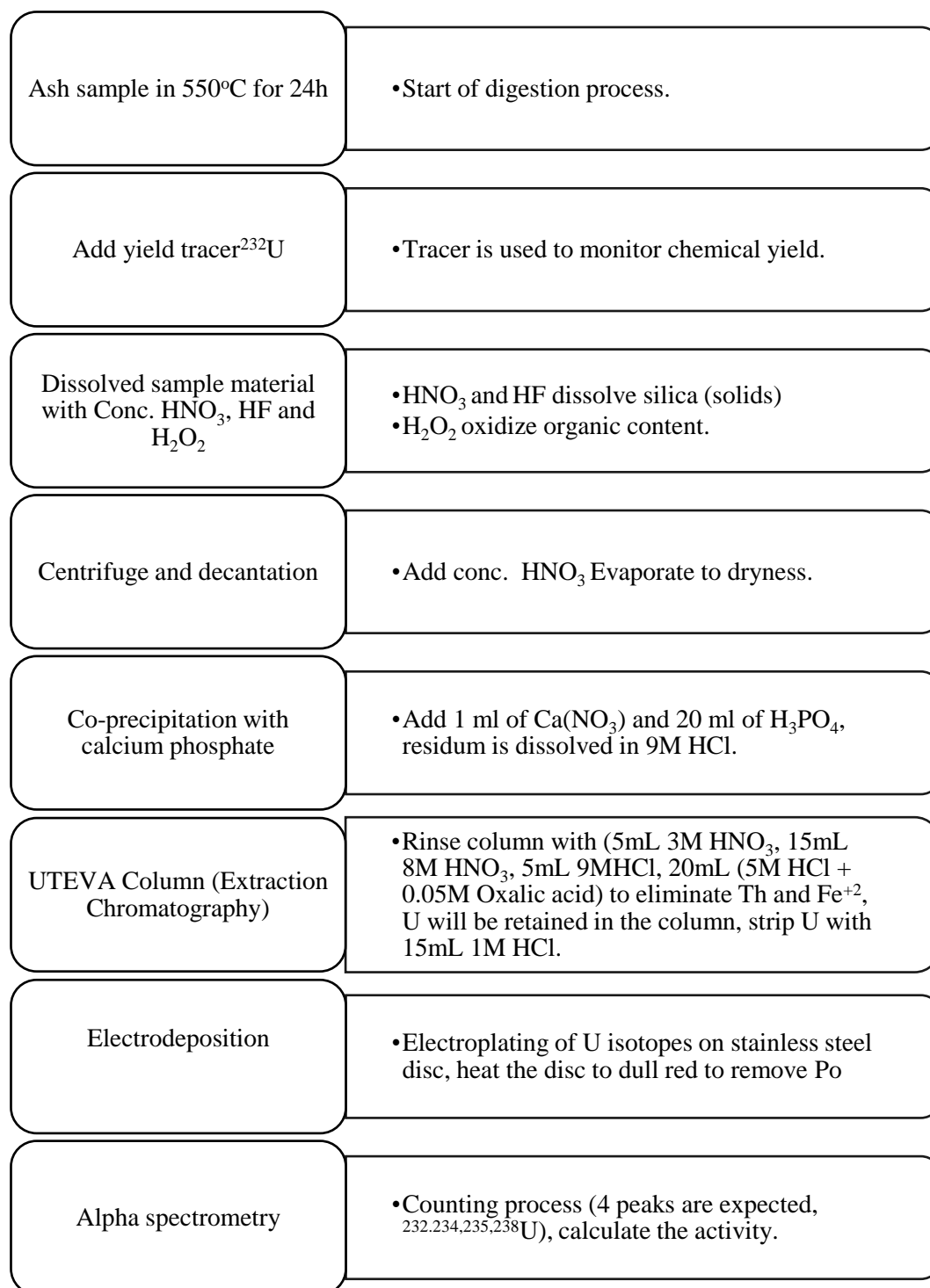


Figure 2.7: Schematic procedure of soil digestion and Uranium separation and measurement

Chapter 3: Results

3.1 Grain-Size Analysis

Grain size analysis was carried out to identify the depositional environment. In addition the grain size mean and cumulative weight were plotted and used to interpret the grain-size frequency distribution in the studied soil, shore and bottom samples. Calculation of the grain-size statistical parameters (M_z , σ_I , S_{ki} and KG) were done through applying the equations of Folk and Ward (1957).

3.1.1 Mean Size (M_z)

The parameter reflects the overall average size of the samples, which is influenced by the beach samples source, mode of transportation and environment of deposition (Udden 1914; Folk, 1966). The base two logarithmic (ϕ) scale is one useful and commonly used way to represent grain size information for a sediment distribution. The measured mean size values of soil samples (Tables 3.1 & 3.4) range between 0.23 mm (fine sand) to 1.07 mm (very coarse sand) with an average value of 0.49 mm (medium sand). The values of mean size in the shore samples (Tables 3.2 & 3.4) range between 0.22 mm (fine sand) to 0.5 mm (medium sand) with an average value of 0.35 mm (medium sand). On the other hand, the bottom sediments of the studied area show that the mean size (Table 3.3 & 3.4) ranges from 0.33 mm (medium sand) to 1.71 mm (very coarse sand) with an average value of 0.56 mm (coarse sand).

3.1.2 Inclusive Standard Deviation (σI)

The inclusive standard deviation is a measure of the uniformity of grain-size distribution within the beach samples. It depends on the size range in the source rock, extent of weathering distance of transportation and the energy variation of the depositing medium (Folk and Ward, 1957; Amaral and Prayor, 1977). The average standard deviations for the soil and shore samples (Tables 3.1, 3.2 & 3.4) are in the moderately sorted group with mean values of 0.82 ϕ and 0.98 ϕ , respectively, and that is reflected by the narrow range of grain sizes. For the bottom sediments (Tables 3.3 & 3.4), the range of the grain sizes is wide, as also shown from the mean value of standard deviation which is 1.08 ϕ , suggesting a poor sorting of the grains.

3.1.3 Skewness (SKI)

This parameter describes the abnormality of grain-size distribution and represents the most sensitive parameters of geologic processes (Folk, 1966). The mean size values in the soil, shore and bottom samples (Table 3.4) are on average -0.32, -0.11 and -0.17, respectively. Both average skewness values of shore and bottom samples fall into the coarse skewed class while average skewness values of soil samples fall into the very coarse skewed class. The skewness values in the soil, shore and bottom samples range from -0.63 to 0.19, -3.5 to 0.35 and from -0.67 to 0.6, respectively. The average skewness values in all cases are negative, meaning that the data are graphically skewed to the positive phi values.

3.1.4 Kurtosis (KG)

This parameter measures the normality of grain size distribution using the ratio of sorting in the central part of the curve to that in its extremities (Folk, 1966).

The soil samples show kurtosis values (Tables 3.1 & 3.4) ranging from 0.77 to 2.81 with an average value of 1.09, which represents leptokurtic class. The minimum and maximum kurtosis values for shore samples (Tables 3.2 & 3.4) is 0.50 and 1.52 with an average value of 1.04, which represents mesokurtic class. The kurtosis value of the bottom sediment samples (Tables 3.3 & 3.4) ranges between 0.74 to 1.36 with an average value of 1.09 (mesokurtic). The kurtosis values for the shore and bottom samples suggest that the peak of the data distribution is rather flat. The data distribution in the soil is light tailed.

Table 3.1: Statistical parameters and Phi percentiles for the analyzed soil samples

S	Phi percentile							Statistical Parameters			
	Φ_5	Φ_{16}	Φ_{25}	Φ_{50}	Φ_{75}	Φ_{84}	Φ_{95}	$M_Z(\Phi)$	$\sigma_1(\Phi)$	SK_1	KG
S1	-5.5	-2	-0.3	1.3	2	2.2	2.9	0.5	-0.34	-0.6	1.5
S2	-0.4	0.4	0.7	1.3	1.9	2.1	2.6	1.27	0.96	-0.1	1.03
S3	-1.6	-0.5	0.2	1.1	1.7	2	2.6	0.87	0.53	-0.28	1.15
S4	-1	0	0.6	1.3	1.7	1.9	2.4	1.07	0.69	-0.36	1.27
S5	0.5	1.3	1.5	1.9	2.3	2.5	2.8	1.9	1.45	-0.11	1.18
S6	-2.4	-0.6	0.3	1.2	1.7	1.9	2.4	0.83	0.33	-0.47	1.4
S7	-2.5	0.5	1.7	2.5	2.7	3	3.5	2	1.02	-0.63	2.46
S8	-3.5	-1.7	-0.6	1	1.7	1.9	2.5	0.4	-0.1	-0.5	1.07
S9	-0.7	1.1	2	2.4	2.6	2.8	3.4	2.1	1.39	-0.52	2.81
S10	-3.9	-1.4	0	1.4	2.2	2.4	3.1	0.8	0.13	-0.47	1.3
S11	-3.7	-2	-1.3	0.6	1.8	2.1	2.5	0.23	-0.16	-0.33	0.82
S12	-1.8	-0.4	0.3	1	1.8	2.1	2.8	0.9	0.58	-0.16	1.26
S13	-3.4	-1.4	-0.3	1.2	2	2.3	2.9	0.7	0.15	-0.43	1.12
S14	-1.3	-0.4	0.1	0.8	1.8	2.1	3.1	0.83	1.29	0.04	1.06
S15	-2.6	-1.5	-0.9	0.2	1.2	1.4	2	0.03	1.42	-0.2	0.9
S16	-4	-2.6	-1.3	1	2.3	2.6	3.2	0.33	-0.12	-0.39	0.82
S17	-4	-2	-1	1	1.7	1.9	2.4	0.3	1.94	-0.55	0.97
S18	-9.5	-0.5	0.4	1.6	2.3	2.6	3.4	1.23	-0.4	-0.54	2.8
S19	-4.2	-0.4	1.1	1.5	2.2	2.4	3.3	1.16	1.83	-0.44	2.8
S20	-3.2	-2	-1.5	-0.4	1.7	2.1	2.8	-0.1	1.93	0.14	0.77
S21	-1.3	1.4	1.6	2	2.4	2.6	3	2	0.95	-0.27	2.21
S22	-0.3	0.9	1.5	2.3	2.7	3	3.4	2.06	1.08	-0.37	1.26
S23	0.3	0.6	0.9	1.6	2.7	3	3.6	1.73	1.1	0.19	1.63
S24	-3.6	-1.3	0	1.3	2.3	2.7	3.4	1.35	2.06	-0.35	1.24
Min	-9.5	-2.6	-1.5	-0.4	1.2	1.4	2	-0.1	-0.4	-0.63	0.77
Max	0.5	1.4	2	2.5	2.7	3	3.6	2.1	2.06	0.19	2.81
Ave.	-2.65	-0.60	0.24	1.30	2.06	2.32	2.92	1.02	0.82	-0.32	1.45

Table 3.2: Statistical parameters and Phi percentiles for the analyzed shore samples

S	Phi percentile							Statistical Parameters			
	Φ_5	Φ_{16}	Φ_{25}	Φ_{50}	Φ_{75}	Φ_{84}	Φ_{95}	$M_Z(\Phi)$	$\sigma_1(\Phi)$	SK_1	KG
B1	-0.7	0.3	0.8	1.4	1.8	2	2.4	1.23	0.83	-0.19	1.27
B2	0.5	1	1.3	1.7	2.4	2.5	3	1.73	1.41	0.05	0.96
B3	-0.9	0	0.5	1.5	2.3	2.6	3.2	1.4	1	-0.16	0.93
B4	0.7	1.4	1.7	2.2	2.6	2.7	3.2	2.1	1.62	-0.22	1.14
B5	-0.4	0.2	0.4	1	1.6	1.9	2.4	1	0.82	0.03	0.96
B6	0.7	1.1	1.4	1.8	2.2	2.4	2.8	1.77	1.41	-0.06	1.08
B7	0.2	0.5	0.6	0.9	1.5	1.7	2.4	1.03	0.63	0.35	1
B8	0.3	0.9	1.2	1.6	2	2.2	2.6	1.56	0.67	-0.1	1.18
B9	-0.9	-0.4	0	1.5	2.2	2.4	2.7	1.16	1.25	-0.35	0.67
B10	-0.4	0.5	1	1.9	2.4	2.6	3	1.66	1.04	-0.34	0.99
B11	0.1	0.7	1.1	1.4	1.8	2	2.4	1.36	0.67	-0.1	1.35
B12	0	0.9	1.5	1.8	2.2	2.4	2.6	1.7	0.77	-0.29	1.52
B13	-0.3	0.5	1	1.5	2	2.3	2.7	1.43	0.9	-0.16	1.23
B14	-0.4	0.2	0.8	1.6	2.3	2.6	3.2	1.46	1.23	-0.14	0.98
B15	0.9	1.4	1.6	2.2	2.7	2.8	3.4	2.16	0.75	-0.05	0.93
B16	0.5	0.9	1.3	1.6	2.1	2.3	2.7	1.6	0.68	0	0.5
Min	-0.9	-0.4	0	0.9	1.5	1.7	2.4	1	0.63	-0.35	0.5
Max	0.9	1.4	1.7	2.2	2.7	2.8	3.4	2.16	1.62	0.35	1.52
Ave.	-0.01	0.63	1.01	1.60	2.13	2.34	2.79	1.52	0.98	-0.11	1.04

Table 3.3: Statistical parameters and Phi percentiles for the analyzed bottom sediments

S	Phi percentile							Statistical Parameters			
	Φ_5	Φ_{16}	Φ_{25}	Φ_{50}	Φ_{75}	Φ_{84}	Φ_{95}	$M_z(\Phi)$	$\sigma_1(\Phi)$	SK_1	KG
M1	-2.7	-1.3	-0.5	1	2	3	3.7	0.9	2.05	-0.05	1.05
M2	-1	-0.4	0	0.4	1	1.3	2	0.43	0.88	0.06	1.23
M3	-0.5	0.3	0.5	1	1.5	1.7	2.3	1	0.77	-0.04	1.15
M4	-1.8	-1.5	-1.2	-0.7	-0.2	-0.1	0.4	-0.77	0.68	-0.07	0.9
M5	-1.5	-0.3	0.2	1	1.8	2.2	2.6	0.97	1.25	-0.13	1.05
M6	-0.7	-0.4	0	0.5	1	1.3	1.7	0.47	0.79	-0.03	0.98
M7	-0.8	0.5	1	1.5	2.3	2.5	3	1.5	1.08	-0.11	1.2
M8	-1	0.5	1	1.6	2.5	2.7	3.5	1.6	1.23	-0.08	1.23
M9	-0.7	0	0.5	1.2	1.7	2	2.5	1.06	0.98	-0.19	1.1
M10	-1	-0.5	-0.3	0.3	0.6	1	1.7	0.27	0.79	-0.01	1.23
M11	-0.6	0	0.3	0.6	1	1.2	1.5	0.6	0.62	-0.57	1.23
M12	-1.3	-0.5	0	0.7	1.5	1.7	2.4	0.63	1.11	-0.53	1.01
M13	-1.1	0	0.4	1.2	1.8	2	2.5	1.07	1.05	-0.24	1.06
M14	-0.3	0.4	0.6	1.3	1.7	2	2.5	1.23	0.82	-0.13	1.04
M15	-0.5	0	0.4	1	1.6	1.8	2.4	0.93	0.89	-0.08	0.99
M16	-1	0	0.3	0.7	1.2	1.5	2	0.73	0.83	-0.04	1.36
M17	-3.5	-2	-1	2	2.6	2.9	3	0.97	2.21	-0.67	0.74
M18	-1.4	0	0.5	1.5	2.3	2.6	3.3	1.37	1.36	-0.2	1.07
Min	-3.5	-2	-1.2	-0.7	-0.2	-0.1	0.4	-0.77	0.62	-0.67	0.74
Max	-0.3	0.5	1	2	2.6	3	3.7	1.6	2.21	0.06	1.36
Ave.	-1.19	-0.29	0.15	0.93	1.55	1.85	2.39	0.83	1.08	-0.17	1.09

Table 3.4: Statistical summary of grain size parameters in studied samples

		$M_z(mm)$	$M_z(\Phi)$	$\sigma_1(\Phi)$	Classification	Sk_1	Classification	KG	Classification
					according to $\sigma_1(\Phi)$		according to Sk_1		according to KG
Soil	Min	0.23	-0.1	-0.4		-0.63		0.77	
	Max	1.07	2.1	2.06		0.19		2.81	
	Average	0.49	1.02	0.82	Moderately sorted	-0.32	Very coarse skewed	1.45	Leptokurtic
Shore	Min	0.22	1	0.63		-0.35		0.5	
	Max	0.5	2.16	1.62		0.35		1.52	
	Average	0.35	1.52	0.98	Moderately sorted	-0.11	Coarse skewed	1.04	Mesokurtic
Bottom	Min	0.33	-0.77	0.62		-0.67		0.74	
	Max	1.71	1.6	2.21		0.06		1.36	
	Average	0.56	0.83	1.08	Poorly sorted	-0.17	Coarse skewed	1.09	Mesokurtic

3.1.5 Determination of the Mechanical and Environments of Deposition

According to Sahu (1964), the statistical method of analysis of the sediments to interpret the variations in the energy and fluidity factors seems to have excellent correlation with the different processes and environment of deposition. The application of Sahu's (1964) discriminate functions will be only applied to shore and soil samples since applying it to the bottom sediments according to Ali et al. (1987) resulted in 70.6% of the analyses being compatible with the field observations. Linear discriminate function (LDF) analysis of the shore and soil samples was carried out using the following equations:

Aeolian/beach:

$$Y1 = -3.5688 Mz + 3.7016 \sigma_1 - 230766 SK1 + 3.1135 KG$$

If Y is >-2.7411 , the environment is 'Beach' but if Y is <-2.7411 , the environment is 'Aeolian'.

Beach/shallow agitated water:

$$Y2 = 15.6534 Mz + 65.7091 \sigma_1 + 18.1071 SK1 + 18.5043 KG$$

If Y is <63.3650 , the environment is 'Beach' but if Y is >63.3650 , the environment is 'Shallow marine'.

Shallow marine/fluvial environment:

$$Y3 = 0.2852 Mz - 8.7604 \sigma_1 - 4.8932 SK1 + 0.0482 KG$$

If Y is >-7.4190 , the environment is 'Shallow marine' but if Y is <-7.4190 , the environment is 'Fluvial'.

After applying the above equations on the shore and soil sample parameters, results are shown in Table 3.5.

Table 3.5: discriminate function of grain size parameters in soil and shore samples

S		Y1	Y2	Y3	S		Y1	Y2	Y3
soil	S1	2.87	2.38	6.13	shore	B1	3.03	93.85	-5.93
	S2	2.44	100.21	-7.51		B2	1.93	138.4	-12.06
	S3	3.02	64.65	-2.97		B3	1.93	101.94	-7.53
	S4	3.44	79.07	-3.92		B4	2.51	156.43	-12.46
	S5	2.49	144.86	-11.57		B5	2.39	87.84	-7
	S6	3.59	52.07	-0.29		B6	2.39	139.25	-11.5
	S7	5.61	132.44	-5.16		B7	1.04	82.36	-6.89
	S8	2.57	10.44	3.49		B8	0.79	88.47	-4.88
	S9	7.48	166.79	-8.9		B9	3.3	106.35	-8.87
	S10	2.65	36.61	1.45		B10	1.71	106.48	-6.93
	S11	1.83	2.28	3.12		B11	2.04	88.48	-4.93
	S12	3.19	72.62	-3.98		B12	2.12	100.08	-4.77
	S13	2.44	33.75	1.04		B13	2.39	101.39	-6.63
	S14	5.03	118.1	-11.21		B14	2.68	119.27	-9.63
	S15	8.37	106.81	-11.41		B15	-1.93	99.4	-5.66
	S16	1.74	5.39	3.09		B16	-1.64	78.98	-5.48
	S17	10.27	140.16	-14.17					
	S18	3.97	35	6.63					
	S19	12.27	182.25	-13.41					
	S20	9.61	142.04	-17.58					
	S21	3.82	129.74	-6.32					
	S22	1.34	119.83	-7					
	S23	2.58	132.96	-9.99					
	S24	7.39	173.1	-15.89					

3.2 Mineralogy

The mineralogical composition of the studied shore, soil and bottom samples was obtained by XRD technique. Few samples were excluded to minimize the number of analyzed samples especially where they are close to each other and no changes in the mineralogy is expected. The results obtained are given in Tables 3.6, 3.7 and 3.8.

3.2.1 Soil Samples Mineralogy

Soil samples exhibit some variations among the selected sites as shown in Table 3.6, however quartz is the only major mineral in all soil samples except S13 and S20. Ca-Na feldspars are the major minerals in S13 and S20, respectively. K-feldspars, calcite, Ca-Na feldspars, halite, aragonite and gypsum are moderate mineral found in soil samples. It appears that some of the moderate minerals are also found as a minor in some soil samples with few appearances of some minor minerals such as basanite and dolomite.

3.2.2 Shore Samples Mineralogy

The mineralogical composition of the 12 shore samples show that quartz and aragonite are the dominant primary minerals in almost all sites (Table 3.7), with little exception in few samples. In samples B13, Ca-Na feldspars occurs as a major mineral, whereas magnesite is a minor in B6, B13, B15 and B16 and a major mineral in B9. Some minor minerals such as dolomite is found in B5. Moreover, calcite is present as minor minerals in many samples while Ca-Na feldspars are present in B1, B4 and B15 as moderate mineral.

3.2.3 Bottom Sediment Samples Mineralogy

The mineralogical composition of the 18 bottom sediments also shows the predominant of quartz and aragonite as major minerals in all sites (Table 3.8) in similarity with those of the shore samples. However, magnesite becomes more existing, occurring in many sites as a minor mineral. In addition, calcite and dolomite are also common minor minerals, while aragonite and Ca-Na feldspars are found in a moderate quantity of many bottom samples.

Table 3.6: Mineralogical composition of soil samples

S	Major	Moderate	Minor
S1	Quartz	Aragonite, Gypsum	Halite, Ca-Na feldspars
S2	Quartz	Aragonite	Calcite, Ca-Na feldspars, Gypsum, Dolomite, Halite
S4	Quartz	Halite	Ca-Na feldspars, Aragonite, Gypsum, Calcite, Dolomite
S6	Quartz		Ca-Na feldspars, Halite, Calcite
S7	Quartz		Halite, Ca-Na feldspars
S8	Quartz	Aragonite	Calcite, Ca-Na feldspars, Halite, Dolomite
S9	Quartz		Calcite, Halite, Ca-Na feldspars
S10	Quartz	Halite, Ca-Na feldspars	Dolomite, Calcite
S11	Quartz	Ca-Na feldspars, K-feldspars	Halite, Calcite, Gypsum
S13	Ca-Na feldspars	Quartz	Halite
S16	Quartz	Calcite, Ca-Na feldspars	
S18	Quartz	Halite, Dolomite	Calcite, Ca-Na feldspars,
S19	Quartz		Calcite, Dolomite, ferroan, Ca-Na feldspars,
S20	Ca-Na feldspars	Quartz	Calcite, Gypsum, Bassanite

Table 3.6: Mineralogical composition of soil samples (continued)

S	Major	Moderate	Minor
S21	Quartz	K-feldspars, Ca-Na feldspars	
S22	Quartz	Calcite	Gypsum
S23	Quartz	Calcite, Ca-Na feldspars, Gypsum	
S24	Quartz	Ca-Na feldspars	Dolomite, Gypsum

Table 3.7: Mineralogical composition of shore samples

S	Major	Moderate	Minor
B1	Quartz	Aragonite, Ca-Na feldspars	
B2	Quartz, Aragonite		Calcite, Ca-Na feldspars
B4	Quartz, Aragonite	Ca-Na feldspars	Calcite
B5	Quartz, Aragonite		Calcite, Ca-Na feldspars, Dolomite
B6	Aragonite	Quartz	Ca-Na feldspars, Magnesite
B7	Quartz, Aragonite		Calcite
B9	Quartz, Magnesite	Aragonite, calcite	
B10	Quartz	Aragonite	Calcite
B11	Quartz, Aragonite		Calcite
B13	Quartz, Ca-Na feldspars	Aragonite	Magnesite
B15	Quartz, Aragonite	Ca-Na feldspars	Magnesite
B16	Aragonite	Quartz, Calcite	Magnesite

Table 3.8: Mineralogical composition of bottom sediment samples

S	Major	Moderate	Minor
M1	Aragonite	Quartz, Ca-Na feldspars	Calcite, Dolomite, Magnesite
M2	Quartz	Aragonite, Ca-Na feldspars	Magnesite, Calcite, Dolomite
M3	Quartz	Aragonite	
M4	Quartz, Aragonite		Calcite
M5	Quartz, Aragonite	Ca-Na feldspars	
M6	Quartz, Aragonite		Magnesite
M7	Quartz	Aragonite	Magnesite, Calcite, Dolomite, Ca-Na feldspars
M8	Quartz	Aragonite	Magnesite, Calcite, Dolomite, Ca-Na feldspars
M9	Quartz	Aragonite	Calcite
M10	Aragonite	Quartz	Magnesite
M11	Aragonite	Calcite	Magnesite
M12	Aragonite	Ca-Na feldspars	Magnesite, Calcite, Quartz
M13	Aragonite	Quartz	Calcite
M14	Quartz	Ca-Na feldspars	Aragonite, Calcite
M15	Quartz, Aragonite		Magnesite
M16	Aragonite	Ca-Na feldspars	Magnesite, Quartz, Calcite
M17	Quartz	Ca-Na feldspars	Dolomite, Calcite, Aragonite
M18	Quartz	Aragonite	Magnesite, Calcite, Dolomite, Ca-Na feldspars

3.3 Carbonate Content

The carbonate content of soil is an important parameter determining soil chemistry. The measurement of this parameter is based on the reaction between carbonates and strong acids, which results in carbonate dissolution and CO₂ development.

The carbonate content percentage in all of the collected samples is estimated and shown in Table 3.9. Generally, measured carbonate content in the studied samples is high. The percentage of carbonate content in the soil samples (Tables 3.9) range between 4.13% to 63.96% with an average value of 35.38%. While the percentage average of shore and bottom samples shows an average of 67.7% and 72.24%, respectively ranging from 46.25% to 85.12% and from 11.02% to 97.8%, respectively. Based on the measured average carbonate content, the following order is observed: soil < shore < bottom.

Table 3.9: Carbonate content (%) of soil, shore and bottom sediment samples

soil	Carbonate content (%)	shore	Carbonate content (%)	bottom	Carbonate content (%)
S1	63.96	B1	81.71	M1	85.3
S2	44.27	B2	85.12	M2	86.1
S3	51.58	B3	80.75	M3	23.22
S4	47.52	B4	68.12	M4	89.3
S5	41.54	B5	82.02	M5	66.86
S6	37.92	B6	46.25	M6	75
S7	23.71	B7	48.51	M7	60.69
S8	60.87	B8	53.57	M8	59.11
S9	26.47	B9	67.26	M9	65.61
S10	30.18	B10	60.12	M10	97.8
S11	34.98	B11	82.11	M11	95.43
S12	41.14	B12	74.02	M12	96.03
S13	38.42	B13	55.12	M13	97.4
S14	32.28	B14	71.15	M14	58.96
S15	17.16	B15	54.42	M15	84.8
S16	40.67	B16	72.92	M16	91.7
S17	37.55	Min	46.25	M17	11.02
S18	29.82	Max	85.12	M18	55.98
S19	23.32	Ave.	67.7	Min	11.02
S20	27.59			Max	97.8
S21	4.13			Ave.	72.24
S22	31.21				
S23	35.57				
S24	27.22				
Min	4.13				
Max	63.96				
Ave.	35.38				

3.4 Major Oxides

The Major oxides include SiO_2 , Al_2O_3 , TiO_2 , FeO , MnO , MgO , CaO , Na_2O , K_2O and P_2O_5 . Because these are reported as a percentage, they are usually greater than 1%, as the total should sum to 100 %, ideally, however acceptable totals lie in the range 98.5 to 101 weight percentage. Studying the major oxides can help to describe the geochemical compositions of the studied area. Major oxides of the studied area are listed in Tables 3.10 to 3.12. Generally, major oxides are dominated by CaO and SiO_2 . Major oxides in soil samples (Table 3.10) are characterized with higher SiO_2 content than CaO content unlike the shore and bottom sediments ranging from 21.97 to 82.92 wt.%, with an average of 49.84 wt.%. The next most abundant element is CaO ranging between 1.75 to 33.22 in wt.% and with an average of 14.08 wt. % while the Lost of Ignition (LOI) range from 13.35 to 52.29 wt. % with an average of 30.73. Both of Na_2O and MgO show a range of 0.11 – 6.74 wt. %, and 0.46 – 4.97 wt. % and average of 2.84 and 2.04 wt. %, respectively.

The shore samples have moderate to high CaO contents, with abundances ranging 30.04 to 45.94 wt.% (Table 3.11), and average of 38.95 wt.% well consistent with 3.9 wt.% present in the sandstone reported by Turekian and Wedepohl (1961). The high value of CaO content in the shore samples reflects their biogenic carbonate content. The next most abundant element is SiO_2 ranging between 6.57 to 32.05 wt.%, averaging 17.48 wt.%, much less than in sandstone (36.80 wt.%). LOI (41.03 wt.%, range 35.02 – 47.69 wt.%,) and MgO (1.59 wt.%, range 1.04 – 2.19 wt.%). All other oxides are present in smaller amount. The higher CaO and LOI contents of all samples, suggesting that marine biogenic CaCO_3 component is dominant in Barakah beach sediments.

Major oxides in bottom sediments of the studied area are listed in Table 3.12. Similar to shore samples, bottom sediments are characterized with high contents of CaO and SiO₂ with an average of 34.9 and 21.99 wt. %, respectively. Furthermore, LOI (39.26 wt.%, range 19.31 – 50.88 wt.%), Na₂O (2.16 wt.%, range 0.71 – 3.14 wt.%), and MgO (1.15 wt.%, range 0.68 – 2.1 wt.%), are the most abundant on average.

The major oxides variation in the soil, shore and bottom sediments samples are consistent with their general mineralogy. The higher silica contents and relatively lower CaO content in soil samples than shore and bottom sediments may be attributed to a different source of the last one.

Table 3.10: Major oxides Wt.% of soil samples (analytical error is <0.01)

S	SiO ₂	FeO	CaO	P ₂ O ₅	MgO	TiO ₂	Al ₂ O ₃	Na ₂ O	K ₂ O	MnO	LOI
S1	21.97	0.22	33.22	0.02	1.16	0.02	0.26	3.10	0.07	0.006	39.96
S2	47.28	0.33	20.93	0.03	1.49	0.02	0.38	0.78	0.08	0.009	28.66
S3	47.15	0.32	24.14	0.03	1.69	0.02	0.34	0.30	0.07	0.009	25.94
S4	28.49	0.48	15.59	0.03	2.57	0.02	0.40	>6.74	0.13	0.012	52.29
S5	51.02	0.40	20.39	0.03	1.39	0.03	0.45	0.15	0.07	0.011	26.05
S6	50.97	0.85	11.77	0.04	3.70	0.03	0.91	1.89	0.27	0.028	29.56
S7	52.86	0.55	8.48	0.02	1.13	0.04	0.57	0.55	0.12	0.009	35.68
S8	25.86	0.23	25.87	0.03	1.72	0.01	0.25	3.82	0.10	0.007	42.11
S9	59.60	0.89	9.12	0.04	0.98	0.04	0.79	1.95	0.13	0.022	26.43
S10	55.27	0.90	4.62	0.04	2.59	0.04	0.77	5.93	0.23	0.022	29.59
S11	58.88	0.69	8.05	0.03	2.57	0.03	0.59	2.11	0.16	0.021	26.88
S12	41.02	0.69	12.02	0.03	2.47	0.03	0.68	>6.74	0.25	0.015	42.78
S13	52.42	0.86	10.87	0.04	2.27	0.05	0.89	4.20	0.18	0.017	28.19
S14	48.16	1.33	16.41	0.05	1.74	0.03	1.81	1.68	0.31	0.016	28.45
S15	62.07	1.09	5.71	0.04	2.87	0.05	0.94	2.87	0.19	0.030	24.13
S16	51.38	0.77	15.22	0.05	2.70	0.04	0.79	1.94	0.13	0.021	26.94
S17	49.75	0.81	10.44	0.03	1.69	0.04	0.81	>6.74	0.22	0.017	36.19
S18	59.83	0.77	7.16	0.04	2.39	0.04	0.81	5.12	0.22	0.022	23.60
S19	65.40	0.82	11.88	0.03	1.01	0.05	0.81	0.13	0.13	0.019	19.71
S20	35.73	0.84	18.37	0.05	4.97	0.04	1.08	2.44	0.16	0.021	36.31
S21	82.92	0.63	1.75	0.02	0.46	0.03	0.60	0.11	0.12	0.010	13.35
S22	42.16	0.69	12.41	0.03	1.94	0.03	0.47	>6.74	0.07	0.016	42.17
S23	48.27	0.42	21.32	0.03	1.67	0.02	0.34	0.19	0.06	0.008	27.66
S24	57.62	0.60	12.09	0.03	1.89	0.03	0.59	2.02	0.14	0.016	24.98
Min	21.97	0.22	1.75	0.02	0.46	0.01	0.25	0.11	0.06	0.01	13.35
Max	82.92	1.33	33.22	0.05	4.97	0.05	1.81	6.74	0.31	0.03	52.29
Ave.	49.84	0.68	14.08	0.03	2.04	0.03	0.68	2.84	0.15	0.02	30.73

Table 3.11: Major oxides Wt.% of shore samples (analytical error is <0.01)

S	SiO ₂	FeO	CaO	P ₂ O ₅	MgO	TiO ₂	Al ₂ O ₃	Na ₂ O	K ₂ O	MnO	LOI
B1	17.85	0.12	37.58	0.02	1.66	0.01	0.13	0.58	0.04	0.003	42.02
B2	11.26	0.09	38.73	0.02	1.43	0.01	0.11	0.62	0.04	0.003	47.69
B3	14.32	0.12	40.90	0.03	1.71	0.01	0.13	0.63	0.04	0.004	42.12
B4	26.06	0.17	34.78	0.03	2.19	0.02	0.21	0.62	0.05	0.005	35.87
B5	19.31	0.00	36.18	0.03	1.84	0.01	0.15	0.59	0.04	0.005	41.83
B6	22.14	0.14	35.60	0.03	1.64	0.01	0.15	0.60	0.05	0.004	39.65
B7	13.45	0.10	42.13	0.03	1.72	0.01	0.11	0.62	0.04	0.003	41.79
B8	22.84	0.09	37.65	0.03	1.56	0.01	0.11	0.68	0.05	0.003	36.99
B9	28.03	0.24	33.94	0.02	1.21	0.01	0.19	0.64	0.06	0.004	35.64
B10	17.45	0.12	40.25	0.02	1.04	0.01	0.15	0.73	0.05	0.003	40.17
B11	6.57	0.06	45.38	0.02	1.16	0.00	0.08	0.59	0.04	0.001	46.09
B12	8.27	0.08	45.94	0.02	1.26	0.01	0.11	0.60	0.04	0.002	43.67
B13	9.33	0.08	43.16	0.02	1.71	0.01	0.09	0.53	0.04	0.002	45.03
B14	10.63	0.09	42.37	0.03	2.07	0.01	0.09	0.59	0.04	0.003	44.08
B15	32.05	0.19	30.04	0.03	1.76	0.01	0.19	0.64	0.06	0.005	35.02
B16	20.15	0.17	38.52	0.03	1.54	0.01	0.17	0.61	0.05	0.005	38.75
Min	6.57	0.01	30.04	0.02	1.04	0.01	0.08	0.53	0.04	0.001	61.67
Max	32.05	0.24	45.94	0.03	2.19	0.02	0.21	0.73	0.06	0.005	18.53
Ave.	17.48	0.12	38.95	0.03	1.59	0.01	0.14	0.62	0.04	0.003	41.03

Table 3.12: Major oxides Wt.% of bottom samples (analytical error is <0.01)

S	SiO ₂	FeO	CaO	P ₂ O ₅	MgO	TiO ₂	Al ₂ O ₃	Na ₂ O	K ₂ O	MnO	LOI
M1	6.54	0.36	36.32	0.05	3.13	0.01	0.43	2.10	0.16	0.006	50.88
M2	14.88	0.15	34.67	0.03	2.21	0.02	0.16	1.09	0.05	0.004	46.74
M3	60.38	0.26	17.77	0.02	0.71	0.02	0.16	0.78	0.05	0.003	19.85
M4	10.56	0.13	38.71	0.04	3.06	0.01	0.10	1.89	0.06	0.004	45.45
M5	24.91	0.15	33.13	0.03	2.20	0.01	0.17	1.00	0.05	0.004	38.33
M6	18.87	0.20	35.59	0.03	2.30	0.01	0.17	1.28	0.06	0.003	41.49
M7	29.54	0.21	30.66	0.02	2.04	0.01	0.19	1.11	0.06	0.004	36.16
M8	25.16	0.28	31.44	0.03	2.39	0.01	0.31	1.60	0.09	0.007	38.66
M9	27.36	0.20	32.45	0.03	2.13	0.01	0.25	0.76	0.06	0.006	36.73
M10	5.94	0.07	46.39	0.03	2.06	0.01	0.08	1.12	0.06	0.002	44.24
M11	0.84	0.04	48.83	0.04	2.07	<.002	0.05	0.98	0.04	0.002	47.10
M12	1.21	0.04	49.26	0.04	1.88	<.002	0.06	1.03	0.04	0.002	46.44
M13	2.27	0.05	45.44	0.06	3.14	<.002	0.06	1.08	0.05	0.003	47.86
M14	37.00	0.21	28.46	0.03	2.01	0.02	0.23	0.68	0.06	0.006	31.30
M15	14.03	0.11	42.12	0.04	2.09	0.01	0.12	0.86	0.06	0.003	40.56
M16	8.30	0.13	44.46	0.05	2.43	0.01	0.13	1.04	0.06	0.004	43.39
M17	71.14	0.68	5.57	0.03	1.23	0.04	0.78	1.02	0.18	0.016	19.31
M18	36.92	0.36	26.92	0.05	1.73	0.02	0.38	1.24	0.10	0.010	32.27
Min	0.84	0.04	5.57	0.02	0.71	0.01	0.05	0.68	0.04	0.00	19.31
Max	71.14	0.68	49.26	0.06	3.14	0.04	0.78	2.10	0.18	0.02	50.88
Ave.	21.99	0.20	34.90	0.04	2.16	0.01	0.21	1.15	0.07	0.00	39.26

3.5 Heavy Metal

Heavy metal concentrations in the soil, shore and bottom samples are presented in Tables 3.13-3.15. Generally, both Fe and Mn are present in the highest concentrations, while Cd has the lowest concentrations in all areas. Furthermore, the shore samples had the lowest level of heavy metal concentrations followed by bottom sediments then soil samples.

Heavy metal concentrations show some elevation in soil samples as shown in Table 3.13. Both of Fe and Mn values ranged from 1700 to 10300 ppm (average 5250 ppm) and from 49 to 231 (average 124 ppm), respectively. Both of Cr and Ni show wide variations in the studied soil sample with a standard deviation of 8 for each. Their concentrations vary between 5.9 and 58.1 ppm and between 5.3 and 45.1 ppm with average of 17.4 and 15.4, respectively. Vanadium and zinc show similar minimum and maximum values (5 and 23 ppm) with average concentration values of 13 and 11.5 ppm, respectively. The remaining heavy metal concentrations fluctuate in the study samples as following: Cu from 1.58 to 8.11 ppm (average 4.18 ppm); and Co from 0.8 to 4.4 ppm (average 2.6 ppm). Pb (1.07 to 4.04 ppm; average 2.43), As (0.8 to 2.9 ppm, average 1.6 ppm), Mo (0.18 to 2.18 ppm; average 0.89 ppm), and finally Cd (0.02 to 0.09; average 0.05 ppm).

According to Table 3.14, Fe and Mn are the most abundant heavy metals in shore samples, with average value of 975 and 26 ppm, ranging between 500 to 1900 and 11 to 42 ppm, respectively. The next most abundant metal is Cr ranging between 2.4 to 5.7 ppm, averaging 3.7 ppm followed by V and Zn with concentration values range from 2 to 5 ppm, and from 1.5 to 3.9 ppm with a mean value of 3 and 2.8, respectively. The average concentration in ppm for the remaining heavy metals

as order of the occurrence is 2.1, 1.4, 1.14, 0.78, 0.4, 0.1 and 0.03 for Ni, As, Pb, Cu, Co, Mo and Cd, respectively.

Bottom sediments show moderate heavy metal concentrations relative to shore and soil samples. According to Table 3.15, both Fe and Mn show the highest average concentration of 1463 and 33.33 ppm. The average remaining heavy metals concentration (in ppm) is, in order of occurrence, Cr (6), V(4.67), Ni (4.3), Zn (3.23), As (1.9), Pb (1.44), Cu (1.41), Co (0.6), Mo (0.23) and finally Cd (0.03).

Table 3.13: Heavy metal concentrations (in ppm) for the soil samples (analytical error is <0.01)

S	Cu	Pb	Zn	Ni	Co	Mn	Fe	Cd	V	Cr	As	Mo	Sr
S1	1.62	1.29	5	5.3	1.1	49	1700	0.02	5	5.9	1.4	0.25	4818
S2	2.06	1.97	6.8	8	1.3	72	2600	0.03	6	8.3	2.6	0.19	2374
S3	2.09	2.77	5.9	7.1	1.1	68	2500	0.03	6	8.2	2.9	0.18	2345
S4	3.43	3.08	13.4	45.1	3.3	92	3700	0.04	7	22.9	1.8	1.17	1756
S5	3.21	2.31	7	10.1	1.7	88	3100	0.03	8	9.9	2.5	0.24	2313
S6	5.86	4.04	21	19.2	3.8	213	6600	0.09	19	21.3	2	1.21	1378
S7	3.32	2.23	9.4	9.4	1.9	70	4300	0.02	11	15.5	0.9	0.23	810
S8	1.58	1.07	7.9	5.4	0.8	51	1800	0.05	5	6.3	1.6	0.31	2523
S9	4.82	2.61	13.9	20.7	3.3	170	6900	0.08	16	22.4	1.3	0.51	10000
S10	4.9	2.45	11.4	19.9	3.3	167	7000	0.07	15	23.5	0.9	0.62	313
S11	3.92	3.65	10.4	9.2	2.5	162	5400	0.06	13	13.1	1.2	1.75	5215
S12	4.56	2.46	12.5	21.6	2.5	118	5400	0.04	13	19.2	1.4	0.55	1598
S13	4.89	2.48	14.7	18.1	3	133	6700	0.03	17	28.7	1.4	0.76	1678
S14	8.11	2.66	22.5	18.7	4.4	122	10300	0.04	19	58.1	1.1	0.53	2001
S15	5.91	3.03	16.1	24	4.2	231	8500	0.07	23	29.3	2	1.97	1043
S16	5.26	2.79	12.2	23.2	3.3	165	6000	0.07	15	21	1.8	1.26	3074
S17	5.24	2.59	11.9	16.9	3	128	6300	0.04	16	19.8	1.2	0.63	1729
S18	4.5	2.23	13.2	15.6	3.2	169	6000	0.08	16	19.5	0.8	2.18	1233
S19	4.75	2.97	12.9	14.1	3.1	151	6400	0.05	14	18.2	1.2	0.53	1273
S20	6.28	2.34	15.9	21.9	3.7	166	6500	0.05	22	38.3	2.9	1.75	2740
S21	3.19	2.34	8.6	8.6	2.1	77	4900	0.03	9	12.4	0.8	0.49	198
S22	4.37	1.75	8.6	12.6	2.3	127	5400	0.04	11	13	1.5	1.67	1212
S23	2.7	1.45	7	5.9	1.3	64	3300	0.04	6	9.5	1.3	1.02	2432
S24	3.83	1.78	8.9	9.7	2.3	122	4700	0.05	12	13.8	1.3	1.25	1296
Min	1.58	1.07	5	5.3	0.8	49	1700	0.02	5	5.9	0.8	0.18	198
Max	8.11	4.04	22.5	45.1	4.4	231	10300	0.09	23	58.1	2.9	2.18	10000
Ave.	4.18	2.43	11.5	15.4	2.6	124	5250	0.05	13	17.4	1.6	0.89	2306
St.Dev.	1.58	0.69	4.5	8.8	1	51	2108	0.02	5	8.2	0.6	0.62	2021

Table 3.14: Heavy metal concentrations (in ppm) for the shore samples

S	Cu	Pb	Zn	Ni	Co	Mn	Fe	Cd	V	Cr	As	Mo	Sr
B1	0.65	1.07	2.5	2.4	0.2	23	900	0.03	3	3.3	1.9	0.11	4743
B2	0.79	1.9	3.9	1.8	0.5	20	700	0.04	<2	2.9	1.4	0.05	4771
B3	0.77	1.16	3.4	5	0.6	28	900	0.02	2	4	0.7	0.09	4884
B4	1.21	2.42	3.9	4	0.8	42	1300	0.03	4	5.7	1.4	0.12	3498
B5	0.88	1.1	3	3	0.4	37	1200	0.04	5	4.2	1.6	0.11	4148
B6	0.97	1.21	3.7	2.4	0.4	32	1100	0.02	4	4.3	1.4	0.25	4380
B7	0.75	1.48	3.2	1.6	0.3	22	800	0.02	3	3.2	1.3	0.21	4396
B8	0.5	0.89	1.5	0.9	0.3	21	700	0.03	<2	3.1	1.8	0.08	4483
B9	0.9	1.56	2.5	2.1	0.4	29	1900	0.01	3	4.6	1.2	0.17	4367
B10	0.58	0.94	1.9	1.8	0.3	20	900	0.02	2	3.5	1.5	0.07	5819
B11	0.49	0.93	1.9	1.6	0.1	11	500	0.02	<2	2.4	1.4	0.07	6366
B12	0.52	0.84	2	1.5	0.2	19	600	0.02	3	3.1	1	0.06	6564
B13	0.67	0.85	2	1.3	0.6	18	600	0.02	3	2.6	1.5	0.06	5446
B14	0.69	0.93	3.5	1.5	0.5	21	700	0.02	3	3.2	1.2	0.08	4627
B15	1.15	0.88	2.7	3.1	0.7	39	1500	0.03	4	5	1.6	0.12	3198
B16	1.03	1.33	2.9	1.9	0.7	35	1300	0.03	3	4.6	1.5	0.12	4486
Min	0.49	0.84	1.5	0.9	0.1	11	500	0.01	2	2.4	0.7	0.05	3198
Max	1.21	2.42	3.9	5	0.8	42	1900	0.04	5	5.7	1.9	0.25	6564
Ave.	0.78	1.14	2.8	2.1	0.4	26	975	0.03	3	3.7	1.4	0.1	4761
St.Dev.	0.22	0.31	0.8	0.8	0.2	9	382	0.01	1	0.9	0.3	0.04	911

Table 3.15: Heavy metal concentrations (in ppm) in bottom sediment samples (analytical error is <0.01). The grain size notations “C”, “M” and “F” stand for coarse, medium and fine

S	Cu	Pb	Zn	Ni	Co	Mn	Fe	Cd	V	Cr	As	Mo	Sr
M1 C	3.9	1.93	5.5	7.1	1	34	210	<0.01	7	6.7	2.8	0.83	314
M2 C	0.4	0.51	1.8	0.8	0.3	12	500	<0.01	2	1.6	1.4	0.12	284
M3 C	1.1	0.85	1.5	1.1	0.4	21	180	<0.01	<2	3.3	1.2	0.18	129
M4 C	0.4	0.64	2.6	<0.1	0.2	27	400	0.15	<2	0.9	1.8	0.13	274
M5 C	0.5	0.73	0.8	1.8	0.5	16	600	<0.01	2	2	1.7	0.22	311
M6 C	0.6	0.45	0.8	2.1	0.4	14	500	<0.01	4	2.4	1.7	0.11	418
M7 C	2.6	16.11	5.9	2.2	0.5	23	150	0.03	3	3.8	2.1	0.3	376
M8 C	2.9	12.19	5.6	3.8	0.6	33	170	0.01	5	4.9	2.1	0.71	362
M9 C	0.9	0.84	2.7	3.9	0.4	26	100	0.03	4	4.4	1.4	0.19	364
M10 C	0.3	0.9	2.6	1	<0.1	13	300	0.04	<2	1.5	1.1	0.13	486
M11 C	0.3	0.56	1.2	1.5	<0.1	13	200	0.04	<2	1.6	0.9	0.09	451
M12 C	0.3	0.98	2.2	1	<0.1	13	300	0.02	<2	1.6	1	0.15	520
M13 C	0.3	0.63	2.1	0.9	0.1	19	300	0.05	<2	1.8	1.1	0.13	297
M14 C	0.9	1.38	2.6	2.5	0.4	25	100	0.03	2	4.3	1.6	0.27	289
M15 C	0.6	0.75	1.7	2	0.2	23	600	0.03	3	2.7	1.6	0.17	466
M16 C	0.9	1.36	3.5	2.1	0.2	32	900	0.04	6	3.6	2.5	0.32	391
M17 C	5.4	2.09	30.8	29.3	2.8	147	610	0.11	17	21.5	1.4	0.49	379
M18 C	6.6	1.75	11.4	12.7	1	59	210	0.07	6	7.7	2.4	1.12	259
Ave.	0.6	1.02	2.7	2.1	0.4	24	929	0.03	3	3.2	1.7	0.2	335
St.Dev.	0.2	0.52	1.6	1.7	0.3	12	662	0.02	2	1.9	0.5	0.11	120

Table 3.15: Heavy metal concentrations (in ppm) in bottom sediment samples (analytical error is <0.01). The grain size notations “C”, “M” and “F” stand for coarse, medium and fine (continued)

S	Cu	Pb	Zn	Ni	Co	M	Fe	Cd	V	Cr	As	Mo	Sr
M1 M	5.04	5.58	7.1	9	1.3	41	2800	0.04	9	9.3	4.3	1.14	431
M2 M	1.33	5.87	3.1	2.7	0.4	16	700	<0.01	3	2.5	2.1	0.18	366
M3 M	2.35	11.2	6.7	3.2	0.4	23	2100	<0.01	<2	3.7	1.4	0.38	178
M4 M	1.41	6.62	2.9	2.4	0.4	21	1000	0.01	2	3.3	1.4	0.28	408
M5 M	0.76	2.15	2.1	2.8	0.4	23	900	<0.01	3	3.9	1.7	0.2	313
M6 M	3.97	2.18	5.8	3.6	0.6	25	1600	0.01	5	5.9	2	0.3	378
M7 M	1.69	1.94	2.6	2.7	0.5	25	1500	<0.01	4	4.8	1.7	0.24	384
M8 M	2.15	1.96	3.6	6.4	0.8	42	2000	0.02	8	7	2.5	0.77	290
M9 M	1.2	0.96	3.8	4	0.5	35	1300	0.03	4	5.7	1.4	0.21	320
M10 M	0.48	0.57	1.2	0.7	<0.1	14	400	0.04	<2	2	1.2	0.13	573
M11 M	0.51	0.56	0.8	1	0.2	11	200	0.04	<2	1.7	1.2	0.1	634
M12 M	0.68	0.8	2.1	0.5	<0.1	14	200	0.04	<2	1.8	1.6	0.12	584
M13 M	0.71	0.89	1.8	2.2	0.2	28	300	0.05	3	2.7	1.5	0.13	399
M14 M	1.32	1.18	3.3	4.4	0.6	35	1400	0.03	4	6.9	1.5	0.3	241
M15 M	0.79	1.16	2.2	2	0.2	24	700	0.03	4	3.2	1.7	0.17	449
M16 M	0.9	1.11	2.4	2.6	0.3	24	800	0.03	4	4	2.7	0.25	414
M17 M	4.42	2.36	23.5	15.7	2.4	11	5000	0.08	12	17.3	1.6	0.4	177
M18 M	4.06	1.4	11.7	9.7	1.2	72	2900	0.06	6	9.5	2.1	0.72	148
Ave.	1.88	1.37	3.2	3.5	0.5	25	1433	0.03	4	4.6	1.7	0.23	363
St.Dev...	1.48	0.63	1.8	2.6	0.3	9	1210	0.02	2	2.5	0.4	0.09	155
M1 F	5.75	2.63	8.5	11.5	1.7	63	3400	0.04	12	12.4	4.5	1.07	363
M2 F	1.86	1.73	3.4	11.3	0.8	60	2200	<0.01	8	13.1	3.4	0.32	224
M3 F	1.5	2.2	2.6	7.1	0.7	37	2100	<0.01	5	7.7	1.8	0.28	226
M4 F	1.38	2.75	2.3	11.1	0.6	38	1600	0.04	5	14.3	2.1	0.32	361
M5 F	1.5	1.88	3.6	5.9	1	54	2000	0.02	7	9.3	2.3	0.25	259
M6 F	1.99	3.49	4	18.5	0.8	42	2500	<0.01	6	32.5	2.5	0.41	328
M7 F	1.38	1.75	3.2	5.5	0.9	43	1800	0.04	7	9.1	2.7	0.27	329
M8 F	2.64	1.82	5.2	10.3	1.5	79	2900	0.02	11	10.6	3.2	0.8	227
M9 F	1.81	1.17	4.5	9.6	1.1	73	2400	0.03	8	11	1.7	0.31	212
M10 F	1.21	1.86	4.5	2	0.4	30	900	0.03	3	4.1	1.8	0.18	489
M11 F	0.96	4.29	2.3	0.8	<0.1	16	500	0.03	3	2.8	1.1	0.16	502
M12 F	0.6	0.85	1.9	0.7	0.2	15	400	0.03	<2	2.4	2.8	0.13	590
M13 F	0.6	0.89	1.4	1	0.2	23	500	0.02	3	2.8	1.1	0.14	424
M14 F	1.75	1.27	5	6.7	1.1	79	2500	0.03	8	11	2.5	0.32	213
M15 F	0.95	1.25	3	1.5	0.3	32	1200	0.02	5	4.4	1.8	0.19	380
M16 F	1.34	1.52	4.7	4.6	0.4	36	1400	0.03	4	7	2.3	0.22	353
M17 F	3.84	1.8	21.5	13.1	2.1	11	4800	0.06	12	16.8	1.3	0.34	118
M18 F	4.12	1.56	15.1	9.6	1.4	92	3400	0.06	8	11.5	1.9	0.89	110
Ave.	1.73	1.93	3.8	7.3	0.9	51	2028	0.03	7	10.2	2.3	0.26	311
St.Dev.v	0.99	0.89	1.7	5	0.6	27	1156	0.01	3	7	0.9	0.08	142

In general, some sites show high heavy metal concentration compared to other sites. The map in Figure 3.1 shows the location of S14, B4 and M18, samples with the highest heavy metals concentrations in shore, soil and bottom samples, respectively.



Figure 3.1: Location of the samples with maximum heavy metal concentrations (in ppm) in shore, soil and bottom sediment

3.6 Rare Earth Elements

Rare earth elements (REE) are a set of seventeen chemical elements in the periodic table, specifically the fifteen contiguous lanthanoids (lanthanum (La), cerium (Ce), praseodymium (Pr), neodymium (Nd), promethium (Pm), samarium (Sm), europium (Eu), gadolinium (Gd), terbium (Tb), dysprosium (Dy), holmium (Ho), erbium (Er), thulium (Tm), ytterbium (Yb), and lutetium (Lu)) plus the lighter scandium and yttrium. Scandium and yttrium are considered REE since they tend to occur in the same ore deposits as the lanthanoids and exhibit similar chemical properties. Most REEs are not rare however, because of their geochemical properties, REE minerals are typically dispersed and not often found in concentrated and

economically exploitable forms. REEs are often found together, and are difficult to separate.

The concentration of Pr, Nd, Sm, Eu, Gd, Tb, Dy, Ho, Er, Tm, Yb and Lu are measured in the soil, shore and bottom sediments, as shown in Tables 3.16-3.18.

The REE concentration for soil samples shows higher values than shore and bottom sediment samples. Their order of occurrence is Nd > La > Pr > Sm > Gd > Dy > Er > Yb > Eu > Ho > Tb > Tm = Lu, with average concentration of 3.39, 3.36, 0.83, 0.70, 0.62, 0.27, 0.24, 0.17, 0.11, 0.08, 0.04 and 0.04 (ppm), respectively (Table 3.16).

The REE concentration for shore samples is lower than of soil samples with an order of occurrence (Table 3.17) as follow: La > Nd > Pr > Sm > Gd > Dy > Er = Yb > Eu > Tb = Ho, with average concentration of 0.95, 0.87, 0.23, 0.19, 0.16, 0.15, 0.07, 0.07, 0.05, 0.03 and 0.03 (ppm), respectively. Both Tm and Lu are below the detection limit (0.02).

The order of occurrence of REE in bottom sediments (Table 3.18) is as follows La > Nd > Pr > Sm > Gd > Dy > Er > Yb > Eu > Tb = Ho > Tm = Lu. Their average concentration (in ppm) with the same previous order is 1.5, 1.26, 0.32, 0.26, 0.24, 0.30, 0.11, 0.10, 0.07, 0.05, 0.05, 0.03 and 0.03, respectively.

Overall, all of the sites show narrow differences in REE concentrations in the analyzed samples as revealed by the small values of standard deviation as shown in Tables 3.16 -3.18.

Table 3.16: REE and Al concentrations (in ppm) in soil samples (analytical error is <0.01)

Sample	LREE (ppm)					HREE (ppm)								Al
	La	Pr	Nd	Sm	Eu	Gd	Tb	Dy	Ho	Er	Tm	Yb	Lu	
S1	1.2	0.31	1.28	0.25	0.07	0.22	<0.02	0.24	0.03	0.12	<0.02	0.10	<0.02	1400
S2	2.2	0.57	2.05	0.45	0.11	0.44	0.04	0.36	0.07	0.18	0.03	0.14	0.02	2000
S3	2.0	0.46	1.82	0.35	0.10	0.36	0.04	0.34	0.06	0.15	0.02	0.15	<0.02	1800
S4	1.8	0.43	1.67	0.37	0.09	0.33	0.03	0.32	0.07	0.19	<0.02	0.13	<0.02	2100
S5	2.5	0.58	2.49	0.57	0.13	0.53	0.05	0.41	0.08	0.18	0.03	0.15	0.02	2400
S6	4.7	1.18	4.41	0.98	0.25	0.85	0.11	0.73	0.14	0.38	0.05	0.34	0.04	4800
S7	2.8	0.81	3.35	0.67	0.18	0.69	0.08	0.56	0.10	0.29	0.03	0.20	0.03	3000
S8	1.3	0.33	1.31	0.24	0.07	0.12	0.04	0.22	0.05	0.09	<0.02	0.08	0.02	1300
S9	4.9	1.24	4.73	1.07	0.27	1.05	0.13	0.87	0.16	0.44	0.07	0.43	0.05	4200
S10	4.6	1.12	4.47	0.93	0.22	0.96	0.11	0.74	0.16	0.32	0.06	0.34	0.03	4100
S11	4.2	1.02	3.94	0.83	0.20	0.77	0.12	0.76	0.13	0.33	0.05	0.29	0.04	3100
S12	3.3	0.84	3.59	0.62	0.20	0.79	0.09	0.54	0.12	0.28	0.04	0.27	0.04	3600
S13	3.7	0.97	3.77	0.84	0.18	0.76	0.08	0.65	0.12	0.29	0.04	0.29	0.05	4700

Table 3.16: REE and Al concentrations (in ppm) in soil samples (analytical error is <0.01) (continued)

Sample	La	Pr	Nd	Sm	Eu	Gd	Tb	Dy	Ho	Er	Tm	Yb	Lu	Al
S14	6.4	1.69	6.88	1.42	0.34	1.18	0.16	1.00	0.18	0.49	0.07	0.41	0.06	9600
S15	5.0	1.25	4.98	1.02	0.25	0.99	0.13	0.89	0.15	0.40	0.06	0.34	0.06	5000
S16	3.7	0.93	3.66	0.70	0.20	0.84	0.11	0.67	0.13	0.30	0.04	0.33	0.05	4200
S17	3.7	0.97	3.87	0.86	0.16	0.67	0.09	0.71	0.14	0.31	0.04	0.28	0.04	4300
S18	3.6	0.90	3.64	0.76	0.19	0.62	0.08	0.64	0.12	0.28	0.04	0.26	0.03	4300
S19	5.3	1.31	4.98	1.00	0.24	0.88	0.11	0.76	0.16	0.33	0.05	0.31	0.03	4300
S20	3.5	0.87	3.42	0.72	0.21	0.63	0.11	0.67	0.12	0.29	0.04	0.22	0.04	5700
S21	3.1	0.81	3.55	0.59	0.17	0.62	0.07	0.53	0.07	0.20	0.03	0.19	0.02	3200
S22	2.4	0.60	2.48	0.49	0.13	0.49	0.06	0.40	0.09	0.24	0.03	0.18	0.02	2500
S23	1.8	0.45	1.84	0.40	0.08	0.31	0.03	0.27	0.06	0.15	0.02	0.09	<0.02	1800
S24	3.0	0.76	3.14	0.65	0.13	0.64	0.08	0.49	0.09	0.24	0.04	0.20	0.03	3100
Min	1.20	0.31	1.28	0.24	0.07	0.12	0.03	0.22	0.03	0.09	0.02	0.08	0.02	1300
Max	6.40	1.69	6.88	1.42	0.34	1.18	0.16	1.00	0.18	0.49	0.07	0.43	0.06	9600
Ave.	3.36	0.85	3.39	0.70	0.17	0.66	0.08	0.57	0.11	0.27	0.04	0.24	0.04	3604
St.Dev	1.08	0.27	1.04	0.23	0.06	0.21	0.03	0.18	0.04	0.08	0.01	0.09	0.01	1296

Table 3.17: REE and Al concentrations (in ppm) in shore samples (analytical error is <0.01)

Sample	LREE (ppm)					HREE (ppm)								ppm
	La	Pr	Nd	Sm	Eu	Gd	Tb	Dy	Ho	Er	Tm	Yb	Lu	Al
B1	1.0	0.25	0.78	0.25	0.05	0.19	0.03	0.13	0.03	0.12	<0.02	0.07	<0.02	700
B2	0.7	0.18	0.71	0.14	0.05	0.16	<0.02	0.16	0.03	0.06	<0.02	0.07	<0.02	600
B3	1.0	0.22	0.87	0.24	0.04	0.21	<0.02	0.16	0.03	0.10	<0.02	0.08	<0.02	700
B4	1.4	0.33	1.26	0.30	0.08	0.27	<0.02	0.20	0.04	0.11	<0.02	0.09	<0.02	1100
B5	1.1	0.29	0.99	0.21	0.04	0.13	0.03	0.21	0.05	0.08	<0.02	0.08	<0.02	800
B6	1.1	0.23	1.01	0.22	0.06	0.13	0.03	0.19	0.04	0.05	<0.02	0.07	<0.02	800
B7	0.7	0.18	0.69	0.17	0.03	0.10	0.03	0.16	0.02	0.05	<0.02	0.04	<0.02	600
B8	0.8	0.20	0.74	0.18	0.03	0.16	0.02	0.14	<0.02	0.06	<0.02	0.04	<0.02	600
B9	1.2	0.32	1.26	0.26	0.06	0.19	0.03	0.21	0.03	0.08	<0.02	0.10	<0.02	1000
B10	0.9	0.23	0.81	0.19	0.04	0.12	0.03	0.13	<0.02	0.08	<0.02	0.08	<0.02	800
B11	<0.5	0.11	0.48	0.07	<0.02	0.10	0.02	0.07	<0.02	0.02	<0.02	0.04	<0.02	400
B12	0.6	0.19	0.58	0.14	0.03	0.16	0.04	0.09	<0.02	0.04	<0.02	0.06	<0.02	600
B13	0.6	0.15	0.58	0.12	0.03	0.08	<0.02	0.10	<0.02	0.06	<0.02	0.06	<0.02	500
B14	0.6	0.16	0.67	0.13	0.03	0.13	<0.02	0.08	0.02	0.05	<0.02	0.05	<0.02	500
B15	1.4	0.36	1.39	0.26	0.07	0.24	0.02	0.22	0.04	0.10	<0.02	0.09	<0.02	1000
B16	1.1	0.25	1.04	0.21	0.07	0.18	<0.02	0.22	0.04	0.08	<0.02	0.07	<0.02	900
Min	0.60	0.11	0.48	0.07	0.03	0.08	0.02	0.07	0.02	0.02	-	0.04	-	400
Max	1.40	0.36	1.39	0.30	0.08	0.27	0.04	0.22	0.05	0.12	-	0.10	-	1100
Ave.	0.95	0.23	0.87	0.19	0.05	0.16	0.03	0.15	0.03	0.07	-	0.07	-	725
St.Dev.	0.23	0.05	0.22	0.05	0.01	0.04	0.00	0.04	0.01	0.02	-	0.01	-	165.6

Table 3.18: REE and Al concentrations (in ppm) in bottom sediment samples (analytical error is <0.01)

Sample	LREE (ppm)					HREE (ppm)								ppm
	La	Pr	Nd	Sm	Eu	Gd	Tb	Dy	Ho	Er	Tm	Yb	Lu	Al
M1 C	1.1	0.29	1.27	0.27	0.06	0.22	<0.02	0.14	0.03	0.08	<0.02	0.1	<0.02	8210
M1 M	1.4	0.38	1.5	0.3	0.08	0.27	0.03	0.29	0.05	0.14	<0.02	0.11	<0.02	
M1 F	2.1	0.56	2.15	0.41	0.11	0.42	0.05	0.42	0.07	0.16	<0.02	0.19	0.03	
M2 C	<0.5	0.09	0.25	0.11	<0.02	0.06	<0.02	0.05	<0.02	0.03	<0.02	0.03	<0.02	2974
M2 M	0.5	0.13	0.54	0.12	0.03	0.12	<0.02	0.08	<0.02	0.04	<0.02	0.05	<0.02	
M2 F	1.9	0.43	1.99	0.33	0.1	0.39	0.04	0.29	0.06	0.15	0.03	0.16	<0.02	
M3 C	0.9	0.27	0.95	0.16	0.04	0.15	<0.02	0.18	<0.02	0.07	<0.02	0.05	<0.02	2974
M3 M	1	0.26	1.1	0.18	0.03	0.24	<0.02	0.12	0.02	0.07	<0.02	0.06	<0.02	
M3 F	1.6	0.4	1.6	0.33	0.07	0.36	<0.02	0.24	0.04	0.12	<0.02	0.11	<0.02	
M4 C	<0.5	0.04	0.12	0.03	<0.02	0.04	<0.02	0.04	<0.02	<0.02	<0.02	<0.02	<0.02	1903
M4 M	0.7	0.15	0.56	0.13	0.04	0.11	<0.02	0.09	<0.02	0.06	<0.02	0.05	<0.02	
M4 F	1.2	0.26	1.1	0.26	0.05	0.21	<0.02	0.19	0.04	0.09	<0.02	0.09	<0.02	
M5 C	0.5	0.12	0.61	0.12	0.03	0.09	<0.02	0.1	0.03	0.04	<0.02	0.04	<0.02	3212
M5 M	1	0.26	1.06	0.2	0.05	0.14	<0.02	0.15	0.03	0.07	<0.02	0.06	<0.02	
M5 F	1.8	0.41	1.82	0.39	0.11	0.39	0.02	0.31	0.06	0.19	0.02	0.13	<0.02	
M6 C	0.5	0.14	0.55	0.11	0.03	0.13	<0.02	0.1	0.02	0.03	<0.02	0.05	<0.02	3212
M6 M	1	0.27	1.08	0.3	0.05	0.18	<0.02	0.2	0.03	0.08	<0.02	0.08	<0.02	
M6 F	1.4	0.37	1.31	0.28	0.05	0.3	0.02	0.19	0.04	0.12	<0.02	0.09	<0.02	
M7 C	0.7	0.17	0.72	0.16	0.04	0.09	<0.02	0.14	0.03	0.04	<0.02	0.06	<0.02	3569
M7 M	1.2	0.3	1.3	0.24	0.05	0.19	<0.02	0.15	0.03	0.09	<0.02	0.07	<0.02	
M7 F	1.7	0.43	1.67	0.4	0.1	0.36	0.03	0.29	0.05	0.14	<0.02	0.13	<0.02	

Table 3.18: REE and Al concentrations (in ppm) in bottom sediment samples (analytical error is <0.01) (continued)

Sample	La	Pr	Nd	Sm	Eu	Gd	Tb	Dy	Ho	Er	Tm	Yb	Lu	Al
M8 C	1	0.24	1.14	0.2	0.05	0.21	<0.02	0.17	0.04	0.09	<0.02	0.07	<0.02	5830
M8 M	1.5	0.38	1.43	0.32	0.05	0.41	0.03	0.29	0.04	0.14	<0.02	0.08	<0.02	
M8 F	2.3	0.53	2.46	0.55	0.08	0.54	0.04	0.41	0.08	0.21	0.02	0.2	0.03	
M9 C	2.3	0.25	0.87	0.2	0.04	0.15	0.03	0.18	<0.02	0.09	<0.02	0.08	<0.02	4759
M9 M	1.4	0.32	1.33	0.28	0.05	0.22	0.04	0.23	0.03	0.12	<0.02	0.05	<0.02	
M9 F	2.3	0.56	2.09	0.5	0.1	0.38	0.05	0.38	0.05	0.18	<0.02	0.21	<0.02	
M10 C	<0.5	0.04	0.17	0.03	<0.02	0.06	<0.02	0.04	<0.02	0.03	<0.02	<0.02	<0.02	1546
M10 M	<0.5	0.07	0.30	0.09	<0.02	0.04	<0.02	0.04	<0.02	<0.02	<0.02	0.03	<0.02	
M10 F	0.7	0.19	0.81	0.17	0.04	0.13	0.02	0.1	<0.02	0.06	<0.02	0.08	<0.02	
M11 C	<0.5	0.04	0.15	0.03	<0.02	<0.02	<0.02	0.03	<0.02	<0.02	<0.02	<0.02	<0.02	951
M11 M	<0.5	0.05	0.16	0.04	<0.02	0.02	<0.02	0.03	<0.02	<0.02	<0.02	<0.02	<0.02	
M11 F	<0.5	0.1	0.42	0.07	<0.02	0.05	<0.02	0.08	<0.02	0.03	<0.02	0.02	<0.02	
M12 C	<0.5	0.05	0.21	0.05	<0.02	0.03	<0.02	0.02	<0.02	<0.02	<0.02	<0.02	<0.02	1133
M12 M	<0.5	0.06	0.24	0.04	<0.02	0.05	<0.02	0.03	<0.02	<0.02	<0.02	0.02	<0.02	
M12 F	<0.5	0.08	0.35	0.08	<0.02	0.05	<0.02	0.05	<0.02	0.03	<0.02	0.02	<0.02	
M13C	<0.5	0.05	0.21	0.06	<0.02	0.06	<0.02	0.05	<0.02	0.02	<0.02	<0.02	<0.02	1070
M13 M	<0.5	0.1	0.31	0.04	<0.02	0.11	<0.02	0.05	<0.02	0.03	<0.02	0.03	<0.02	
M13 F	0.6	0.15	0.69	0.13	<0.02	0.12	0.02	0.08	<0.02	0.05	<0.02	0.04	<0.02	
M14 C	0.9	0.23	1.04	0.19	0.04	0.15	0.03	0.14	0.02	0.07	<0.02	0.06	<0.02	4283
M14 M	1.5	0.35	1.33	0.3	0.05	0.21	0.04	0.18	0.04	0.09	<0.02	0.08	<0.02	
M14 F	2.9	0.67	2.62	0.49	0.12	0.46	0.08	0.44	0.07	0.19	0.03	0.18	<0.02	

Table 3.18: REE and Al concentrations (in ppm) in bottom sediment samples (analytical error is <0.01) (continued)

Sample	La	Pr	Nd	Sm	Eu	Gd	Tb	Dy	Ho	Er	Tm	Yb	Lu	Al
M15 C	<0.5	0.11	0.49	0.09	<0.02	0.09	<0.02	0.1	<0.02	0.03	<0.02	0.04	<0.02	2260
M15 M	0.7	0.21	0.76	0.15	0.02	0.13	0.02	0.13	<0.02	0.08	<0.02	0.07	<0.02	
M15 F	1.3	0.36	1.41	0.32	0.06	0.27	0.03	0.18	0.03	0.1	<0.02	0.08	<0.02	
M16 C	0.6	0.17	0.62	0.15	0.02	0.12	0.03	0.12	<0.02	0.06	<0.02	0.05	<0.02	2498
M16 M	0.8	0.22	0.84	0.16	0.05	0.16	0.03	0.17	0.02	0.04	<0.02	0.07	<0.02	
M16 F	1.4	0.34	1.2	0.23	0.06	0.2	0.03	0.16	0.03	0.1	<0.02	0.07	<0.02	
M17 C	4.7	1.29	5.17	1.06	0.23	0.92	0.16	0.82	0.12	0.36	0.05	0.27	0.04	14754
M17 M	4.3	1.16	4.4	0.82	0.21	0.84	0.12	0.62	0.11	0.37	0.04	0.27	0.02	
M17 F	4.3	1.1	4.16	0.89	0.22	0.74	0.13	0.63	0.12	0.34	0.04	0.29	0.04	
M18 C	2	0.51	1.94	0.39	0.1	0.41	0.07	0.39	0.05	0.21	<0.02	0.12	<0.02	7258
M18 M	2.5	0.63	2.45	0.47	0.1	0.44	0.07	0.32	0.06	0.18	0.03	0.15	<0.02	
M18 F	2.9	0.77	2.98	0.72	0.15	0.57	0.1	0.39	0.07	0.2	0.03	0.24	<0.02	
Min	0.50	0.04	0.12	0.03	0.02	0.02	0.02	0.02	0.02	0.02	0.02	0.02	0.02	951
Max	4.70	1.29	5.17	1.06	0.23	0.92	0.16	0.82	0.12	0.37	0.05	0.29	0.04	14754
Ave.	1.59	0.32	1.26	0.26	0.07	0.24	0.05	0.20	0.05	0.11	0.03	0.10	0.03	4022
St.Dev.	0.77	0.20	0.77	0.16	0.04	0.16	0.03	0.12	0.02	0.06	0.01	0.05	0.01	3372

3.7 Radionuclide Activity Concentrations

The natural radioactivity concentrations of ^{238}U (^{226}Ra), ^{232}Th and ^{40}K were measured for soil, shore and bottom sediment samples, using gamma spectrometry, their results are shown in Tables 3.19, 3.20 and 3.21. The average activity concentrations of ^{238}U (^{226}Ra) are 15.68 ± 0.56 , 4.43 ± 0.39 and 4.73 ± 0.47 Bq/kg in soil, shore and bottom sediment samples, respectively. The activity concentrations of ^{238}U (^{226}Ra) fluctuate in the soil samples with a minimum value of 5.33 ± 2.46 and a maximum value of 64.82 ± 8.7 Bq/kg. Further more, ^{238}U (^{226}Ra) shows a narrower range in shore and bottom sediment samples between 3.04 ± 5.78 to 6.2 ± 5.08 and 1.24 ± 1.52 to 10.63 ± 4.62 , Bq/kg, respectively.

The estimated average activity concentrations of ^{232}Th show wide variations in the studied area. The activity concentrations vary between 2.23 ± 0.10 and 18.15 ± 0.43 Bq/kg in soil samples and between 0.87 ± 0.18 and 2.46 ± 0.26 Bq/kg in shore samples, and finally between 0.36 ± 0.49 and 7.29 ± 0.34 Bq/kg in bottom sediments with average of 8.3 ± 0.23 , 1.68 ± 0.17 and 1.83 ± 0.24 Bq/kg, respectively.

The activity concentrations of ^{40}K range from 141.35 ± 8.6 to 611.16 ± 14.9 Bq/kg with an average of 349.72 ± 11.76 Bq/kg in soil and from 40.71 ± 5.59 to 240.91 ± 9.7 Bq/kg with an average of 106.3 ± 7.27 Bq/kg in shore and from 7.81 ± 2.7 to 544.12 ± 14.8 Bq/kg with an average of 105.23 ± 10.03 Bq/kg in bottom sediment samples.

Table 3.19: Radionuclides Activity concentrations and radium equivalent in (Bq/kg) and absorbed dose (nGy/hr) in soil samples

S	^{238}U (^{226}Ra)	^{232}Th	^{40}K	Rad. eq.	Abs. dose
S1	5.33±0.25	2.23±0.10	141.35±8.6	19.41±1.05	9.71±0.21
S2	8.48±0.58	3.82±0.15	323.84±11.3	38.88±1.66	19.73±0.40
S3	9.05±0.31	3.31±0.20	239.4±8.4	32.22±1.23	16.16±0.30
S4	10.29±0.38	4.21±0.20	287.24±10.2	38.43±1.44	19.28±0.33
S5	10.3±0.45	4.51±0.21	308.52±11.7	40.5±1.63	20.35±0.38
S6	14.51±0.39	9.37±0.22	394.97±10.15	58.33±1.50	28.84±0.36
S7	13.3±0.62	11.52±0.23	485.04±12.9	67.11±1.93	33.33±0.47
S8	7.66±0.34	4.65±0.22	258.4±11.05	34.21±1.50	17.12±0.34
S9	15.57±0.47	13.76±0.33	444.97±20.65	69.51±2.53	34.06±0.50
S10	16.92±0.56	8.9±0.22	447.34±10.45	64.1±1.67	31.85±0.43
S11	64.82±0.87	7.08±0.10	455.57±12.65	110.03±1.98	53.22±0.51
S12	12.67±0.39	8.4±0.18	314.95±10.1	48.93±1.42	24.06±0.33
S13	17.59±0.48	12.46±0.23	362.78±10.9	63.34±1.65	30.78±0.41
S14	14.8±0.55	11.34±0.27	347.82±14	57.8±2.01	28.19±0.47
S15	18.63±0.73	10.91±0.22	465.2±12.9	70.05±2.05	34.6±0.53
S16	22.02±0.52	7.6±0.24	307.01±10.7	56.54±1.71	27.57±0.43
S17	14.4±0.62	13.21±0.24	389.62±13.15	63.29±1.98	30.88±0.49
S18	12.9±0.97	8.92±0.27	415.5±10.9	57.65±2.20	28.67±0.66
S19	16.44±0.74	18.15±0.43	340.78±12.7	68.63±2.33	32.77±0.66
S20	15.16±0.54	5.14±0.21	174.07±8.05	35.92±1.45	17.37±0.41
S21	7.97±0.84	8.11±0.31	611.16±14.9	66.62±2.42	34.07±0.63
S22	17.28±0.69	6.47±0.32	251.86±10.95	45.93±1.99	22.4±0.56
S23	17.98±0.66	6.11±0.29	243.16±12.5	45.43±2.04	22.13±0.53
S24	12.21±0.39	9.35±0.19	382.62±12.5	55.04±1.62	27.24±0.35
Min	5.33±0.25	2.23±0.10	141.35±8.6	19.41±1.05	9.71±0.21

Table 3.19: Radionuclides Activity concentrations and radium equivalent in (Bq/kg) and absorbed dose (nGy/hr) in soil samples (continued)

S	$^{238}\text{U}(^{226}\text{Ra})$	^{232}Th	^{40}K	Rad. eq.	Abs. dose
Max	64.82±0.87	18.15±0.43	611.16±14.9	110.03±1.98	53.22±0.51
Ave.	15.68±0.56	8.31±0.23	349.72±11.76	54.5±1.79	26.85±0.44
St.Dev.	11.23	3.87	107.16	18.31	8.84

Table 3.20: Radionuclides Activity concentrations and radium equivalent in (Bq/kg) and absorbed dose (nGy/hr) in shore samples

S	$^{238}\text{U}(^{226}\text{Ra})$	^{232}Th	^{40}K	Rad. eq.	Abs. dose
B1	5.14±0.40	2.04±0.15	101.45±8.25	15.87±1.24	7.84±0.31
B2	4.39±0.34	1.5±0.19	89.33±6.1	13.41±1.08	6.66±0.30
B3	4.22±0.22	1.66±0.21	86.81±5.9	13.29±0.97	6.58±0.25
B4	5.87±0.38	2±0.17	186.42±7.95	23.09±1.23	11.7±0.31
B5	5.77±0.36	2.23±0.13	99.32±6.85	16.61±1.07	8.15±0.27
B6	6.2±0.51	1.82±0.17	142.01±7.9	19.73±1.35	9.88±0.37
B7	3.55±0.51	1.25±0.15	71.94±7.35	10.88±1.30	5.4±0.36
B8	3.22±0.47	1.5±0.22	128.41±7.5	15.24±1.37	7.74±0.39
B9	4.23±0.54	2.17±0.20	116.86±7.25	16.34±1.38	8.14±0.40
B10	4.44±0.51	2.46±0.26	102.19±9.25	15.83±1.60	7.8±0.43
B11	3.15±0.21	0.87±0.18	40.71±5.59	7.53±0.94	3.68±0.24
B12	3.14±0.25	1.1±0.12	47.14±5.9	8.35±0.88	4.09±0.21
B13	3.33±0.28	0.98±0.13	61.62±6.45	9.48±0.97	4.7±0.24
B14	3.04±0.58	1.27±0.11	90.42±7.5	11.82±1.31	5.94±0.37
B15	5.37±0.30	2.22±0.17	240.91±9.7	27.09±1.29	13.87±0.28
B16	5.78±0.36	1.76±0.17	95.19±6.5	15.63±1.11	7.7±0.30
Min	3.04±0.58	0.87±0.18	40.71±5.59	7.53±0.94	3.68±0.24
Max	6.2±0.51	2.46±0.26	240.91±9.7	27.09±1.29	13.87±0.28
Ave.	4.43±0.39	1.68±0.17	106.3±7.27	15.01±1.19	7.49±0.31
St.Dev.	1.12	0.49	50.68	5.19	2.68

Table 3.21: Radionuclides Activity concentrations and radium equivalent in (Bq/kg) and absorbed dose (nGy/hr) in bottom sediment samples

S	$^{238}\text{U}(^{226}\text{Ra})$	^{232}Th	^{40}K	Rad. eq.	Abs. dose
M1	6.98±0.54	2.19±0.49	76.93±14.6	16.04±2.37	7.76±0.61
M2	2.83±0.53	0.95±0.40	38.05±15	7.11±2.24	3.47±0.54
M3	3.59±0.42	2.34±0.35	152.29±19.4	18.66±2.41	9.42±0.49
M4	2.03±0.47	0.64±0.34	21.84±8.2	4.62±1.60	2.23±0.46
M5	5.54±0.74	1.54±0.31	93.65±16.95	14.95±2.50	7.39±0.60
M6	3.66±0.50	1.24±0.22	51.94±7.75	9.44±1.40	4.61±0.40
M7	5.83±0.38	1.89±0.24	112.27±15.25	17.17±1.90	8.51±0.39
M8	8.83±0.79	3.38±0.40	166.91±15.55	26.51±2.55	13.08±0.67
M9	7.12±0.31	1.98±0.11	121.04±10.6	19.28±1.28	9.53±0.25
M10	1.3±0.15	0.36±0.49	10.6±3	2.62±0.45	1.26±0.11
M11	1.24±0.15	0.54±0.45	7.81±2.7	2.6±0.42	1.22±0.11
M12	1.53±0.16	0.42±0.15	11.45±2.7	3.01±0.58	1.44±0.18
M13	1.96±0.17	0.54±0.69	15.95±3.05	3.95±0.50	1.89±0.13
M14	10.63±0.46	1.6±0.14	99.87±6.7	20.6±1.18	10.04±0.33
M15	2.49±0.20	1.17±0.61	58.51±4.95	8.67±0.66	4.3±0.15
M16	3.2±0.67	1.12±0.24	30.49±4.95	7.14±1.40	3.42±0.48
M17	9.47±0.86	7.29±0.34	544.12±14.8	61.79±2.49	31.47±0.67
M18	6.88±0.87	3.71±0.41	280.48±14.4	33.78±2.57	17.11±0.71
Min	1.24±0.15	0.36±0.49	7.81±2.7	2.6±0.42	1.22±0.11
Max	10.63±0.46	7.29±0.34	544.12±14.8	61.79±2.49	31.47±0.67
Ave.	4.73±0.47	1.83±0.24	105.23±10.03	15.44±1.58	7.68±0.40
St.Dev.	3.01	1.67	130.14	14.58	7.43

3.8 Radium Equivalent Activity Concentrations and Absorbed Dose Rates

The Estimated values of Radium equivalent and absorbed dose are shown in Tables 3.19, 3.20 and 3.21. The estimated average value of Radium equivalent activities concentrations in soil, shore and bottom sediment samples are 54.50 ± 1.79 , 15.01 ± 1.19 and 15.44 ± 1.58 Bq/kg. Their activity concentrations vary between 19.41 ± 1.05 and 110.03 ± 1.98 in soil samples and between 7.53 ± 0.97 and 27.09 ± 1.29 in shore samples and between 2.60 ± 0.42 and 61.79 ± 2.49 Bq/kg in bottom sediments. The average values of the estimated absorbed dose in soil, shore and bottom sediment samples are 26.85 ± 0.44 , 7.49 ± 0.31 and 7.68 ± 0.40 nGy/hr, respectively. The estimated absorbed dose (in nGy/hr) rang from 9.71 ± 0.21 to 53.22 ± 0.51 and from 3.08 ± 0.24 to 13.87 ± 0.28 in soil and shore samples, respectively and from 1.22 ± 0.11 to 31.47 ± 0.66 in bottom sediments.

3.9 Alpha Spectrometry

Among the different uranium isotopes, both ^{234}U and ^{238}U are of particular interest, as the shorter half-life ^{234}U (2.45×10^5 year) is in secular equilibrium in closed system with long half-life ^{238}U (4.47×10^9 year). However, any closed system is disturbed by physico-chemical weathering processes, that operate when rocks become exposed at the Earth's surface, which affect the $^{234}\text{U}/^{238}\text{U}$ equilibrium. Monitoring the $^{234}\text{U}/^{238}\text{U}$ activity ratio will be a good indicator of the origin of uranium either natural (from weathering of igneous rocks and ore bodies) or anthropogenic (from industrial use, manufacturing or handling of depleted U) (Dresel et al., 2002). Monitoring also can help in indicating activities associated with variation of $^{234}\text{U}/^{238}\text{U}$ activity ratio in the studied environment. On the other hand, differences in $^{234}\text{U}/^{238}\text{U}$ ratio can be used in some cases to study the pathway of U

applied with fertilizers from an agricultural field downstream (Zielinski et al., 2000). In order to determine the isotopic composition of uranium, alpha spectrometry (measuring alpha particle emitting) is used. Table 3.22 shows $^{234}\text{U}/^{238}\text{U}$ ratios for ten samples, which were selected based on their gamma activity concentrations. Based on the current alpha spectra, the peaks of ^{234}U and ^{238}U are most common while ^{235}U peak is weak. That is because both ^{234}U and ^{238}U emit distinct alpha particles at specific energy level while ^{235}U emits a mixed energy particles as the crustal uranium contains lower percentage of ^{235}U , compared with ^{234}U and ^{238}U (NNDC 2011). The small radioactive percentage of ^{235}U gave very small peak, which was not distinguished in current alpha spectra. The results indicate that the $^{234}\text{U}/^{238}\text{U}$ activity ratios show wide range from 0.59 to 2.24.

Table 3.22: ^{234}U and ^{238}U activity ratios for selected samples

S	^{234}U Bq/kg	^{238}U Bq/kg	$^{234}\text{U}/^{238}\text{U}$ ratio
S7	0.7±0.04	0.5±0.03	1.40
S9	12±0.72	13±0.78	0.92
S5	15.9±0.95	13.4±0.80	1.19
S11	3.9±0.24	2.2±0.13	1.77
S16	5.6±0.34	2.5±0.15	2.24
S17	6.9±0.42	7±0.42	0.99
S20	18.7±1.30	31.5±1.10	0.59
S23	26.3±1.58	28±1.68	0.94
B12	56.8±3.51	50.7±3.04	1.12
M11	14.0±0.84	11.3±0.68	1.24
Ave.	16.07±0.98	14.25±0.88	1.24

3.10 Relationship between Heavy Metals, REE and Natural Radioactivity Concentrations

Despite the variability of concentrations of heavy metals, REE and the natural radioactivity concentrations measured in the studied samples, their highest values are recorded in three samples (Figure 3.1). All measured concentrations (Figure 3.2) in S14, B4 and M17 from soil, shore and bottom sediment samples, respectively, show higher values than the measured averages. Highest concentrations of REE, Cu, Pb, Co, Mo, V and Cr are recorded in S14 while M17 shows the highest values of Rad_{eq}, Zn, Ni, As and Cd, as shown in Figure 3.2.

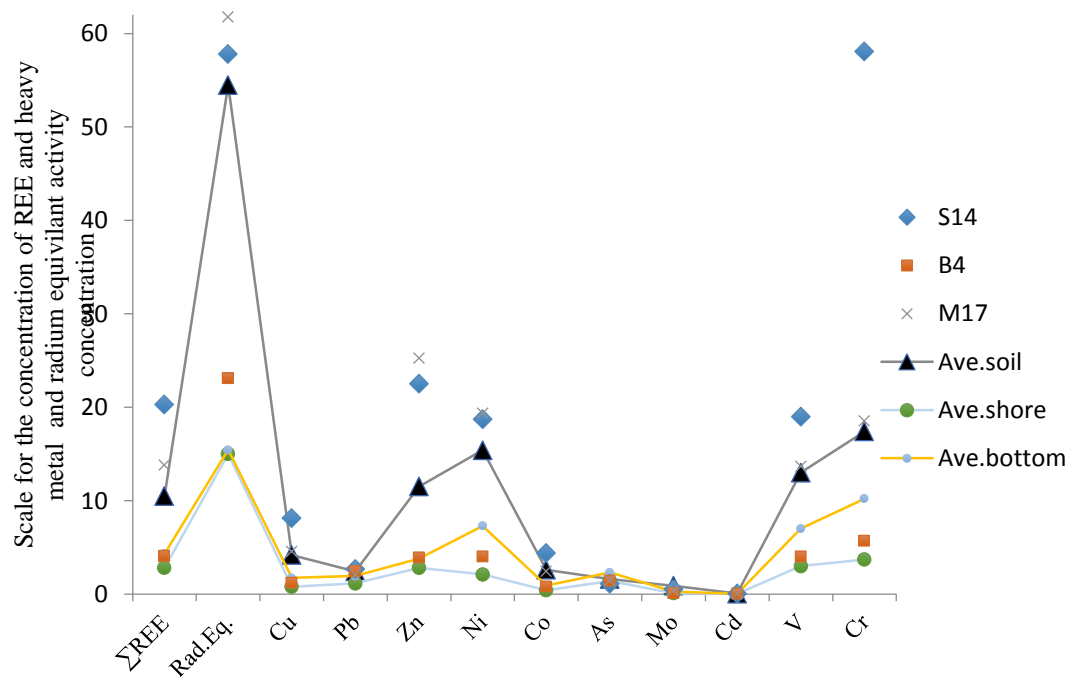


Figure 3.2: Concentrations of heavy metals, total REE and radium equivalent in S14, B4 and M17, in addition to their average values in soil, shore and bottom sediments

Chapter 4: Discussion

4.1 Grain Size Analysis

4.1.1 Grain Size Parameters

The mean size values in the shore, soil and bottom samples are on average 0.35 mm, 0.49 mm and 0.56 mm, respectively. According to Udden (Udden, 1914), the ranges of the sizes for very coarse, coarse, medium, fine, and very fine sand grain sizes are 1-2 mm, 0.5-1 mm, 0.25-0.5 mm, 125-250 μm and 62.5-125 μm , respectively. The grain size of shore and soil is between medium to coarse sand. However, the mean size of shore samples lies in medium sand, while most of the soil samples consists of coarse sand. The dominance of coarse sand in soil samples suggests a higher energy in the depositional environment, which is mainly controlled by wind. Shoreline turbulence prevents small particles from settling and transports them towards the sea (Yuan et al., 2008).

The bottom samples are dominated by coarse and medium sand with a mean size average value of 0.56 mm (coarse sand). The highest mean size reading appears in sample M4 of Sila area, which is associated, during the sampling process, with the presence of very coarse shell fragments and coarse sediments. Figure 4.1 shows that most of the grains range in size from 0.13 to 1.00 mm; i.e. the samples consist of fine to coarse sand. This result is also presented in Figure 4.2. Compared to the rest of the samples, the soil samples, S1-S24, contained more grains with size greater than 2 mm, but they also contained more grains with size 0.06 mm or less, which means that the standard deviation is relatively high. Figure 4.2 also shows the variation in the composition of each samples even if they are located in the same area.

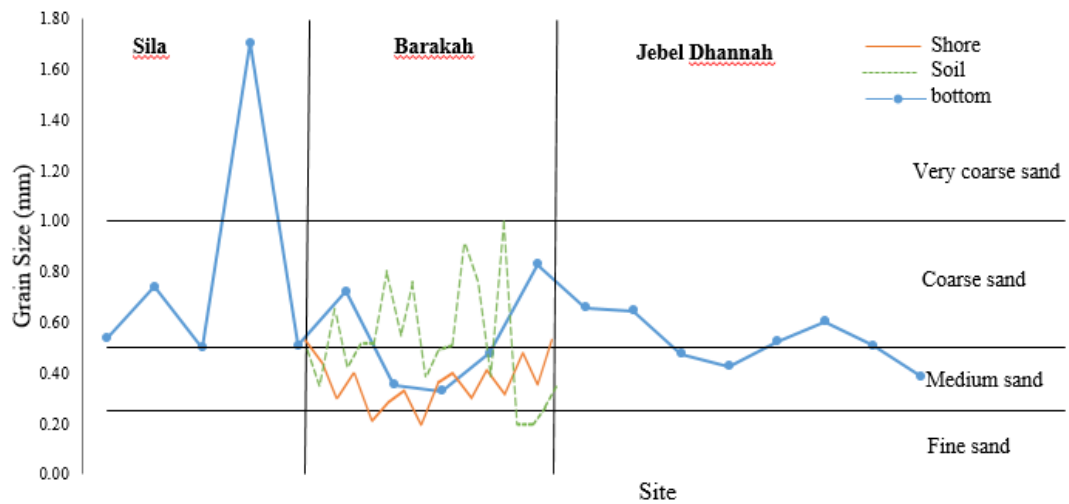


Figure 4.1: Mean size distribution for all 58 samples in mm. All the samples, grouped in soil, shore and bottom, are shown in this plot. The locations are listed from left to right in chronological order as shown in Table 2.1. The vertical lines separate the samples according to the area they were taken from. The horizontal line show the threshold for the classification of fine, medium and course sand according to Udden classification

The sorting of the grain size depends on several factors such as the extent of weathering, distance of transportation and the energy variation of the depositing agents. The statistical analysis of the grain size values of the 58 samples considered in this study are summarized in Table 3.4. The standard deviations for the shore and soil samples suggesting that the grain sizes are relatively within a narrow range, but they are moderately sorted. The large standard deviation for the marine sediments is suggesting a scattered sorting of the grains as shown in the stacked column (Figure 4.2).

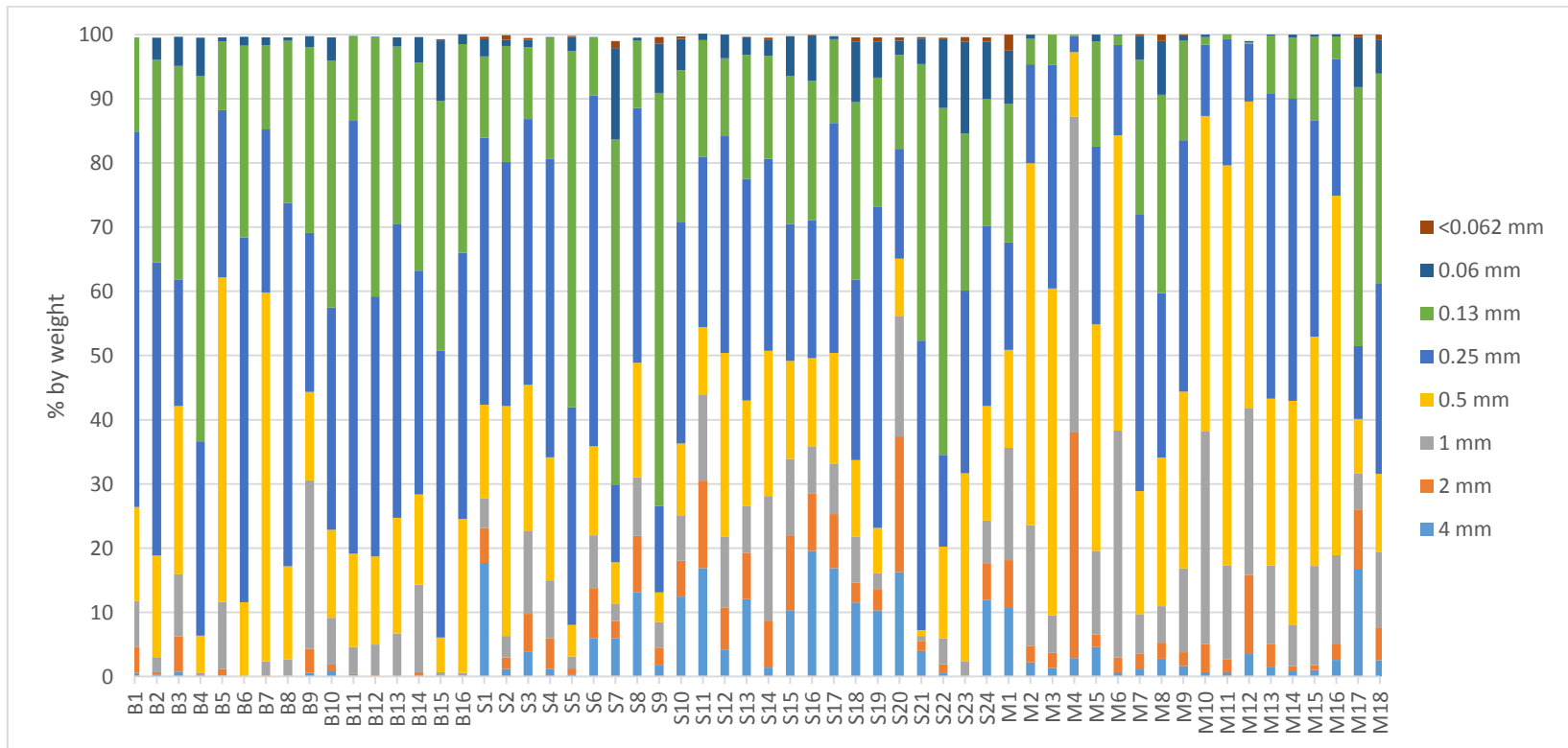


Figure 4.2: Stacked column showing the percent by weight of the grains in the different size ranges

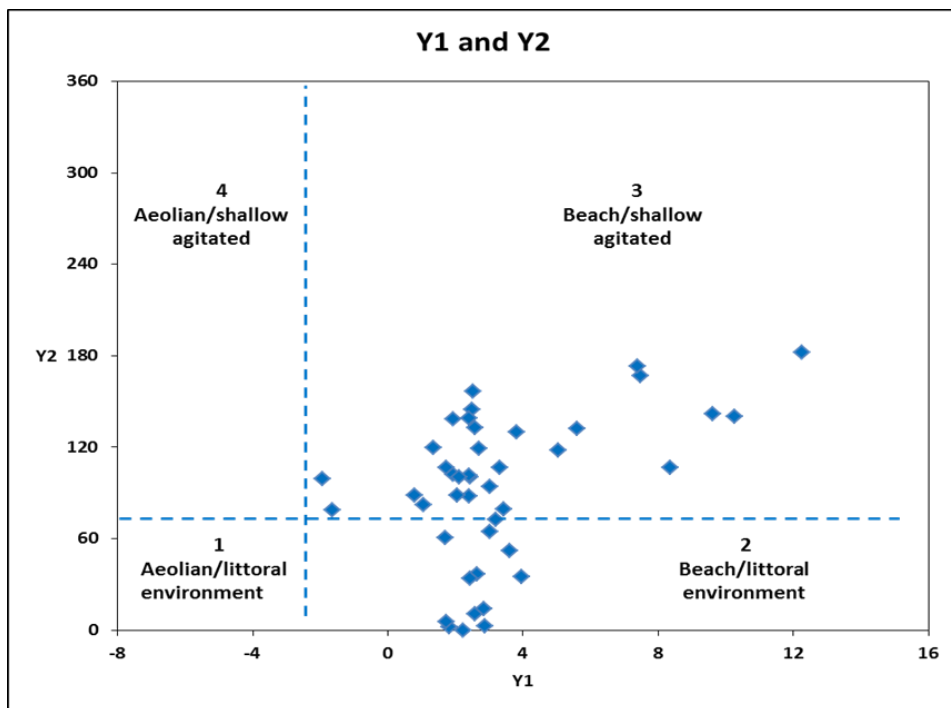


Figure 4.3: Graphical plot of Y1 against Y2

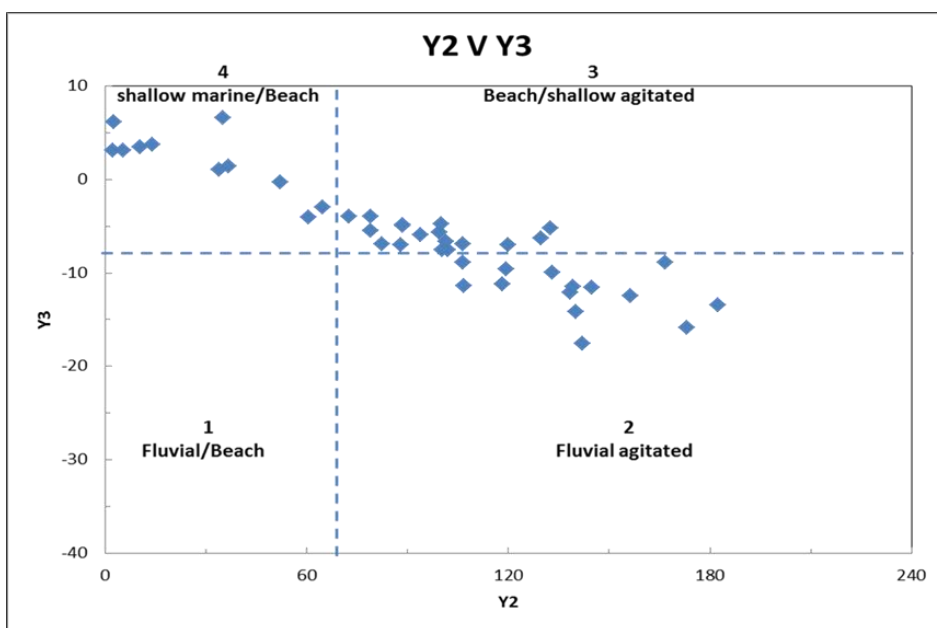


Figure 4.4: Graphical plot of Y2 against Y3

4.1.2 Mechanical and Environments of Deposition

The application of Sahu's (1964) discriminate functions for shore and soil samples was done for determination of the mechanical and environments of deposition. A graphical plot of Y1 vs. Y2 and Y2 vs. Y3 allows four fields of depositional environments (Sahu, 1964) to be distinguished (Figs 4.3 & 4.4). The values of Y1 is greater than -2.74 which indicated that all the studied samples are identified as beach deposits. Values of Y2 calculated for the studied samples indicate that 77.5% of sediments are concluded to be derived from shallow agitated marine environments. While the 22.5 % of the sediments are beach deposition. The 22.5% comes from the soil samples, which mean 100% of the shore sediment samples are derived from shallow agitated marine. Values of Y3 shows that 60% of the sediment samples are shallow marine deposits, while the rest (40%) are fluvial deposits.

4.1.3 Grain Size vs. Heavy Metals in the Bottom Sediment Samples

The relationship between the average concentrations of heavy metal and the grain size of the bottom samples is shown in Figure 4.5. Samples were classified into three size categories: coarse (> 0.5 mm) medium (> 0.25 mm) and fine (> 0.125 mm). The results confirm the inverse relationship between the grain size and levels of concentration of heavy metals. As the grain size gets finer, the specific surface area increases causing an increase in the heavy metal concentration. The only exception is that of Cu, where Cu concentration in fine particles (on average) were less than the medium particles.

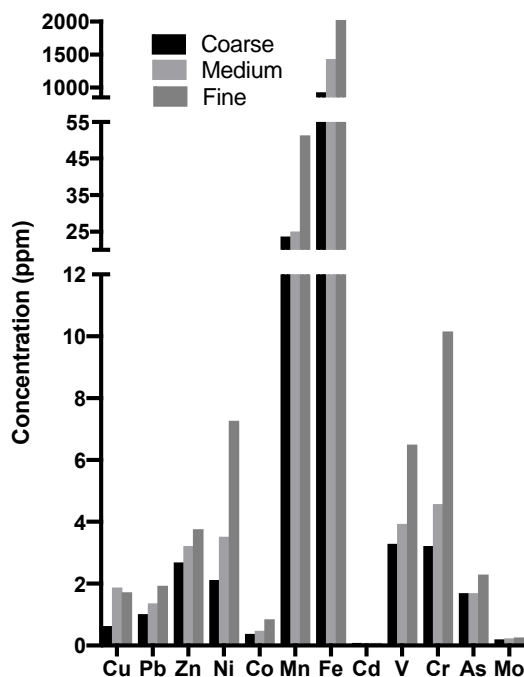


Figure 4.5: Average concentrations (in ppm) of various heavy metals for each of the course, medium and fine grains of the bottom samples

Although, that inverse relationship between the heavy metals concentrations and the grain size is well defined for all heavy metal in Figure 4.5, Table 3.15 in the previous chapter shows some samples with higher values (Ni and Cd) in coarse grains than in fine grains. The formation of agglomerates from contaminated fine grains could be the reason for these exceptions. The agglomeration of the small particles could happen either in the presence of organic matter or by sea salts from the marine sediments (Parizanganeh 2008). Chakraborty et al. (2009) concluded that a higher contamination of heavy metals in the coarse grains is also related to the quality and quantity of organic matter and the distribution of different mineral phases.

4.1.4 Grain Size vs. Carbonate Content in Soil, Shore and Bottom Sediment Samples

Generally, Carbonate content percentage values reveal wide variation in the shore, soil and bottom samples. The bottom samples show highest carbonate content values while soil is the least. Grain size analysis shows that both soil and shore mean grain size fall in medium sand class while the mean grain size for bottom sediment samples is in coarse sand class. A comparison between mean grain size and carbonate content percentage is presented in Figure 4.6. The higher carbonate percentage in both shore and bottom sediments is because coastal sediments usually contain bioclastic carbonate (shell) as well as siliciclastic components. The correlation between mean grain size and carbonate content in soil, shore and bottom samples shows a decreasing trend (Figure 4.7) with weak correlation coefficient of 0.24 or less. The negative correlation between the mean grain size and carbonate content suggest that finer-grain contain more carbonate material. This inverse relation can be due to those coastal sediments have various shapes and densities (Prager et al., 1996).

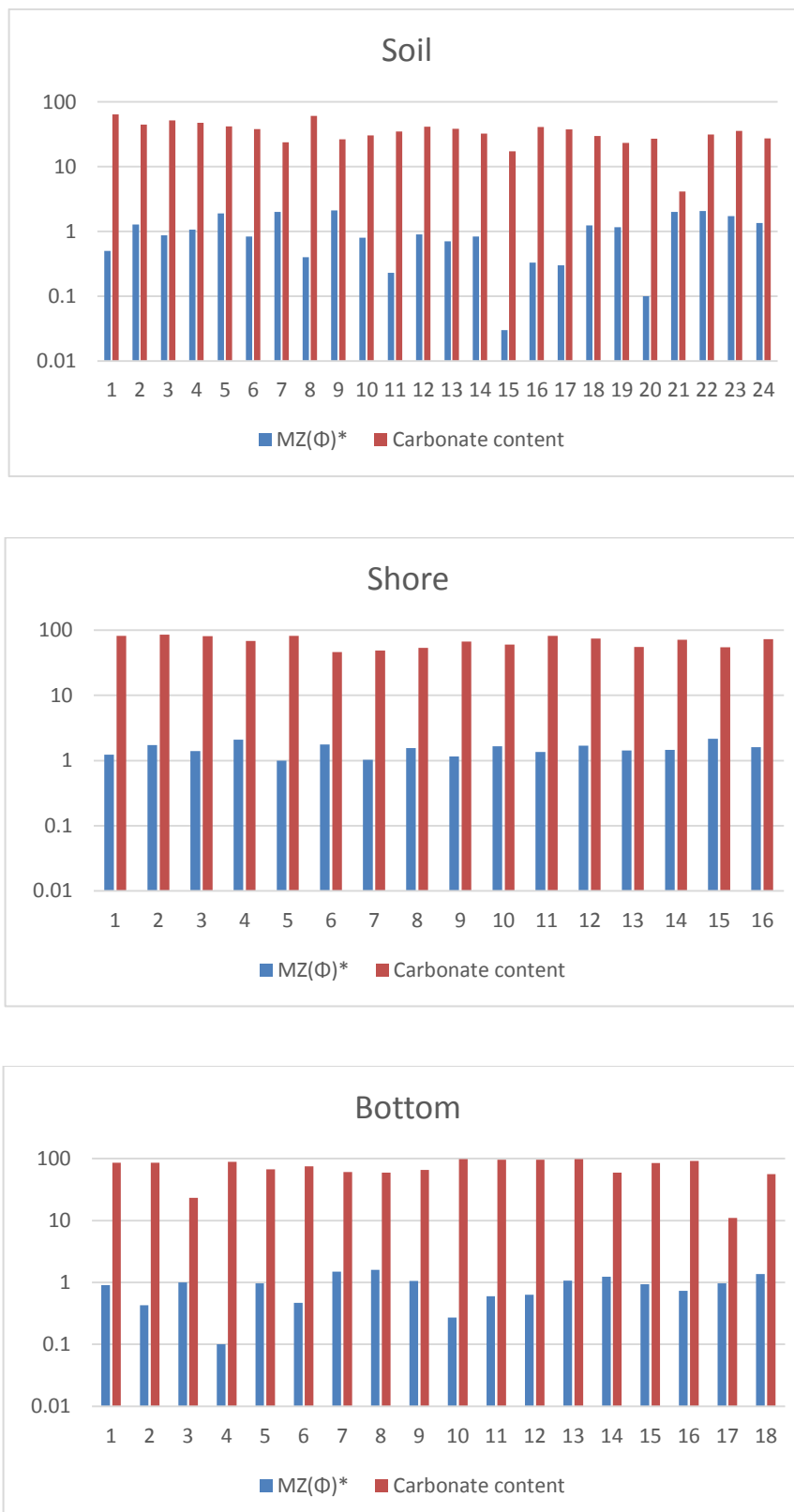


Figure 4.6: Comparison between mean grain size and carbonate percentage in soil, shore and bottom sediment samples

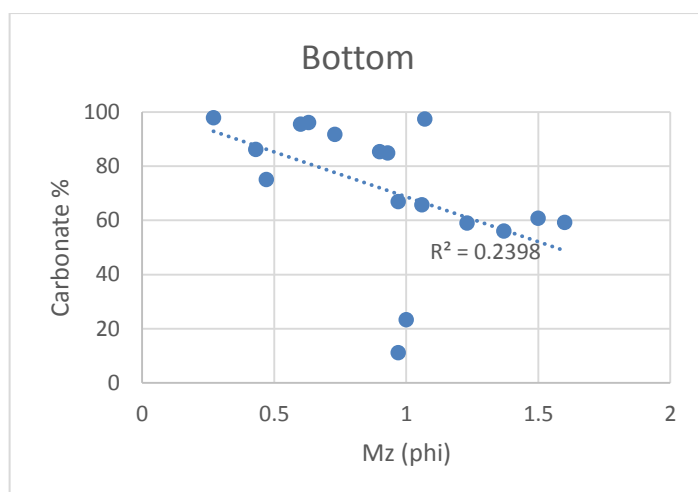
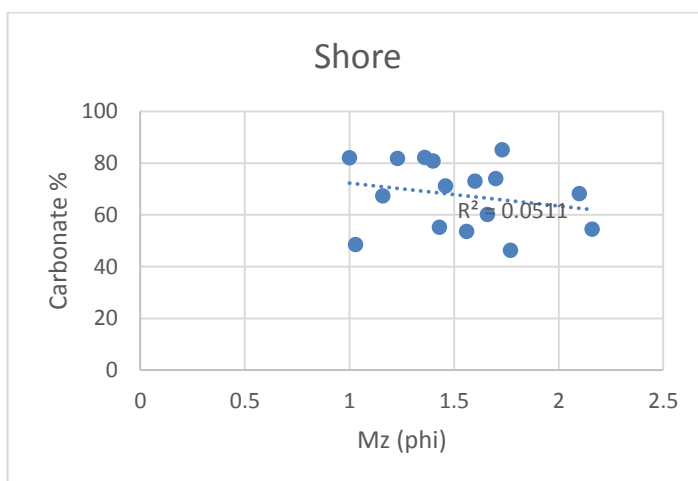
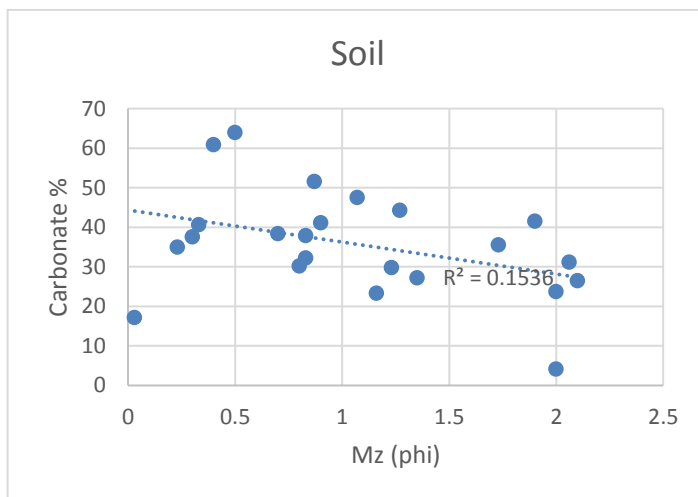


Figure 4.7: Correlation between mean grain size and carbonate percentage in soil, shore and bottom sediment samples

4.2 Geochemistry

4.2.1 Major Oxides Indication

The relationship between the three primary components, CaO for biogenic carbonate, SiO₂ and Al₂O₃ in the beach sand sediments of all samples are shown in ternary diagram in Figure 4.8. The data from the beach sand and bottom sediments of Barakah plot mostly in CaO corner, thus pointing marine biogenic carbonate materials. While the data from Barakah soil plot more closely to SiO₂ side indicating quartz sand. This plot are parallel with the finding from mineralogical composition of the samples where quartz is the major mineral in soil while the major minerals in shore and bottom sediments are aragonite and quartz.

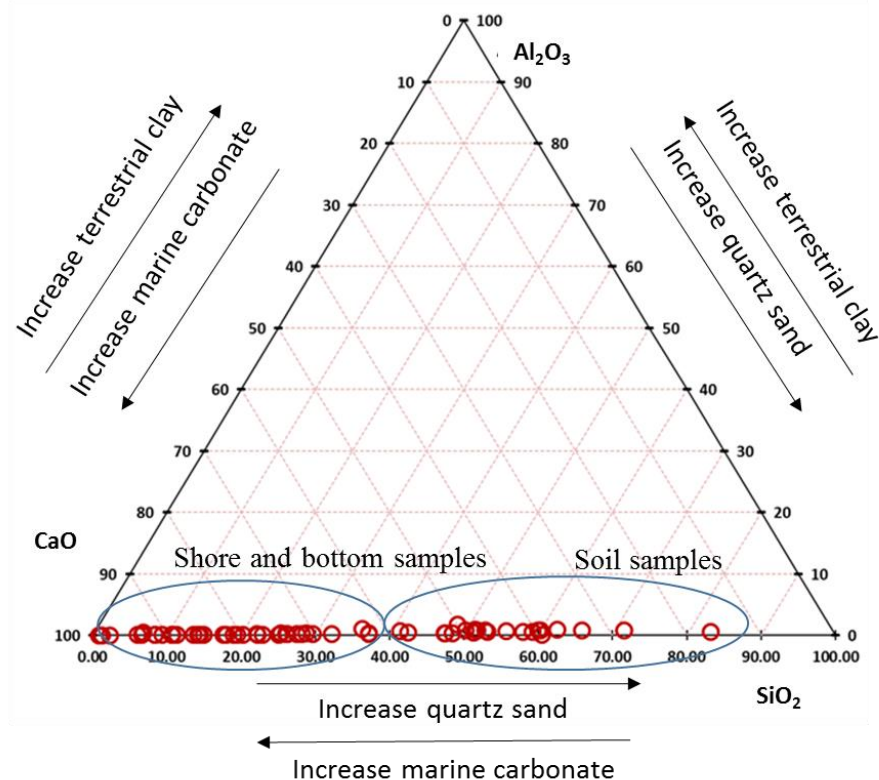


Figure 4.8: CaO, SiO₂ and Al₂O₃ ternary plot for shore, soil and bottom sediments of study area

4.2.2 Heavy Metals Concentration

The average distributions of all heavy metals in the shore, soil and bottom samples is illustrated in Figure 4.9. Both Fe and Mn are present in the highest concentrations, while Cd has the lowest concentrations in all areas. The shore samples reveal the lowest level of the heavy metal concentrations despite having the smallest grain size average (0.35 mm) (Table 3.4) compared to the soil (0.49 mm) and bottom (0.56 mm) samples. Although soil samples are not the finest in the grain size, they show the highest concentrations relative to shore and bottom sediment samples. The correlation between grain size and levels of heavy metal concentrations is not clear in this case because the samples vary from soil samples to shore or bottom sediments. The shore and bottom sediments are subject to the convection cycle of water along with possible tidal activities and turbidities; which can wash away heavy metals (Scoullou et al., 2014). The most contaminated samples are those of the soil, ~ 200 m away from the coastal water. The soil samples are more contaminated than the bottom sediments by almost a factor of four for Cu, Zn, Ni, Co, Mn, Fe, and Mo; by a factor of three for V and Cr; by a factor of two for Pb and Cd and the ratio is close to unity for As. The level of contaminations of the bottom compared to the shore samples are almost equal or higher by a factor of maximum 1.6 with two exceptions, Ni and Mo, where the level is doubled.

The average of heavy metal concentrations in the soil ranked from the lowest to the highest is as of the following: Cd < Mo < As < Pb < Co < Cu < Zn < V < Ni < Cr < Mn < Fe while in shore is Cd < Mo < Co < Cu < Pb < As < Ni < Zn < V < Cr < Mn < Fe and finally in bottom sediment is Cd < Mo < As < Pb < Co < Cu < Zn < V < Ni < Cr < Mn < Fe.

These rankings clearly show that the soil, shore and bottom samples are highly enriched with iron followed by manganese (Figure 4.9). Cadmium and molybdenum show the lowest level of contamination. In the middle range, the contamination level of zinc, nickel, vanadium and chromium is found in upper level whereas lead, copper, cobalt and arsenic is in the lower level.

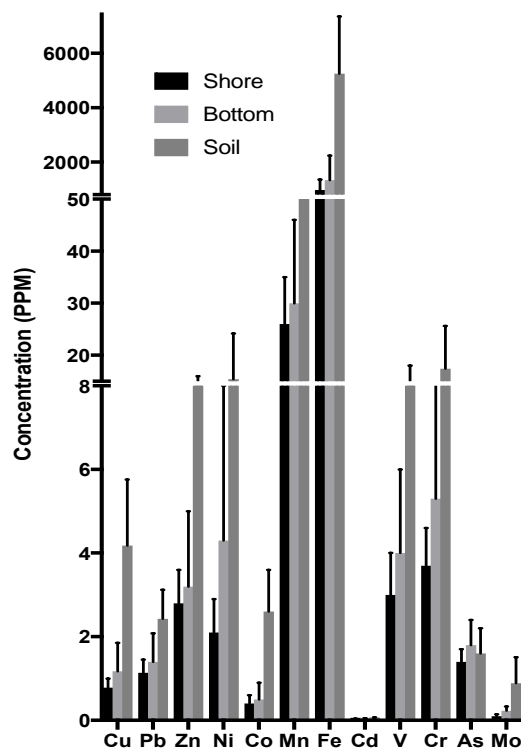


Figure 4.9: Average concentrations (in ppm) of the heavy metals and their standard deviations in the shore, soil and bottom samples

Compared to other soil samples, the soil sample S14 and S15 show higher concentrations of heavy metals. The high concentration depends on the nature of these samples, which consist mainly of salt flat (sabkha). S14 is exceptionally more enriched with Cu (8.11 ppm), Zn (22.5 ppm), Co (4.4 ppm), Fe (10300 ppm), V (19 ppm) and Cr (58.10 ppm). Moreover, B4 shows higher heavy metal concentrations compared to other shore samples, which can be related to the large presence of shell

fragments in the sample. The slightly higher metal concentrations in B4 is as follow: Cu (1.2 ppm), Pb (2.42 ppm), Zn (3.9 ppm), Ni (4.0 ppm), Co (0.8 ppm), Mn (42 ppm), Fe (1300 ppm), V (4 ppm) and Cr (5.7 ppm). The bottom sample M17 is also exceptionally more contaminated with Cu (4.57 ppm), Zn (25 ppm), Ni (19.37 ppm), Co (2.43 ppm), Mn (123.33 ppm), Fe (5300 ppm), Cd (0.08 ppm), V (13.67 ppm) and Cr (18.53 ppm) compared to other bottom samples. The M17 site is 2 km North the Shuwei hat power company, and it is adjacent to a harbor that is 760 m North this site. Table 4.1 shows some characteristics of the locations with highest heavy metal concentrations. It is well established that granulometry, carbonate and organic matter content are important controlling factors in the abundance of heavy metals (McCave, 1984; Horowitz, 1987).

Table 4.1: Characteristics samples location with the maximum heavy metal concentrations (in ppm) in shore, soil and bottom sediment

	Sample	Location/depth of water	Nature of sediments	grain size class	% of carbonate content
soil	S14	2 km south of shoreline	Salt flat	0.83 (coarse sand)	32.28
	S15	2 km south of shoreline	Salt flat	0.03 (fine sand)	17.16
shore	B4	Beach sediment	Shell fragments	2.1 (fine sand)	68.12
	B15	Beach sediment	Shell fragments	2.16 (fine sand)	54.42
bottom sediments	M17	2 km north of a power company 0.7 km north of a harbor 5 meters depth	Dark green sediments	0.97 (coarse sand)	11.02
	M18	4.8 km north of a power company, 2.8 km north of a harbor 6 meters depth	Dark green sediments	1.37 (fine sand)	5.98

4.2.3 Spatial Distribution of Heavy Metals

The maps in Figure 4.10 provide a comprehensive illustration of the spatial distribution of the heavy metals over the studied area. These maps clearly show how soil samples (from areas coded with blue) are more contaminated than the shore and bottom sediments. The shore sediments show lower levels of contamination likely due to the tidal fluctuation and wave currents (Caetano et al., 1997). The relatively higher concentration of heavy metals in the soil samples could be related to the erosion of the bedrock. The studied area is dominated sandstones and limestones from the Miocene age (Alsharhan and Kendall 2003). The southern part of the study area is occupied by sand dunes that are thought to originate from the extensive erosion of the Miocene rocks. On the other hand, Baynunah Formation is composed mainly of sandstones and mudstones from fluvial settings with fossil accumulation at various levels, this Formation is exposed along more than 200 km of the Abu Dhabi coast in the western Al Gharbia region, and extends more than 30 km inland (Whybrow, 1989).

The distributions of Cr, Ni and Mn in shore, soil and bottom samples are in a very similar pattern, as shown in Figure 4.10. The concentrations decrease significantly from the south to the north; with relatively mild contaminations in the east while the west remains virtually intact. V, Fe, Co, Mo, Zn and Cu exhibited similar distribution patterns; the maximum concentrations were found in the south central zone with relatively elevated concentrations (especially for Cu) to the east (Jebel AlDhannah) and west (Sila). Overall, for the Cr, Ni, Mn, V, Fe, Co, Mo, Zn and Cu, the general trend of the concentrations distribution is maximal in the center

of the southern Barakah area and minimal in the shore and bottom sediments in the northern area.

The spatial distribution maps of Pb, Cd and As (as shown in Figure 4.10) are unique compared to the distributions of the rest of the heavy metals considered in this study. The lead is mainly concentrated around the western part of the studied area near the Sila area; cadmium is spread intermittently in the eastern part (Jebel AlDhannah), the central southern part (Barakah), with exceptionally high concentrations in the western part (Sila); and arsenic is spread across the entire area, with particularly higher concentrations in the western part (Sila). The toxicity generated by the elevated concentrations of lead in the western part of the studied area may lead to extinctions of endangered marine species, thus causing a change in the structure of the marine biota (Moriarty 1975; Bowen 1979). Despite its unique distribution, cadmium (as shown in Figure 4.10) is found in the lowest concentrations among other metals considered in this study; with the highest value, 0.15 ppm, being in M4 in the Arabian Gulf. Al Abdali et al. (1996) concluded that Cd is a natural constituent of the Gulf marine environment, and not an element derived from pollutant sources.

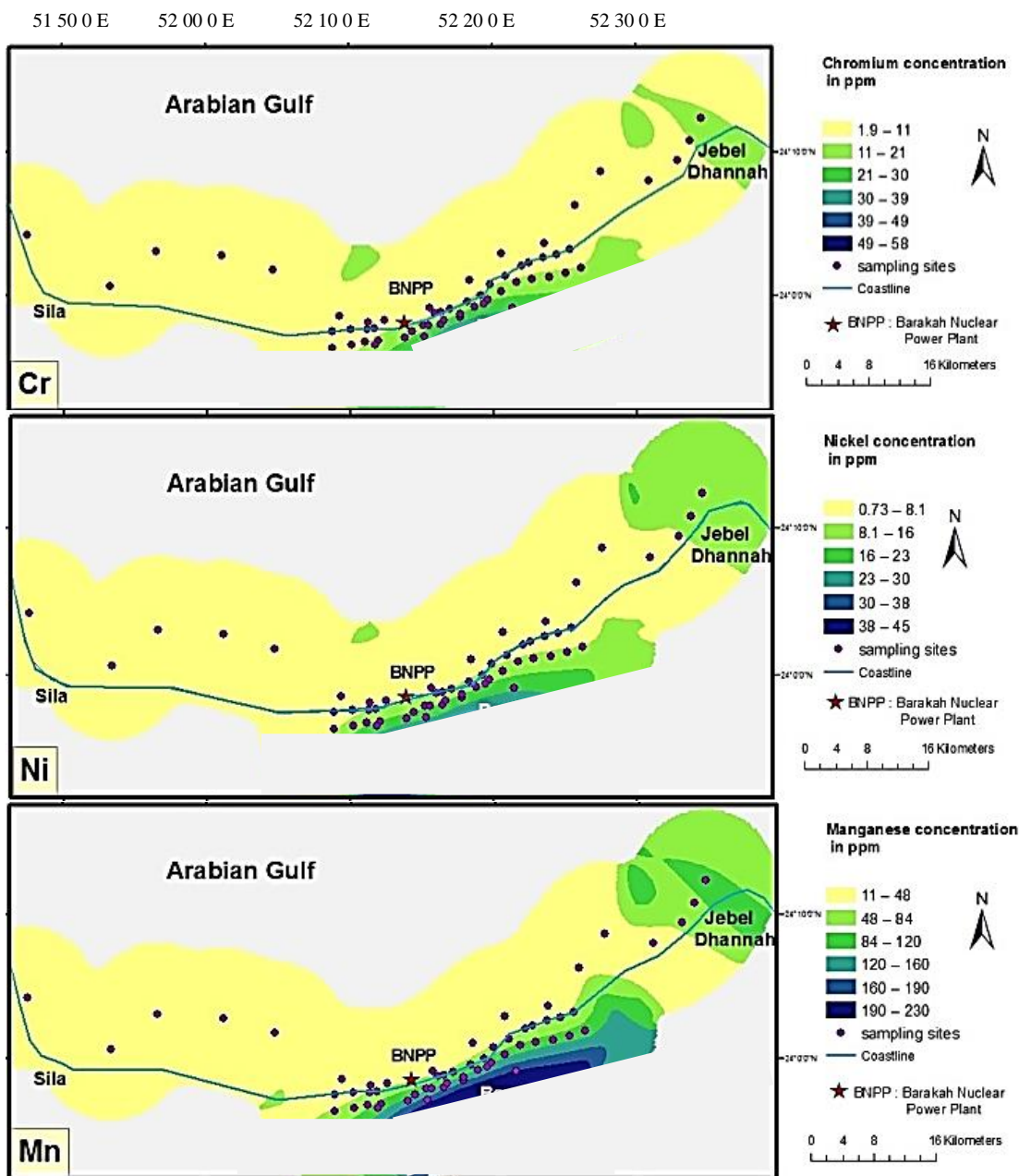


Figure 4.10: Spatial distribution maps showing the heavy metal distributions across all 58 sampling sites, which are represented by dots. The blue line represents the coastline and the star is the location of the BNPP. The color codes from yellow to green to blue correspond to concentrations from low to medium to high, respectively

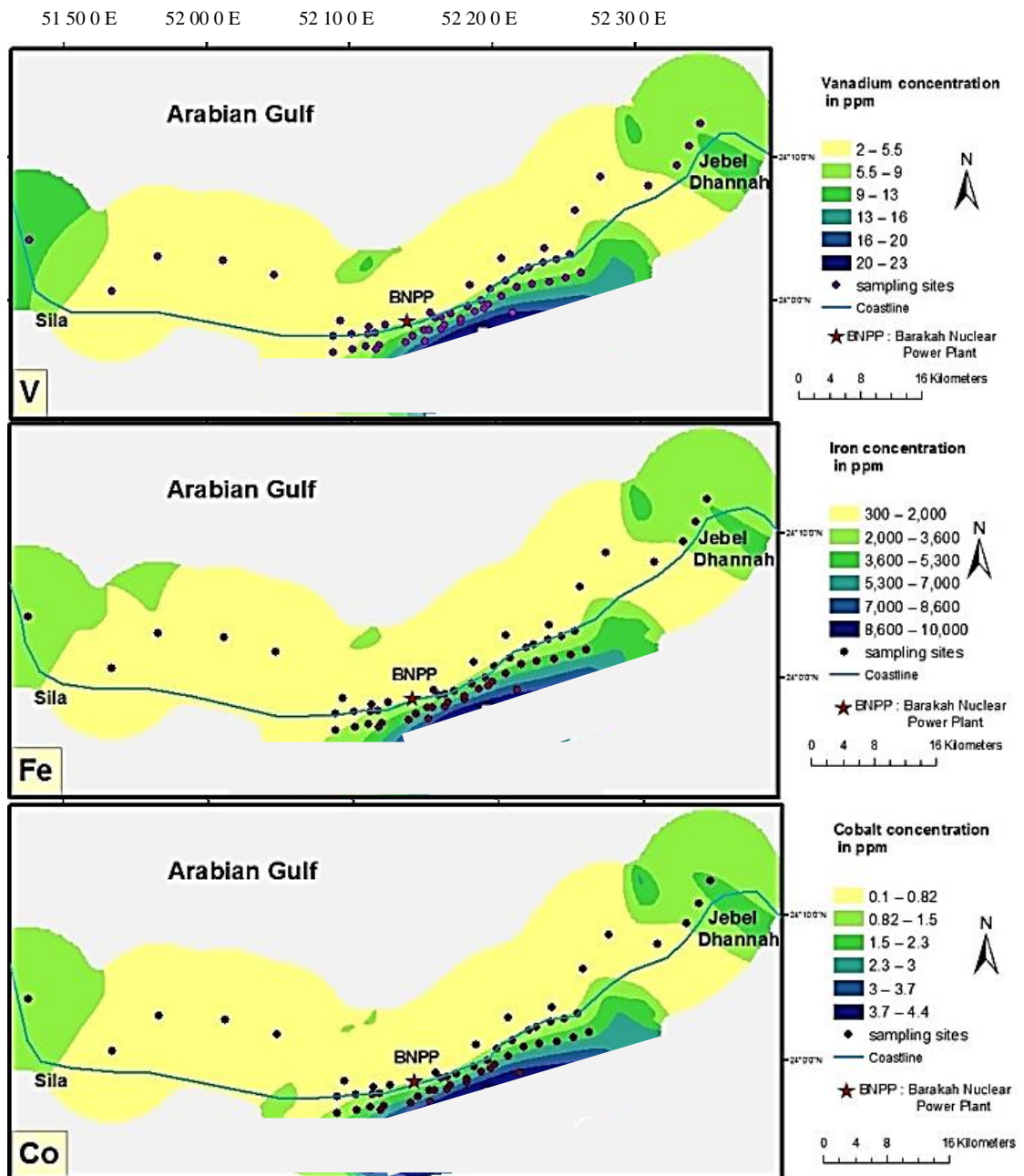


Figure 4.10: Spatial distribution maps showing the heavy metal distributions across all 58 sampling sites, which are represented by dots (continued)

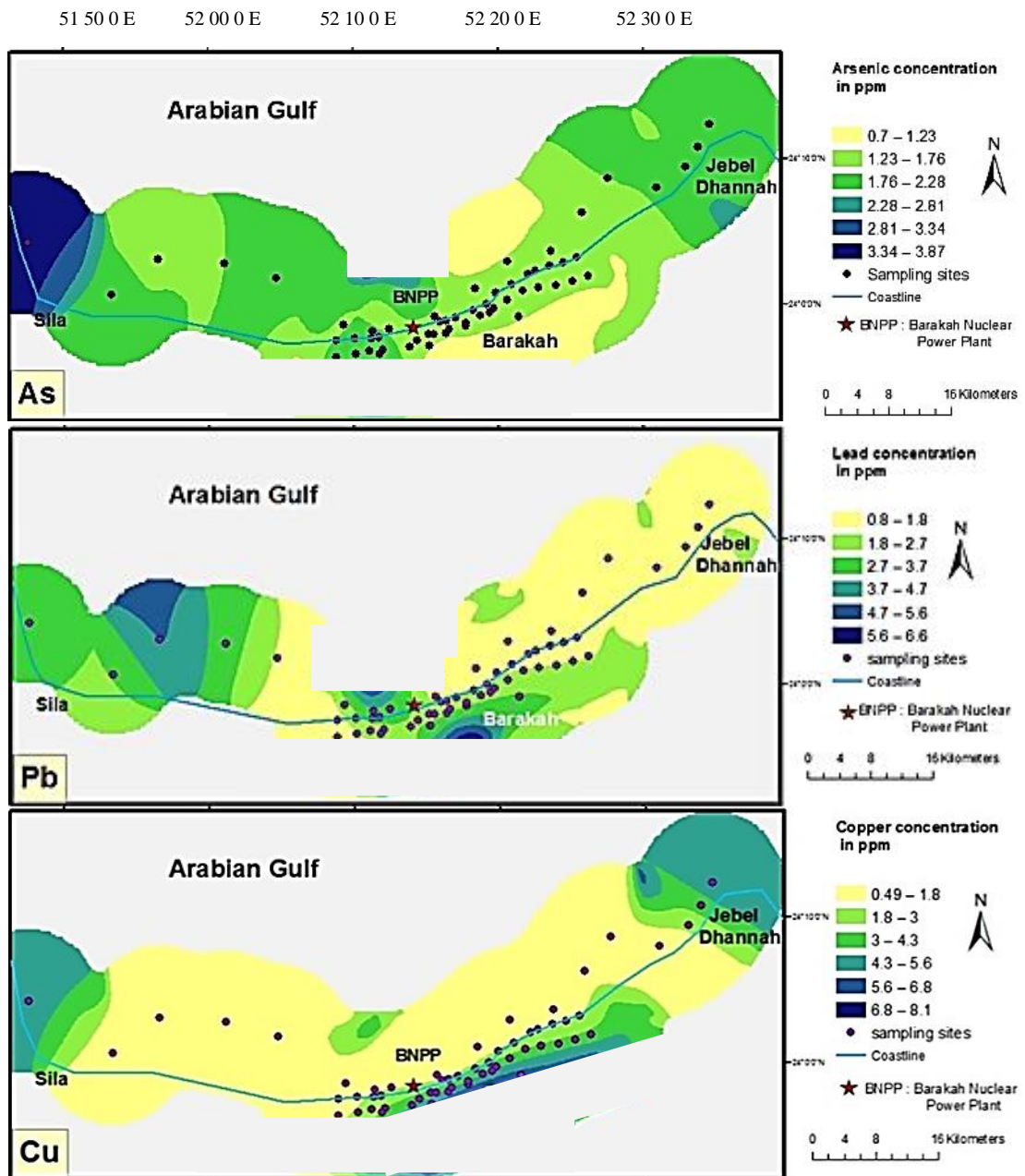


Figure 4.10: Spatial distribution maps showing the heavy metal distributions across all 58 sampling sites, which are represented by dots (continued)

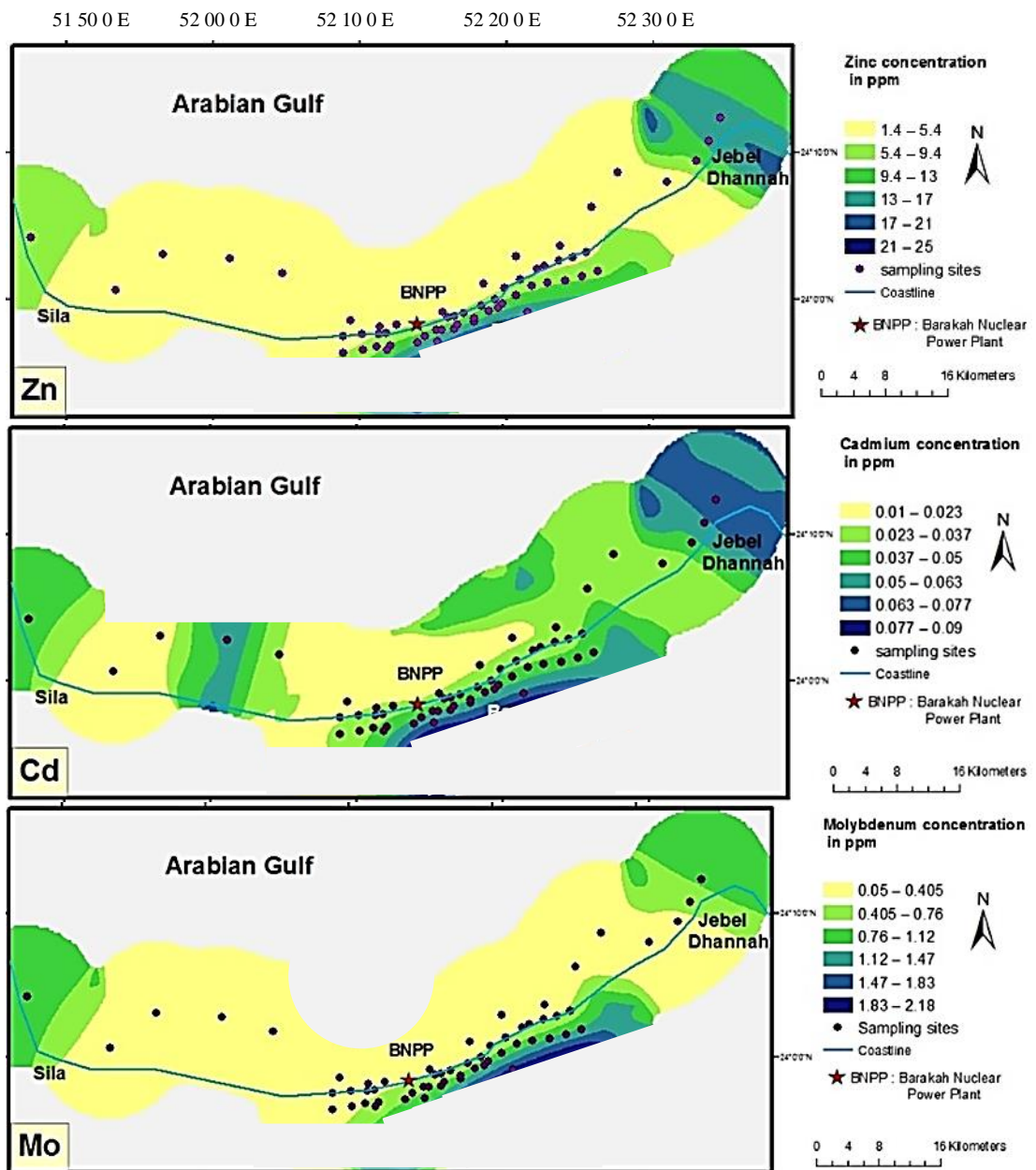


Figure 4.10: Spatial distribution maps showing the heavy metal distributions across all 58 sampling sites, which are represented by dots (continued)

4.2.4 Regional and International Comparison of Heavy Metal Average Concentrations

The average concentrations of some heavy metals in this study, BNPP, is compared with previous studies done by Al Rashdi et al. (2015) on shore sediments in Abu Dhabi and Al-Abdali et al. (1996) and El Tokhi et al. (2016) on bottom sediments of the Arabian Gulf (Table 4.2). The results of Al Rashdi et al. (2015) study for the shore sediments are higher than the current study, which proves that there is a wide variation in the distributions of heavy metals in Abu Dhabi depending on the specific areas considered. In this case, the Barakah area is less contaminated than Abu Dhabi (the capital) coastal line. The results by Al Rashdi et al. (2015), however, are comparable, for all metals, with the results found for the soil samples in this study. This observation needs further investigations to assess the reasons (if any) for this similarity. For the bottom sediments, compared to the results reported by El Tokhi et al. (2016), the values in this study are less than half for all metals except for lead, which is present in roughly equal concentrations, 1.91 and 1.4 ppm, respectively. Results of Al Abdali et al. (1996) were significantly higher for all metals compared to those reported in this study. The significant drop in Pb from 15-30 ppm (according to Al Abdali et al., 1996) to 1.9 ppm in 2015 (according to El Tokhi et al., 2016 and to this study) may be attributed to the banned use of the leaded gasoline in the UAE since January 2003. Nevertheless the average concentrations of all heavy metals are less than the safe limits set by the Dutch guidelines (Lijzen et al., 2001) (Table 4.2), i.e. the guidelines accepted and referred to in Abu Dhabi. Thus, the area is considered unpolluted and safe.

Table 4.2: Heavy metal contaminations (in ppm) in BNPP (for shore, soil and bottom samples) in comparison with other studies in the UAE and with Dutch guidelines (Lijzen et al., 2001)

	Cd	Mo	Co	Cu	Pb	As	Zn	Ni	V	Cr	Mn	Fe
Shore (BNPP)	0.03	0.1	0.4	0.78	1.14	1.4	2.8	2.1	3	3.7	26	975
Bottom (BNPP)	0.03	0.23	0.5	1.17	1.4	1.8	3.2	4.3	4	5.3	30	1339
Soil (BNPP)	0.05	0.89	2.6	4.18	2.43	1.6	11.5	15.4	13	17.4	124	5250
(Al-Abdali et al., 1996)	1.2-2	-	-	15-30	15-30	-	30-60	70-80	20-30	-	300-600	10000-20000
(Al Rashdi et al., 2015)	0.1	0.5	4.1	3.8	1.9	2.8	8.2	25.3	-	-	-	-
(El Tokhi et al., 2016)	0.08	-	1.28	-	1.91	-	11.94	10.55	11.43	17.53	92.26	2800
Dutch guidelines (Lijzen et al., 2001)	13	200	240	190	530	85	720	210	-	220	0	0

Table 4.3: Heavy metal concentrations (in ppm) in soil samples from BNPP in comparison with other international studies

References	Location	Cd	Co	Cu	Pb	As	Zn	Ni	Cr	Mn	Fe
This study (soil)	UAE	0.05	2.6	4.18	2.43	1.6	11.5	15.4	17.4	124	5250
(Pradhan and Kumar 2014)	India	1.3	12.4	4291	2645	17.1	776.8	126	115		4130
(Velea et al., 2008)	Romania	7		350	750		1300				
(Zhou et al., 2013)	China	0.2			25	12	74	35	79		
(Hu et al., 2013)	China		8.6		51.4			26	67.2	371	5092
(Malik et al., 2009)	Pakistan	36.8	35.5	26.85	121.4		94.2	85.5	155		17992

A comparison of heavy metal concentrations (in ppm) in soil samples from the BNPP to those reported in other countries similar to the current study in grain size and geographical latitude is shown in Table 4.3. Levels of some heavy metals reported from surface soils of waste recycling areas in India exceeded the safe limits suggested by the US Environmental Protection Agency (Pradhan and Kumar 2014) exposing human health to serious hazard. The heavy metal values recorded near an industrial area in Romania decrease with increasing the distance from the focal point of the industry (Velea et al., 2008). This reflects the impact of the industrial activities on the accumulation of heavy metals in the surrounding area. The high concentration values of Pb, As, Zn and Ni measured in China are due to anthropogenic sources, which are atmospheric deposition, sewage irrigation/fertilizers usage, and atmospheric deposition/ irrigation water (Zhou et al., 2013). Another study of heavy metals in the surface soils in one of the world's most densely populated regions in China shows high mean values of Cd, Cu, Zn, and As concentrations that were over two times higher than the background values. The source of Cd, Cu and Zn could be anthropogenic sources while Mn, Co, Fe, Cr, and Ni could be primarily derived from lithogenic sources (Hu et al., 2013). The exceptionally high values of Cd (36.8 ppm) in Pakistan emerge from effluents of pharmaceutical industries (Malik et al., 2009).

Table 4.4: Heavy metal concentrations (in ppm) in shore samples from BNPP in comparison with other international studies. BDL stands for below detection limit

References	Location	Cd	Co	Cu	Pb	Zn	Ni	Cr	Fe
This study (shore)	UAE	0.03	0.4	0.78	1.14	2.8	2.1	3.7	975
(Ali et al., 2014)	Pakistan	0.4	1.1	64.2	45	68	34	171	
(Saleh & Marie 2014)	Yemen-polluted site	2.8		39.1	4.4		8.6		100.5
(Saleh & Marie 2014)	Yemen-unpolluted sited	2.8		39.1	4.4		8.6		100.5
(AbuHilal, 1987)	Gulf of Aqaba-Red sea	2-18		7-27		31-260	19-76	15-186	4000-28400
(Gao & Chen 2012)	China	0.22		38.5	34.7	131.1	40.7	101.4	

The heavy metal concentration of the shore samples is compared with values reported in other coastal regions of the world that have similarity in grain size and geographical latitude (Table 4.4). Based on concentration of heavy metals in Pakistan both enrichment and contamination factors (EF and CF) suggested significant influence of anthropogenic and industrial activities along the coastal belt of Pakistan (Ali et al., 2014). The levels of Cd, Cu, Pb, Ni and Fe in the coastal sediments from the Red Sea coast of Hodeida in Yemen were roughly twice as much in the site surrounded by industrial and domestic water wastes (polluted site) compared to an unpolluted site in the same area (Saleh and Marie 2014). Heavy metal concentrations in surface sediment samples along the Jordanian coast of the Gulf of Aqaba, Red Sea show higher values compared to results from current study and that is due to the anthropogenic activities. The coastal sediments of the Bay of

Bohai Sea in China are rather unpolluted indicating a limited influence of the anthropogenic activities (Gao and Chen 2012).

Concentrations of heavy metals in bottom sediments of many countries across different continents depending on similarities in grain size and geographical latitude are shown in Table 4.5. India, is contaminated with Cd (Raj and Jayaprakash 2007) more than other countries listed in this table. The amount of copper, lead and chromium varies significantly from one place to another with the UAE being the least polluted and India being the most polluted with Cu, Pb and Cr. Arsenic and Zinc levels are high in both of China (Xu et al., 2015) and Ethiopia (Yohannes et al., 2013). Iran is particularly contaminated with nickel (Keshavarzi et al., 2015). China has the highest concentration of Mn (Cheng et al., 2015) compared to the level reported in India which is the second highest. The levels of contaminations of all heavy metals in the UAE are the lowest among all countries listed in Table 4.5 followed by Croatia (Zvab Rozic et al., 2012). Overall, India is the most contaminated country; this is because of anthropogenic activities such as industrial wastewater, coal-fueled iron and steel industries and municipal sewage (Raj and Jayaprakash 2007). The UAE is the least polluted with all metals despite the rapid growth of anthropogenic activity in the area.

Table 4.5: Heavy metal concentrations (in ppm) in bottom sediments of BNPP in comparison with other international studies

References	Location	Cd	Mo	Co	Cu	Pb	As	Zn	Ni	V	Cr	Mn	Fe
This study (Bottom sediments)	UAE	0.03	0.23	0.5	1.17	1.4	1.8	3.2	4.3	4	5.3	30	1339
(Raj and Jayaprakash 2007)	India	4.6-7.5		5.8-11.8	385-657	24.9-40		71.3-201	19.8-53.4		148.6-243.2	284-460	17000 - 37000
(Xu et al., 2015)	China	0.1			31.1	27.9	11.2	102.3			83.3		
(Cheng et al., 2015)	China	0.11			39.3	41.1		72.4			53.6	1633.5	
(Zvab Rozic et al., 2012)	Croatia	0.07-2	0.2-1.4	0.2-2.5	1.05-6.6	3.3-12.3	2.3-8	4.0-33.0	2.8-15.6	5.3-19.3	20-40		
(Yohannes et al., 2013)	Ethiopia	0.21		5.49	8.69	15.7	4.02	93.8	20.2		8.27		
(Keshavarzi et al., 2015)	Iran	0.24			20.45	8.09	4.25	48.89	73.66		48.79		

4.2.5 Heavy Metal Contamination Assessment

To evaluate the anthropogenic influences of heavy metals in the Barakah area, the enrichment factors are calculated using EF equation (Rubio et al., 2000):

$$EF = M_x Fe_b / M_b Fe_x$$

where M_x is the average concentration of the metal in the study area, M_b is the concentration of the metal in the background (in ppm), sandstone average (Turekian and Wedepohl 1961) (in ppm), Fe_x is the average concentration of iron in the samples (in ppm) and Fe_b is the iron concentration in the background (in ppm). Enrichment factors $EF < 1$, $EF = 1-3$, $3-5$, $5-10$, $10-25$, $25-50$, $EF > 50$ indicate no enrichment (I), minor enrichment (II), moderate enrichment (III), moderate severe enrichment (IV), severe enrichment (V), very severe enrichment (VI) and extremely severe enrichment (VII), respectively (Birch, 2003). As shown in Table 4.6, the shore samples are the most enriched group. The enrichment is in As, followed by Cd, then the rest of the metals, with no enrichment exhibited for Cu. The bottom samples are marginally more enriched compared to the soil samples. Overall, the study area had minor enrichment in all metals, but no enrichment in Cu or V. For all samples, Co, Zn and Mn exhibited minor enrichment, but the values are at the lower end of the range.

The level of contamination expressed by the contamination factor (CF) (Pekey, et al., 2004) is calculated as follows:

$$CF = M_x / M_b$$

where M_x is the metal content in the sediment (in ppm) and M_b metal content in natural reference sediment (in ppm) based on sandstone average (Turekian and

Wedepohl 1961). $CF < 1$, $CF = 1-3$, $3-6$, $CF > 6$ indicate low contamination factor, moderate contamination factors, considerable contamination factors and very high contamination factor, respectively. The CF categories are based on the classifications by (Pekey, et al., 2004). Results show that all the heavy metals in all sites and environments had $CF < 1$ which indicate low contamination factor.

The geoaccumulation index (Muller, 1979) is employed in order to determine and define metal contamination in sediments by comparing current concentrations with background levels and it is calculated using:

$$I\text{-geo} = \log_2 [C_n / (1.5B_n)]$$

where C_n is the measured concentration of element n in a sample (in ppm) and B_n is the average for in Earth crust sandstone for the element n (in ppm) by (Turekian and Wedepohl 1961). Classifications of geoaccumulation indices are: class 0 uncontaminated, class 1 uncontaminated to moderately contaminated, class 2 moderately contaminated, class 3 moderately to strongly contaminated, class 4 strongly contaminated, class 5 strongly to extremely contaminated and class 6 extremely contaminated; for $I\text{-geo} < 0$, $0-1$, $1-2$, $2-3$, $3-4$, $4-5$, and >5 (Muller 1979). For soil, shore and bottom samples of the study area, the geoaccumulation index is negative indicating that the area is classified as uncontaminated. The negative geoaccumulation index indicates that there has not been accumulation of heavy metals over the time.

The pollution load index (PLI) proposed by Tomlinson et al. (1980) is obtained as a Enrichment Factor (EF) of each metal with respect to the background value in the sediment, by applying the following equation:

$$PLI = (EF_1 \times EF_2 \times EF_3 \dots \times EF_n)^{1/n}$$

If $PLI < 1$ the place is not polluted, if $PLI > 1$ the area is polluted (Tomlinson et al., 1980). The pollution load index (PLI) is greater than unity in the each of the soil, shore and bottom samples. This means that the study area is polluted. Nevertheless the average concentrations of all heavy metals are an order of magnitude less than the safe limits set by the Dutch guidelines (Lijzen et al., 2001), i.e. the guidelines accepted and referred to in Abu Dhabi. Thus, even though the area is analytically considered polluted, it is still safe.

Table 4.6: The average background values, enrichments factors (EF), contamination factor (CF) and geoaccumulation indices (I-geo) for the soil, shore, bottom areas and overall average

	Cd	Mo	Co	Cu	Pb	As	Zn	Ni	V	Cr	Mn	Fe
Earth crust (Turekian and Wedepohl 1961)	0.03	0.2	0.3	5	0.2	1	16	2	20	35	50	9800
Enrichment Factors (soil)	1.44	3.06	1.23	0.84	1.09	4.97	1.09	2.04	0.88	1.74	1.31	1
Enrichment Factors (shore)	4.03	1.89	1.11	0.84	2.75	5.21	1.42	1.47	1.12	2.01	1.48	1
Enrichment Factors (bottom)	3.43	3.08	0.97	0.92	2.47	1.09	1.2	2.22	1.17	2.8	1.24	1
Enrichment Factors (overall average)	2.97	2.68	1.10	0.87	2.10	3.76	1.24	1.91	1.06	2.18	1.34	1
Contamination factors (soil)	0.01	0.34	0.14	0.09	0.12	0.12	0.12	0.23	0.1	0.19	0.015	0.11
Contamination factors (shore)	0.1	0.04	0.02	0.02	0.06	0.11	0.03	0.03	0.02	0.04	0.03	0.02
Contamination factors (bottom)	0.1	0.09	0.03	0.03	0.07	0.15	0.03	0.06	0.04	0.07	0.04	0.03
Contamination factors (overall average)	0.07	0.16	0.06	0.05	0.08	0.13	0.06	0.11	0.05	0.10	0.03	0.05
Geoaccumulation index (soil)	-3.2	-2.1	-3.5	-4	-3.6	-3.63	-3.6	-2.7	-3.9	-3	-3.4	-3.75
Geoaccumulation index (shore)	-4.2	-5.3	-6	-6.4	-4.7	-3.8	-5.7	-5.6	-6	-5.2	-5.6	-6.1
Geoaccumulation index (bottom)	-3.9	-4.1	-5.8	-5.8	-4.4	-3.41	-5.5	-4.6	-5.5	-4.7	-5.4	-5.7
Geoaccumulation index (overall average)	-3.77	-3.83	-5.10	-5.40	-4.23	-3.61	-4.93	-4.30	-5.13	-4.30	-4.80	-5.18

4.2.6 REE Concentration and Normalization

The rare earth elements (REE) concentration in the study area reveals that the LREE are higher than the HREE, which is in accordance with the general distribution of REE in earth crust. Furthermore, this behavior is expected since the REE contents of most shales are normally enriched in LREE relative to HREE (Haskin et. al., 1966). Generally, all REE concentrations in the current study are below the mean REE values in earth crust (Turekian and Wedepohl, 1961) (Table 4.7) and (Figure 4.11). Nd is the most abundant REE in soil samples, whereas La is the most abundant REE in both shore and bottom sediments (Figure 4.12). The order of occurrence of REE in bottom sediments is similar to that in the earth's crust as described by Taylor and McLennan (1995) as show in Table 4.7. Comparison of the distribution of REE amongst the three depositional environments (soil, shore and bottom sediment) showed that soil samples have the highest concentrations of REE. The relatively higher concentration of REE in the soil samples may be attributed to erosion process. However, REE concentration vary with in soil samples, which can be related to the long aeolian transport distance in case of low concentrations and the short aeolian distance in high concentration of REE samples (Kasper-Zubillaga et. al., 2008). The studied samples displayed variations in total REE (\sum REE) contents (Table 4.7) with mean values of 10.48, 2.80 and 4.31 ppm, in soil, shore and bottom sediments, respectively. The \sum REE is higher in soil samples than in shore and bottom sediments. Shore samples that are rich in carbonate showed the lowest values of \sum REE, those samples were characterized with the presence of shell fragments (calcium carbonate contents). Carbonates decrease the concentrations of

REE as calcareous biological debris dilute the REE abundances of the sediments (Chen et. al., 2013).

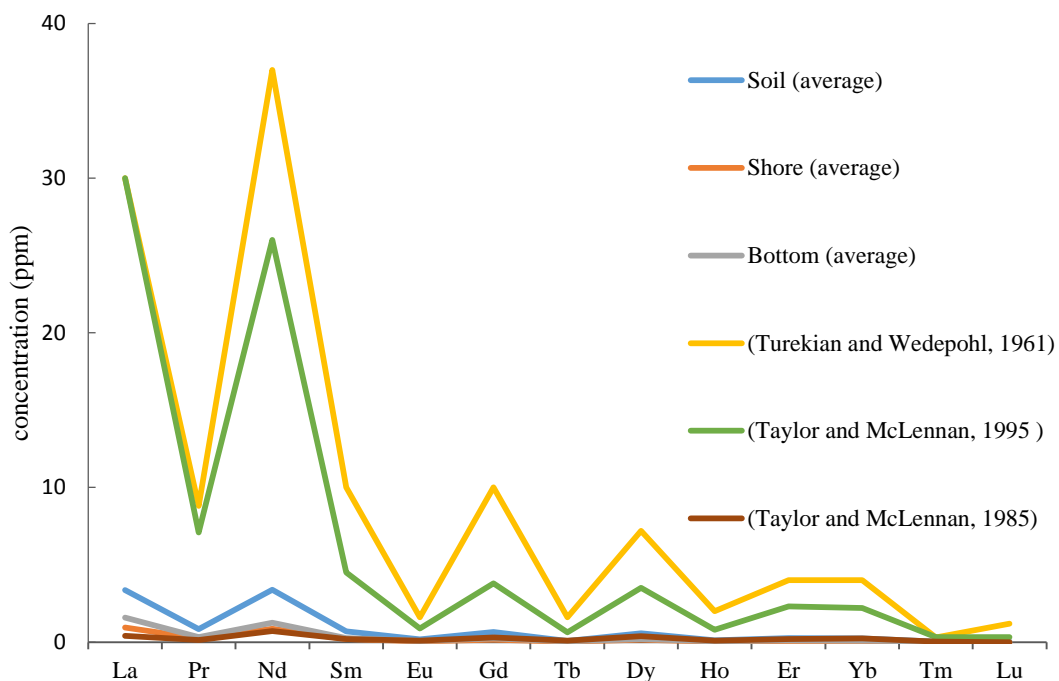


Figure 4.11: REE average concentrations in soil, shore and bottom sediments compared to average background values and chondrite value

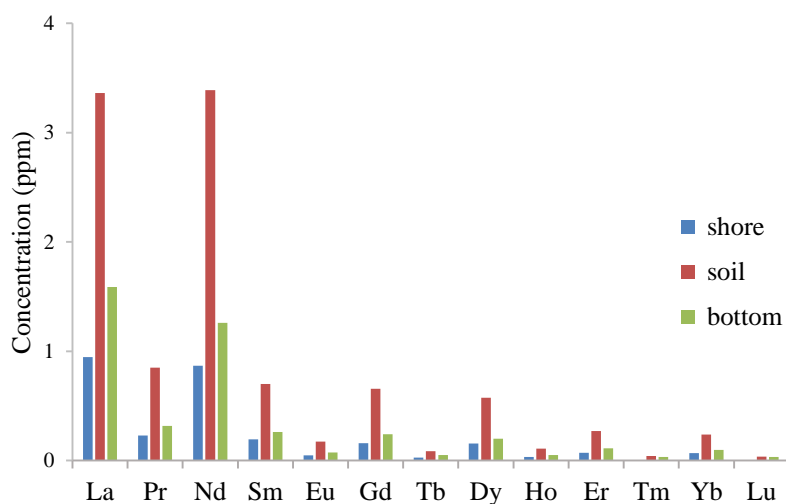


Figure 4.12: Average concentrations of REE in soil, shore and bottom sediments

Table 4.7: REE average concentrations in soil, shore and bottom sediments compared to average background values and chondrite value

	LREE					HREE								Σ REE
	La	Pr	Nd	Sm	Eu	Gd	Tb	Dy	Ho	Er	Tm	Yb	Lu	
Soil (average)	3.36	0.85	3.39	0.70	0.17	0.66	0.08	0.57	0.11	0.27	0.04	0.24	0.04	10.48
Shore (average)	0.95	0.23	0.87	0.19	0.05	0.16	0.03	0.15	0.03	0.07	-	0.07	-	2.80
Bottom (average)	1.59	0.32	1.26	0.26	0.07	0.24	0.05	0.20	0.05	0.11	0.03	0.10	0.03	4.31
Earth crust (sandstone) (Turekian & Wedepohl, 1961)	30	8.8	37	10	1.6	10	1.6	7.2	2	4	0.3	4	1.2	-
Continental crust (Taylor & McLennan, 1995)	30	7.1	26	4.5	0.88	3.8	0.64	3.5	0.8	2.3	0.33	2.2	0.32	
Chondrite value (Taylor & McLennan, 1985)	0.4	0.14	0.71	0.2	0.09	0.31	0.1	0.38	0.09	0.2	0.04	0.25	0.0	-

Normalization of the analyses to reference standards such as chondrite (Taylor and McLennan, 1985) (values are in Table 4.7) were done since chondrites are thought to be compositionally similar to the original earth's mantle (Table 4.8). The REE distribution patterns in soil, shore and bottom sediments indicated an enrichment of LREE over HREE shown by distinctly decreasing LREE trends accompanied by flat HREE trends (Figure 4.13). Similar REE pattern for offshore marine sediments in Abu Dhabi have been reported by El Tokhi (et. al., 2015b). No depletion (anomaly) appeared in the REE distribution patterns. The similarity of REE distribution patterns is not only within the same depositional environments but are also similar among the three depositional environments (shore, soil and bottom sediment). This may indicate that the source rock of the three environments have similar geochemical characteristics, which is in accordance with El Tokhi et.al, (2015b) conclusions. Because soil samples showed the highest REE concentrations, the chondrite normalized REE values were plotted for each soil sample to investigate the variation among sites (Figure 4.14). It can be observed that the normalized values of REE concentrations of all soil samples show a wide variation in the REE concentrations. It is likely that the major differences in REE concentration among soil samples is controlled by the aeolian transport (Kasper-Zubillaga et. al., 2008).

Rare earth elements are mobilized, fractionated and precipitated during weathering processes (Prudincio et al., 1995). Variations in that behavior across the REE are indicated by the degree of LREE enrichment with respect to HREE. This is represented by La/Yb ratio, where $(La/Yb)_n = (La_{\text{sample}} / La_{\text{chondrite}}) / (Yb_{\text{sample}} / Yb_{\text{chondrite}})$; the degree of middle rare earth element (MREE) enrichments with respect to LREE and HREE (Tranchida et al., 2011). The concentration of the previously mentioned REE are used from Turekian and Wedepohl, (1961). The

average calculated $(La/Yb)_n$ for soil, shore and bottom sediment are 6.44, 6.35 and 7.44, respectively (Table 4.7). The $(La/Yb)_n$ values are close to each other (within 17%) indicating a similarity in the behavior across the REE in the three different depositional environments as well as that REE are most unlikely to have the anthropogenic nature. The average $(La/Yb)_n$ value of bottom sediments is slightly higher than those of shore and soil. Slightly higher $(La/Yb)_n$ ratio in the bottom sediments indicate LREE enrichments relative to the HREE, and the LREE enrichment trend become slightly lower in soil and shore where lower $(La/Yb)_n$ values (mean values 6.44 and 6.35, respectively). The results of REE concentration in the current study were compared with REE results of (El Tokhi et. al., 2015b). REE concentrations in the both studies were found to be less than those in the oceanic crust.

Grain size, mineralogy, source rock composition and chemical weathering are the main controlling factors for the REE concentration in the bottom sediments (Yang et al., 2002). The source of REE in the present study is detrital fraction derived from continental land as the final result of weathering processes. Since REE contents increased in the sand-silt-clay series (Dubinin, 2004; Sholkovitz, 1988), REE were measured in three grain size fractions (coarse, medium and fine) for the bottom sediments. Figure 4.15 shows REE concentrations for the different grain size fractions of the bottom sediment. This figure shows an overall inverse relationship between grain size and REE concentrations with an anomaly in Tm. The anomaly could be attributed to the fact that clay minerals are rich sources of REE due to their ability to adsorb REE onto their surfaces and to incorporate REE in their crystalline structure (Dubinin, 2004).

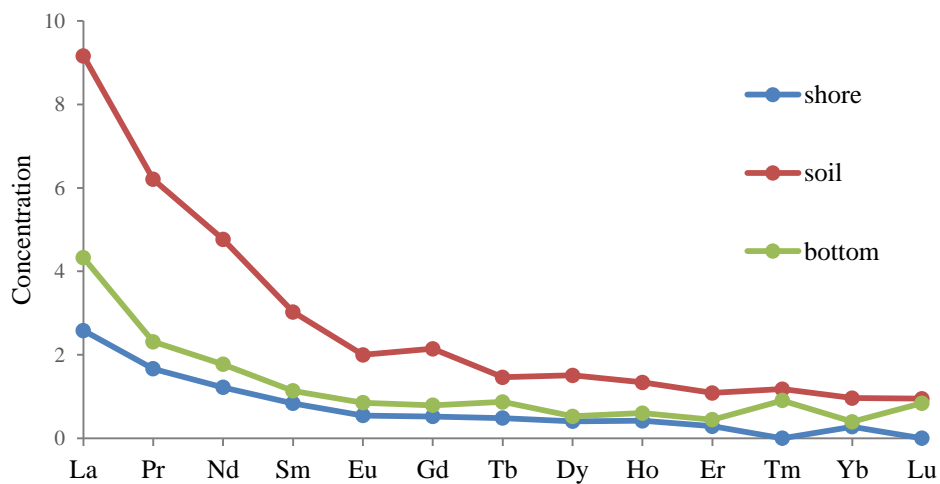


Figure 4.13: Concentrations of REE: LREE (La, Pr, Nd, Sm and Eu) and HREE (Gd, Tb, Dy, Ho, Er, Tm, Yb and Lu) normalized to the concentrations in chondrite in Average of soil, shore and bottom sediments

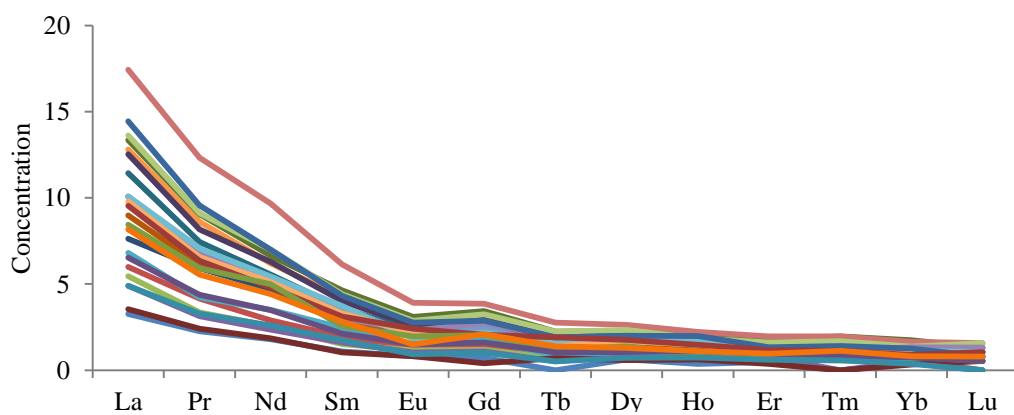


Figure 4.14: Concentrations of REE: LREE (La, Pr, Nd, Sm and Eu) and HREE (Gd, Tb, Dy, Ho, Er, Tm, Yb and Lu) normalized to the concentrations in chondrite for all soil samples

Table 4.8: Basic statistics of REE normalized to the concentrations in chondrite normalized in soil, shore and bottom sediments

	LREE					HREE								(La/Yb) _n
	La	Pr	Nd	Sm	Eu	Gd	Tb	Dy	Ho	Er	Tm	Yb	Lu	
Soil (average)	9.16	6.20	4.77	3.03	2.00	2.14	1.46	1.51	1.34	1.08	1.18	0.96	0.94	6.44
Shore (average)	2.58	1.67	1.22	0.84	0.54	0.52	0.48	0.41	0.42	0.29	<0.02	0.27	<0.02	6.35
Bottom (average)	4.33	2.31	1.77	1.13	0.85	0.79	0.87	0.53	0.60	0.44	0.91	0.39	0.84	7.44

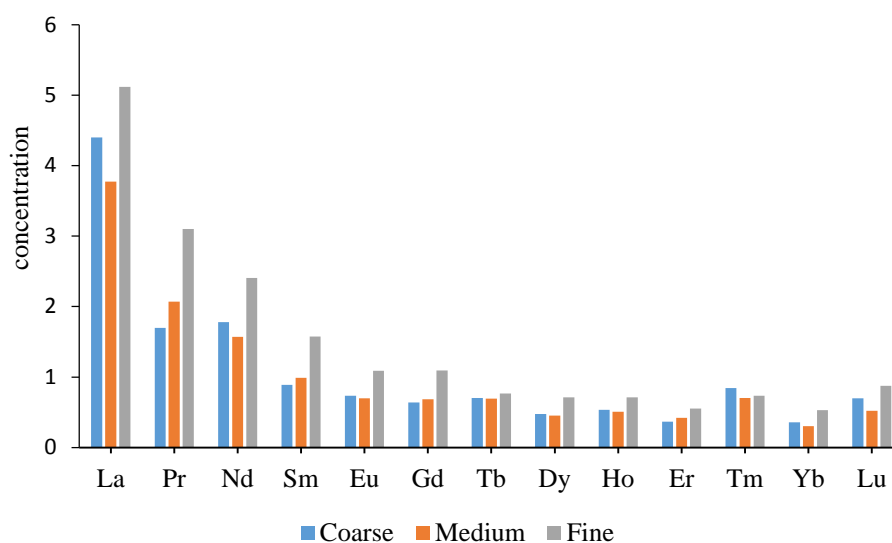


Figure 4.15: Average REE distribution pattern normalized to the concentrations in chondrite in different fraction (C coarse, M medium and F fine) of bottom sediments

Both of Al and REE are considered immobile during the alteration process that result from temperature, chemical variables and time (Reeves et al., 2006 and Liaghat et al., 2003). In this study, REE concentrations in bottom sediments showed significant positive correlations between Al and REE (Figure 4.16). The correlation coefficients range from 0.83 to 0.95, the strong relation between REE and immobile Al (Land et al., 1997) indicates that REE show low or negligible mobility and are resistant to fractionation during weathering processes. This result is in correlation with result obtained by Fu et al. (2011).

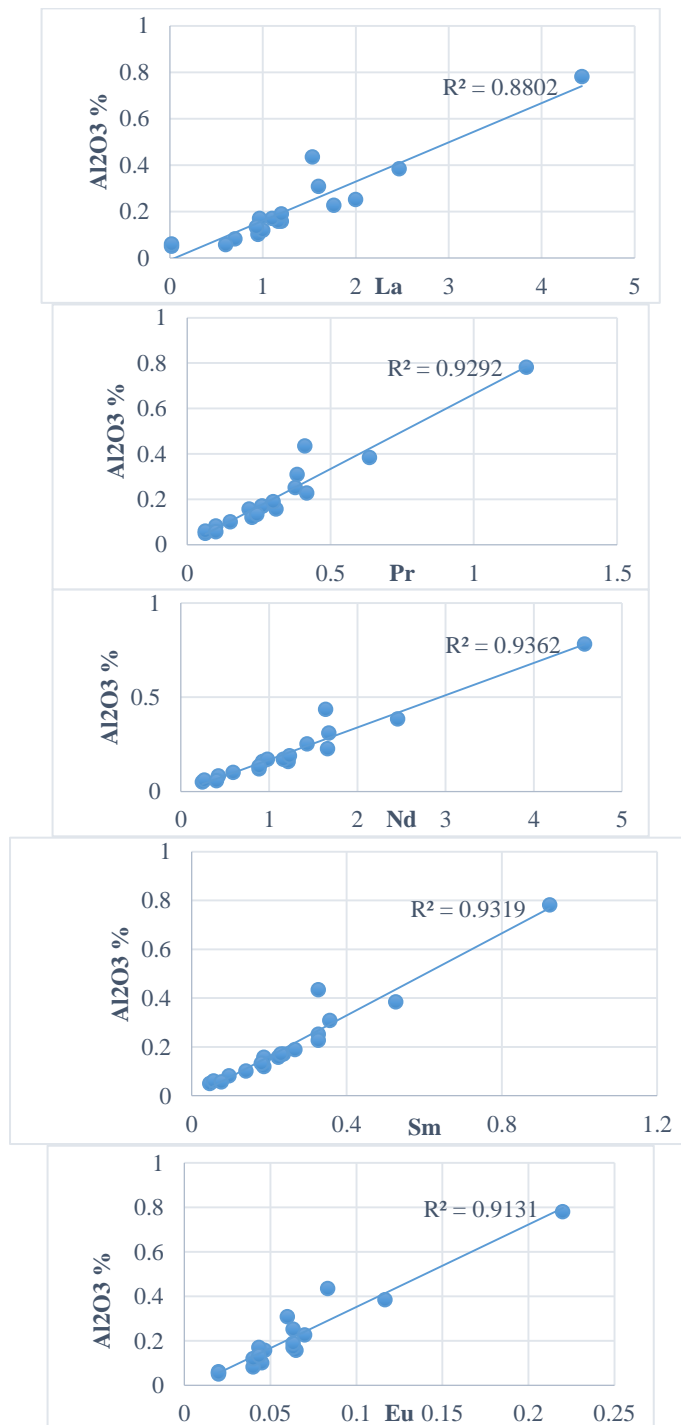


Figure 4.16: Scatter diagram of Al_2O_3 (%) contents against REE concentration in ppm for bottom sediment

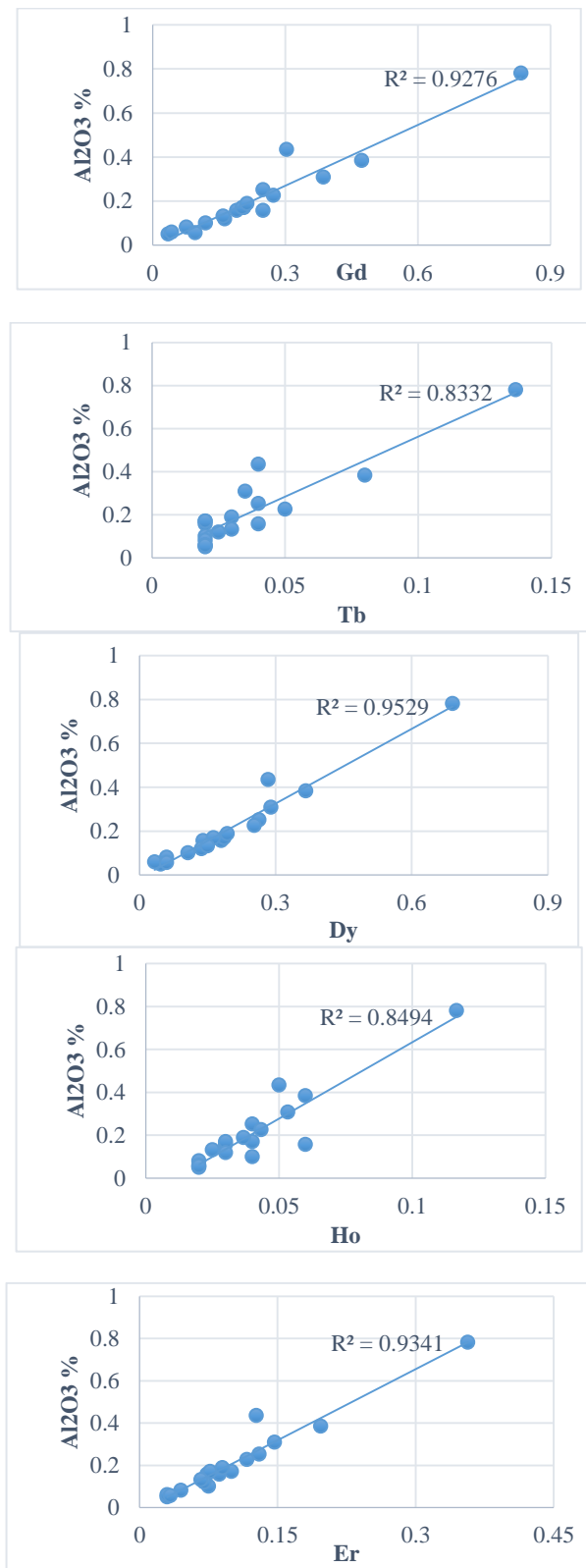


Figure 4.16: Scatter diagram of Al₂O₃ (%) contents against REE concentration in ppm for bottom sediment (continued)

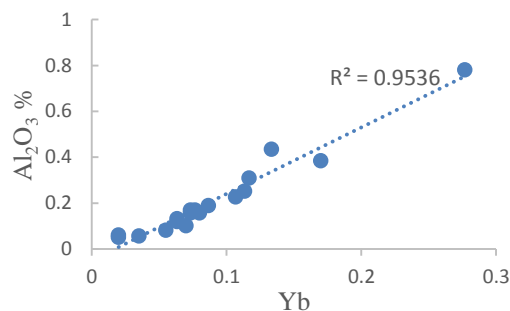


Figure 4.16: Scatter diagram of Al₂O₃ (%) contents against REE concentration in ppm for bottom sediment (continue)

4.2.7 Spatial Distribution of REE

Spatial distribution maps are constructed using Arcmap 10.1 by interpolation method (kernel smoothing). The distribution of La, Pr, Sm, Nd, Sm, Gd, Tb, Dy, Ho, Er, Tm, Yb and Lu are plotted based on their concentrations. The distributions of all REE are very similar, as shown in Figure 4.17. Generally, the highest concentrations are always found in the south; while the minimum concentrations are found in the northern zone towards the shore. All REE exhibit similar distribution pattern with exception of Tm, Tb and Lu. Their concentrations decrease dramatically from the south to the north with some elevated concentrations towards the east and west as shown in Figure 4.17. While the distribution of Tb and Tm lack high concentrations toward the west. A unique distribution is found in Lu concentration, where the maximum concentration are only shown in the south.

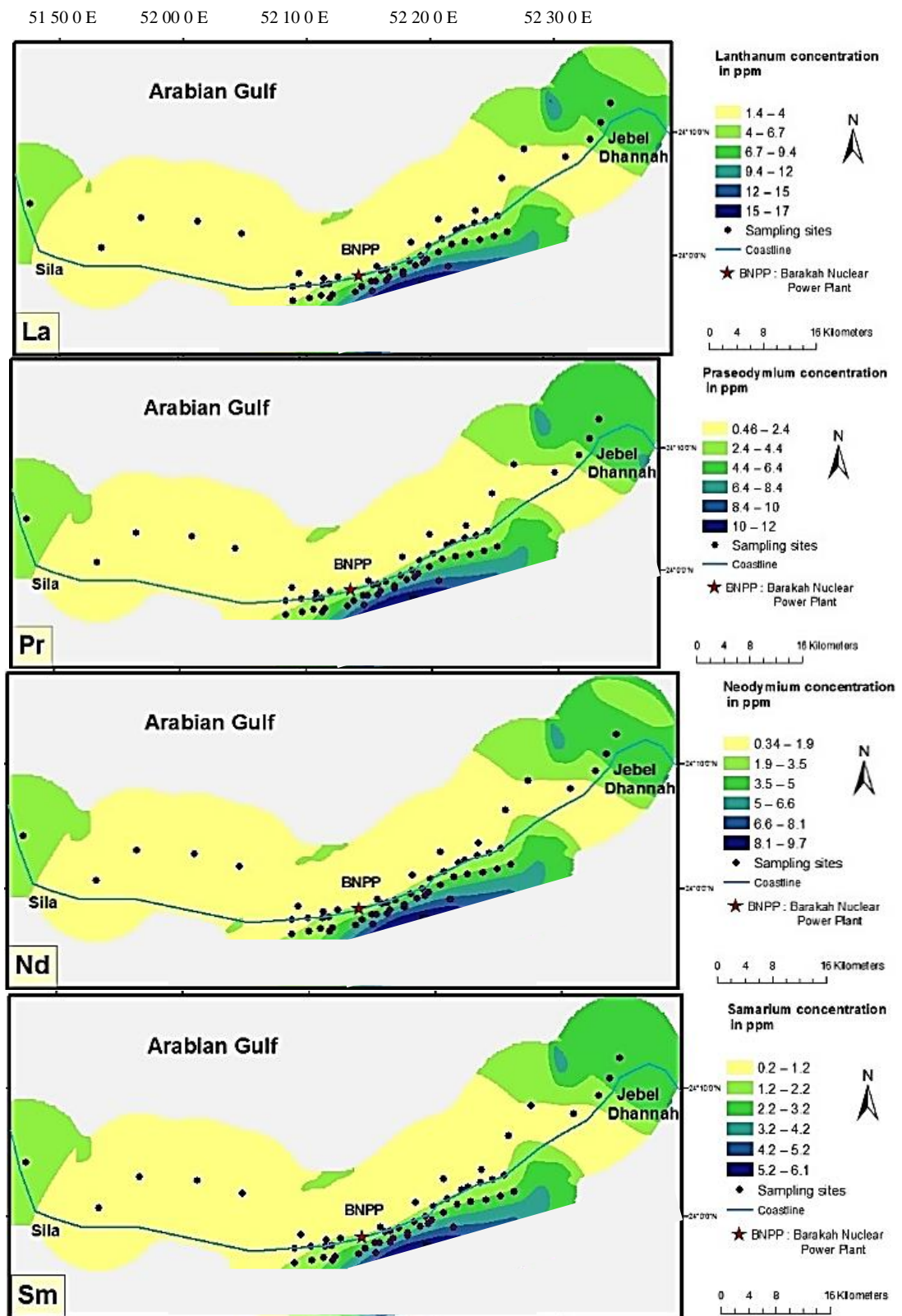


Figure 4.17: The distribution pattern of REE in the studied area

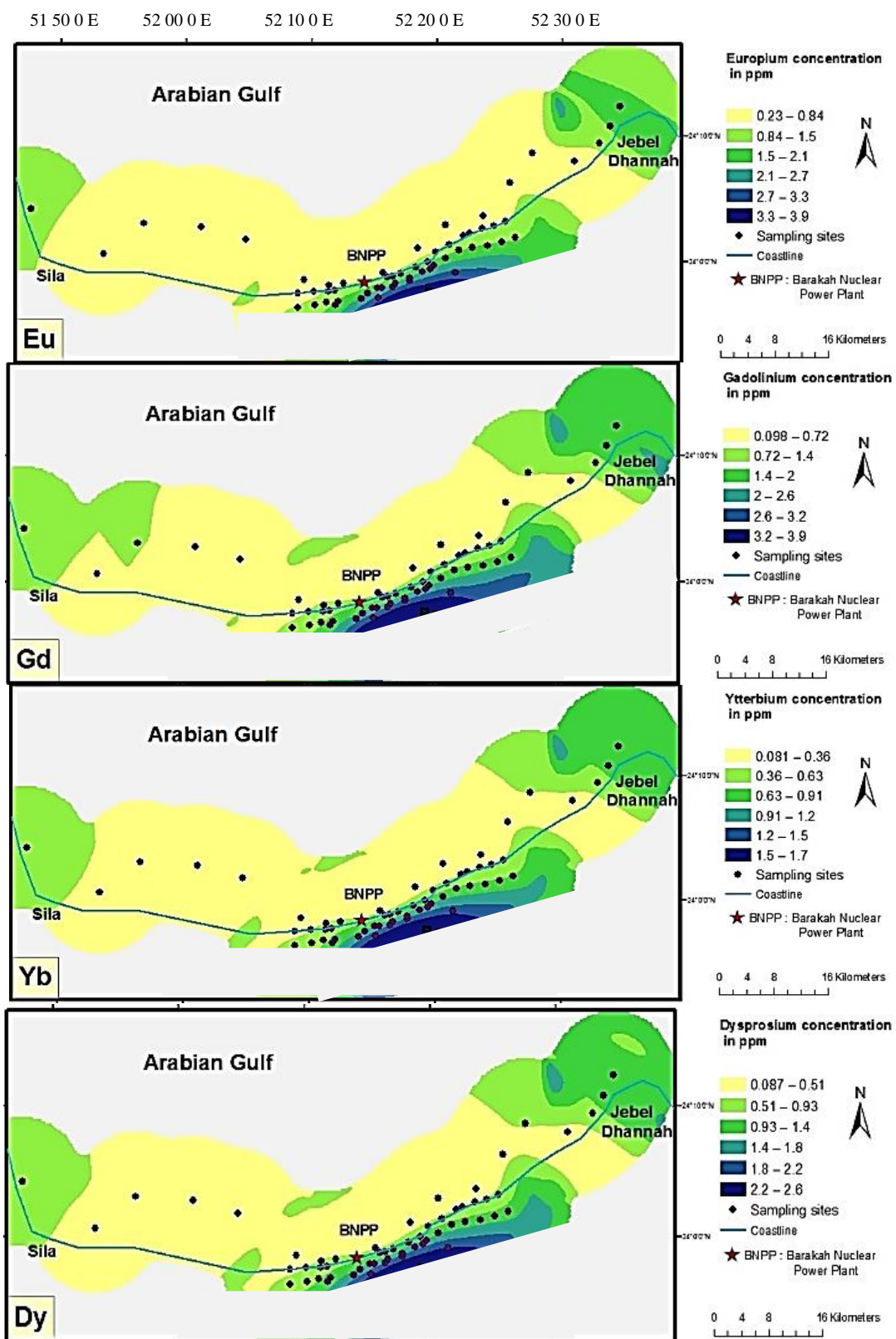


Figure 4.17: The distribution pattern of REE in the studied area (continued)

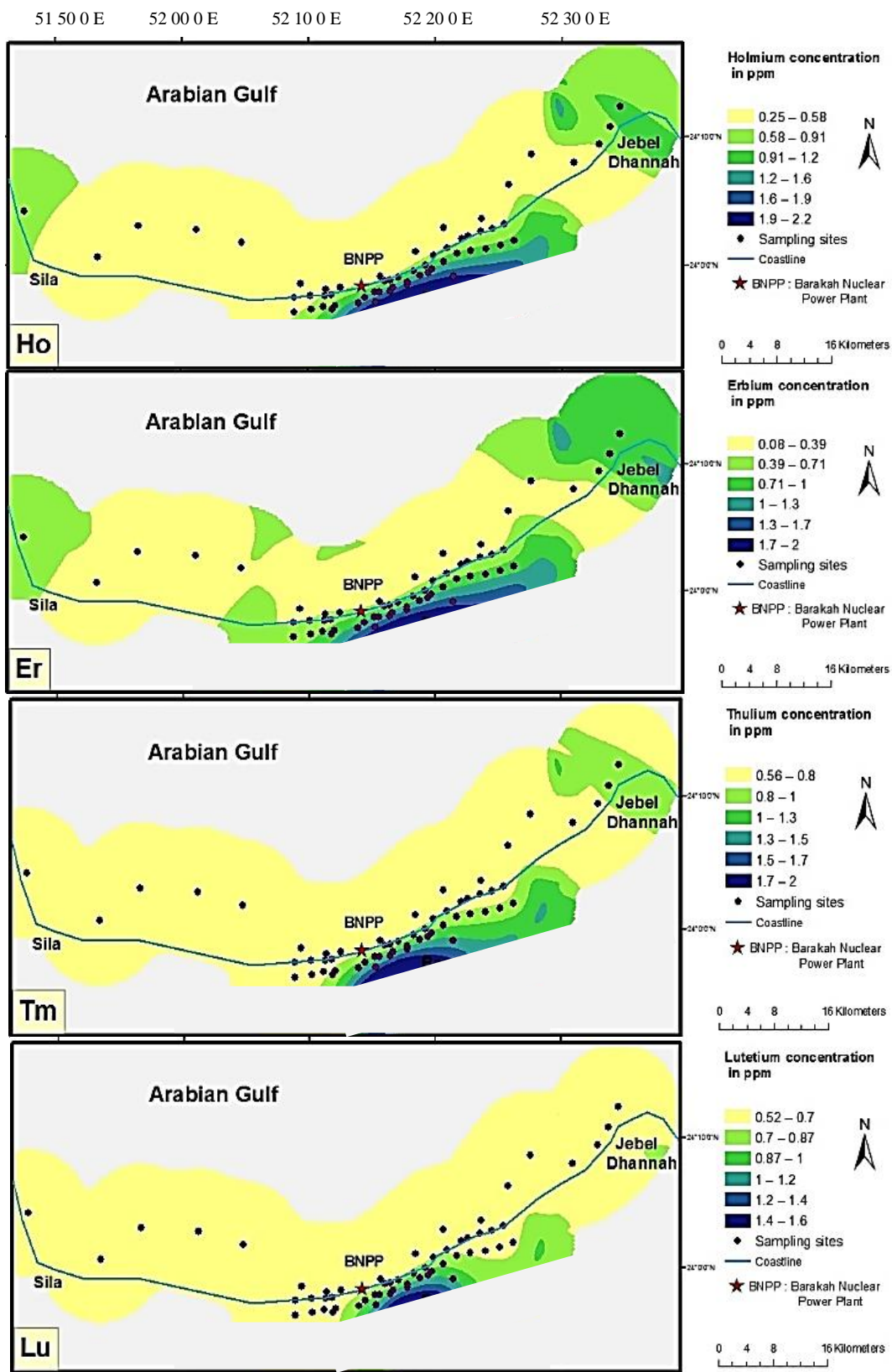


Figure 4.17: The distribution pattern of REE in the studied area (continued)

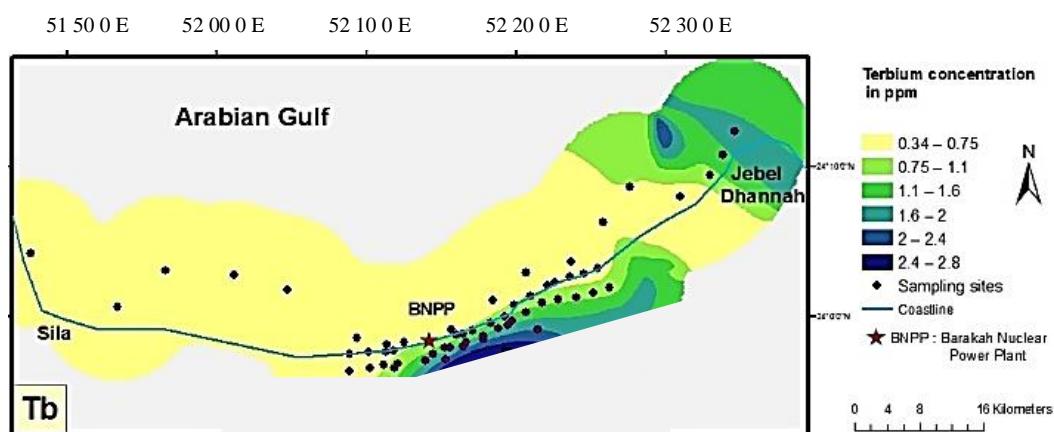


Figure 4.17: The distribution pattern of REE in the studied area (continued)

4.2.8 Regional and International Comparison of REE Average Concentrations

The distribution of REE in many countries across different continents compared to the current study based on similarity in grain size and/or geographical latitude is shown in Table 4.9. The surface soil around a Chinese mining area (Wang & Liang 2015) shows elevated concentration of REE indicating human activities and strong winds in that region. A similar REE investigation near an Iranian mining area (Zaremotlagh & Hezarkhani 2016) reveals high concentrations of REE and thereby their findings are extended to REE geochemical exploration projects. The coastal area of both UAE (current study), Malaysia (Antonina et al., 2013) and India (Naidu et al., 2016) show low REE concentrations compared to the earth crust values, while Gd shows elevated concentration in Nigeria (Akinlua et al., 2016) due to organic matter origin. The bottom sediments of both Korea and China (Xu et al., 2009) show high content of REE while the least concentration is in UAE bottom sediments.

Table 4.9: REE distribution (ppm) in soil, shore and bottom sediments of BNPP in comparison with other international studies

	References	Location	La	Pr	Nd	Sm	Eu	Gd	Tb	Dy	Ho	Er	Tm	Yb	Lu
soil	This study (soil samples)	UAE	3.36	0.85	3.39	0.70	0.17	0.66	0.08	0.57	0.11	0.27	0.04	0.24	0.04
	(Sultan and Shazili 2009)	Malaysia	24.24	3.83	11.71	1.77	3.38	2.41	0.36	1.31	0.25	0.88	0.11	0.72	0.13
	(Zaremotlagh & Hezarkhani 2016)	Iran	454.44	59.89	306.98	52.71	151.92	117.72	34.83	26.36	6.81	13.22	7.64	14.3	4.78
	(Wang & Liang 2015)	China	891.59	355.20	384.44	48.16	2.76	10.30	2.50	7.85	2.06	3.19	1.36	2.90	0.69
shore	This study (shore samples)	UAE	0.95	0.23	0.87	0.19	0.05	0.16	0.03	0.15	0.03	0.07	<0.02	0.07	<0.02
	(Antonina et al., 2013)	Malaysia	16.30	4.30	12.80	4.20	3.39	2.47	0.65	1.54	0.59	1.04	0.42	1.20	0.66
	(Akinlua et al., 2016)	Nigeria	51.10	5.81	7.22	8.56	1.52	297.8	0.81	29.19	0.50	-	12.80	2.77	0.07
	(Naidu et al., 2013)	India	0.17	0.04	0.15	0.02	0.01	0.01	0.01	0.02	0.02	0.01	0.01	0.03	0.01
bottom	This study (Bottom sediments)	UAE	1.59	0.32	1.26	0.26	0.07	0.24	0.05	0.20	0.05	0.11	0.03	0.10	0.03
	(El Tokhi et al., 2015b)	UAE	3.43	0.74	2.83	0.60	0.18	0.50	0.11	0.48	0.16	0.30	0.10	0.27	0.10
	(Xu et al., 2009)	Korea	46.97	9.90	40.89	7.03	1.39	5.02	-	4.52	0.86	2.35	-	2.49	0.38
	(Xu et al., 2009)	China	33.29	7.38	31.15	5.77	1.15	4.41	-	4.24	0.83	2.29	-	2.48	0.38

4.2.9 REE Contamination Assessment

In order to calculate the enrichment factor (EF), which is widely used to estimate the anthropogenic impact on soil, Al is used as a conservative element to calculate the EF of REE (Wang and Liang, 2015). EF is based on the normalization of analytical data against the reference element (Al) using the following formula (Sutherland, 2000):

$$EF = (C_i/C_r)_{\text{sample}} / (C_i/C_r)_{\text{crust}}$$

where C_i is the average concentration of the REE (in ppm) in the study area, C_r is the concentration of the REE in the background (in ppm), sandstone average (Turekian and Wedepohl 1961), C_i is the average concentration of Al in the samples and C_r is the Al concentration in the background.

Calculations were made using content values of REE and Al in the upper continental crust from Turekian and Wedepohl (1961). The EF categories are based on the classifications by Birch (2003). As shown in Table 4.10, with exception of La (1.05) in shore samples, all the REE have an average EF <1 which indicate no enrichment. Even the average EF of the element La value in shore samples is slightly above the limit of this category. Most of LREE had average EF value slightly higher than HREE average, reflecting a relatively LREE enrichment influenced by the prevailing wind in this region. Enrichment factor (EF) of the different REE shows the order shore > soil > bottom, indicating that the shore samples were relatively enriched the most among other samples.

Contamination factor (CF) (Pekey, et al., 2004) is calculated also using the metal content in natural reference sediment is based on (Turekian and Wedepohl

1961). The CF categories are based on the classifications by (Pekey, et al., 2004). Results show that all the REE in all sites and environments had $CF < 1$ which indicate low contamination factor.

The pollution load index is calculated using the same equation used in heavy metal assessment (Tomlinson et al., 1980). Pollution load index of shore, soil and bottom samples (Table 4.10) is 0.68, 0.51 and 0.17, respectively. All PLI is < 1 , indicating no pollution.

The geoaccumulation index is calculated also using the average for sandstone for the element n by (Turekian & Wedepohl, 1961). All shore, soil and bottom sediments show $I\text{-geo} < 1$, which fall in uncontaminated class (Table 4.10). The negative values of geoaccumulation index indicate that the studied area is classified as uncontaminated.

Table 4.10: Average enrichment factors (EF), contamination factors (CF) and geoaccumulation indices (I-geo) for the soil, shore and bottom areas and for all samples together (overall average)

	La	Pr	Nd	Sm	Eu	Gd	Tb	Dy	Ho	Er	Tm	Yb	Lu
Earth crust (Turekian and Wedepohl 1961)	30	8.8	37	10	1.6	10	1.6	7.2	2	4	0.3	4	1.2
Enrichment Factors (soil)	0.81	0.69	0.66	0.5	0.78	0.47	0.36	0.58	0.39	0.49	0.82	0.43	0.17
Enrichment Factors (shore)	1.05	0.89	0.8	0.66	0.96	0.56	0.57	0.73	0.37	0.61	-	0.59	-
Enrichment Factors (bottom)	0.28	0.23	0.22	0.17	0.27	0.15	0.17	0.18	0.16	0.17	0.73	0.16	0.01
Enrichment Factors (overall average)	0.71	0.60	0.56	0.44	0.67	0.39	0.37	0.50	0.31	0.42	0.78	0.39	0.09
Contamination factors (soil)	0.11	0.10	0.09	0.07	0.11	0.07	0.05	0.08	0.06	0.07	0.13	0.06	0.03
Contamination factors (shore)	0.03	0.03	0.02	0.02	0.03	0.02	0.02	0.02	0.02	0.02	-	0.02	-
Contamination factors (bottom)	0.05	0.04	0.03	0.03	0.04	0.02	0.03	0.03	0.03	0.03	0.10	0.03	0.03
Contamination factors (overall average)	0.06	0.06	0.05	0.04	0.06	0.04	0.03	0.04	0.04	0.04	0.12	0.04	0.03
Geo-accumulation index (soil)	-3.7	-3.9	-4.0	-4.4	-3.7	-4.5	-4.8	-4.2	-4.79	-4.4	-3.4	-4.6	-5.6
Geo-accumulation index (shore)	-5.6	-5.8	-6	-6.2	-5.7	-6.5	-6.5	-6.1	-6.4	-6.4	-	-6.4	-
Geo-accumulation index (bottom)	-5.1	-5.3	-5.4	-5.8	-5.2	-5.9	-6.0	-5.7	-6.2	-5.8	-4.2	-6.0	-5.8
Geo-accumulation index (overall average)	-4.8	-5.0	-5.1	-5.5	-4.9	-5.6	-5.8	-5.3	-5.8	-5.5	-3.8	-5.7	-5.7

4.3 Radiology

4.3.1 Radionuclide Gamma and Alpha Activity

To observe the variation in gamma activity concentrations and hazard parameters, Figure 4.18 shows this tendency for each environment and sites, respectively. Generally, the gamma radioactivity concentrations in shore samples are much lower than the concentration in soil (due to tidal fluctuation and wave currents) and slightly lower than bottom sediments (shore samples < bottom sediments < soil samples) (Figure 4.18) and all are lower than the world average set by UNSCEAR (2000). The highest activity concentration of ^{238}U (^{226}Ra) is found in site S11 (soil sample) which is higher than the world average value (33 Bq/kg). In the case were ^{226}Ra concentration activity is much higher than world average, radioactive equilibrium is significantly disturbed with the $^{226}\text{Ra}/^{238}\text{U}$ ratio reaching high values (Anagnostakis et al., 2002). The high activity concentration of ^{226}Ra in S11 indicates a transport of ^{226}Ra to that surface soil. Furthermore, all the averages of the different three environments are below the world average value. These results demonstrate that the source of ^{226}Ra is natural and is coming from ^{238}U that had been incorporated in the sediments long time ago. The activity concentrations of ^{232}Th for all samples are lower than the activity concentration of the world average value (45 Bq/kg).

The activity concentrations of ^{40}K show a maximum value measured in bottom sediment found in M17, which locate to the east of the area where Jebel AlDhannah port is located. Other than anthropologic factor (due to harbor activities), high activity may be due to the muddy texture of M17 sample that lead to adsorption of radionuclides in lattice defects or onto crystal and grain boundaries (Baeza et al., 1995). High ^{40}K activity concentrations indicate high percentage of potassium level

that may come from K-feldspar such as microcline and anorthoclase as showed from mineralogical composition of the samples. Although there are wide variations in the activity concentrations of ^{40}K in the studied area, but all the activity concentrations averages of soil, shore and bottom sediment samples are below the world average values (420 Bq/kg).

Variation of radionuclides activities from one environment to another is expected while the difference in the same environment could be attributed to the physical and chemical sorting processes from one location to another. Activity concentrations are in the order $^{40}\text{K} > ^{238}\text{U} (^{226}\text{Ra}) > ^{232}\text{Th}$ in all sampling sites (except soil samples S19 & S21), where ^{232}Th activity concentrations are slightly higher than $^{238}\text{U} (^{226}\text{Ra})$. The higher activity concentrations found in soil could be explained in relation to geologic structure of the studied area, which is mainly Baynunah Formation (Miocene-age sandstones and limestones) (Whybrow et. al., 1999). The extensively eroded Miocene rocks is thought to be the origin of this sand which has been transported south to create the extensive dune fields that occupy much of the southern part of the area.

Our spectroscopic data indicate absence of ^{137}Cs peak in the runs of all samples. This observation is in accordance with the global distribution of ^{137}Cs atmospheric nuclear tests fallout (UNSCEAR, 1993) which suggests insignificant activity in the UAE soils.

The Estimated values of Radium equivalent and absorbed dose as shown Figure 4.18 are higher in soil while both shore and bottom sediments shows close values. Radium equivalent shows values less than the safe limit value 370 Bq/kg set by (UNSCEAR, 2000). Furthermore, the estimated absorbed dose in shore, soil and

bottom sediment samples is much less than the world average (57 nGy/hr) set by (UNSCEAR, 2000). The estimated contribution by individual components of natural radioactivity shows ^{40}K as the biggest contributor to the absorbed dose.

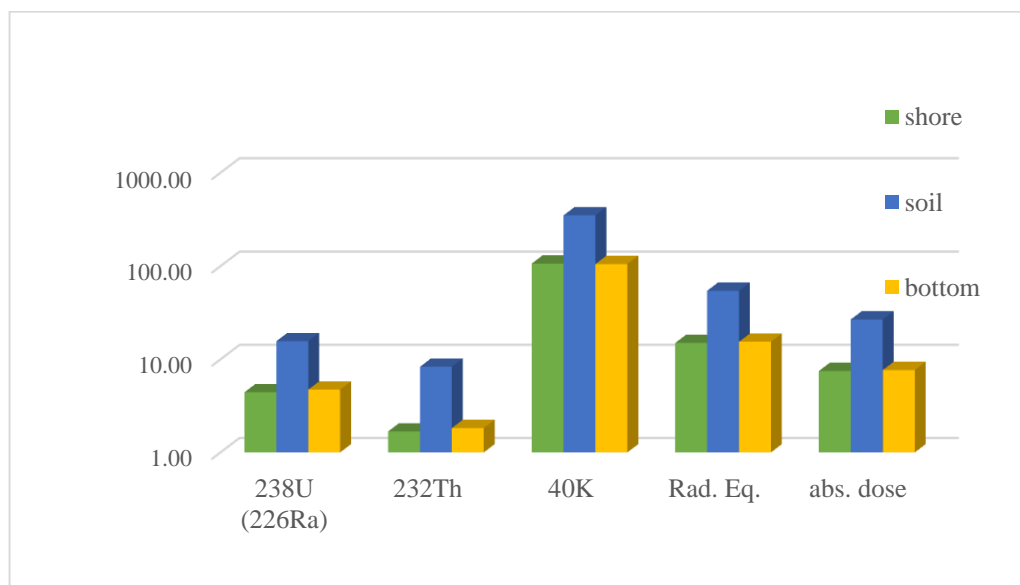


Figure 4.18: Average values of the radiological activities and radium equivalent in (Bq/kg) and absorbed dose (nGy/hr)

The alpha analysis result (see Table 3.22) shows that the $^{234}\text{U}/^{238}\text{U}$ activity ratios show wide range from 0.59 to 2.24. In closed systems older than 10^6 years ^{238}U decay chain should be at equilibrium where $^{234}\text{U}/^{238}\text{U}$ is approximately equal 1 in activity ratio (Holden, 1990, Cheng et al., 2000). The current study is done in open system where the daughter to parent ($^{234}\text{U}/^{238}\text{U}$) activity ratio is out of secular radioactive equilibrium. The depletion of ^{238}U in natural objects is a well-known phenomenon (Rosholt 1959 and Thurber 1962) and more other workers. Two main factors affect the disequilibrium, the direct recoil of ^{232}Th and its fast decay to ^{234}U near mineral grain boundaries and the leaching processes of ^{234}U from crystal lattices

that are damaged by energetic alpha decay (Andersen et al, 2009; Tokarev, 2005). Thus, the observed disequilibrium in the current data can be attributed to the geology of the area. The Western area of Abu Dhabi emirate contains terrestrial sediments related to the Miocene period. The substrate of this Miocene consists of a sequence of marls, sandstone, limestone and evaporation occurred southward and gently dipping (AlSharhan and Kendall, 2003). The presence of evaporites and carbonates can cause high $^{234}\text{U}/^{238}\text{U}$ ratio disequilibrium due to fractionation from water-rock interactions (Riotte and Chabaux, 1999). Faure and Mensing (2005) illustrated how uranyl ion (UO_2^{2+}) tends to form carbonate complexes, thus observable concentrations of U would be found in Ca carbonates minerals.

Correlation between the activities of ^{238}U (^{226}Ra) and ^{232}Th and between ^{238}U (^{226}Ra) and ^{40}K and between ^{232}Th and ^{40}K is presented in Figure 4.19. It is obvious that all the correlations in soil samples is rather weak, with correlation coefficient of 0.3 or less. Correlation between ^{238}U (^{226}Ra) and ^{40}K and between ^{232}Th and ^{40}K activities in shore samples show weak but relatively higher than soil samples. A good correlation exists between ^{238}U (^{226}Ra) and ^{232}Th in shore samples ($R^2=0.52$), which agrees with a previous study on the correlation between ^{238}U (^{226}Ra) and ^{232}Th in Egypt done by Eissa et al. (2010). In bottom samples a significant correlation is found between ^{238}U (^{226}Ra) and ^{40}K ($R^2=0.97$), which indicate that the presence of ^{40}K activities is related to the presence of ^{238}U (^{226}Ra) in bottom samples.

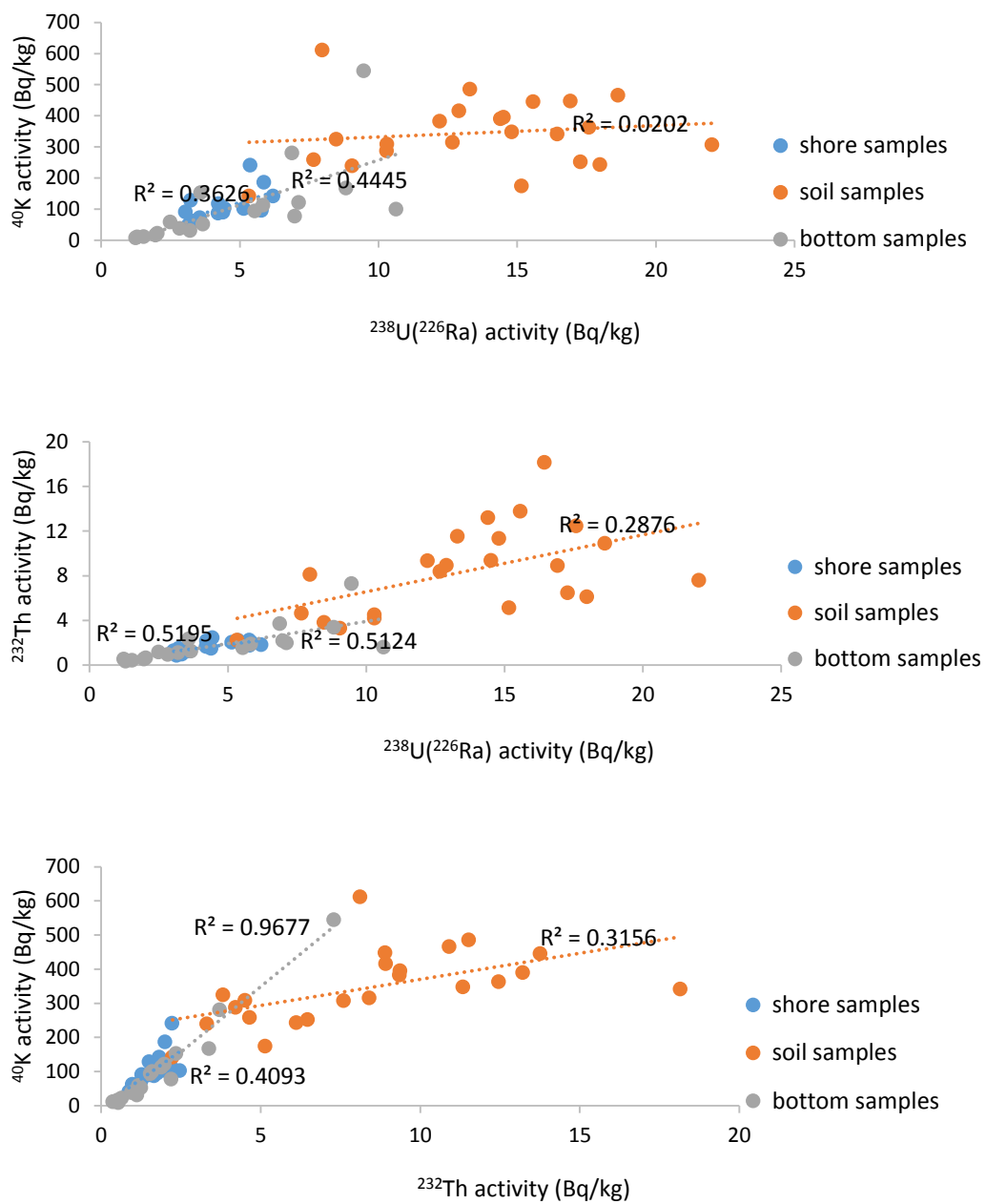


Figure 4.19: Correlation between ^{238}U (^{226}Ra), ^{232}Th and ^{40}K in different environments (shore, soil and bottom)

4.3.2 Spatial Distribution of Radionuclide Activity Concentrations

The spatial distribution (radiological map) of the measured radiological activities, radium equivalent and absorbed dose in the studied area is plotted in Figure 4.20. For plotting spatial distribution, Arcmap 10.1 was used by interpolation method (kernel smoothing). Interpolation method allows us to estimate activity values in a regularly distributed grid and to represent the corresponding activity fields. Two areas are observed with highest values at east and south portions of the map. The concentrations decrease from the south to the north, the highest activity concentrations of radionuclides as well as the absorbed dose are observed in the south where soil samples were collected. The north and west areas of the maps show lower activity concentrations where both shore and bottom sediment samples were collected. Tidal fluctuation and wave currents effectively lower the activity concentrations of radionuclides in shore sediments and that indicate the low measured values in the current study. It can be seen that to the northern east of the map there is a slight increase in the radionuclides activities, Radium equivalent and absorbed dose readings. The eastern part represents Jebel AlDhannah port where some anthropogenic activities are present and that may positively affect the activity concentrations of the radionuclides and other hazard parameters.

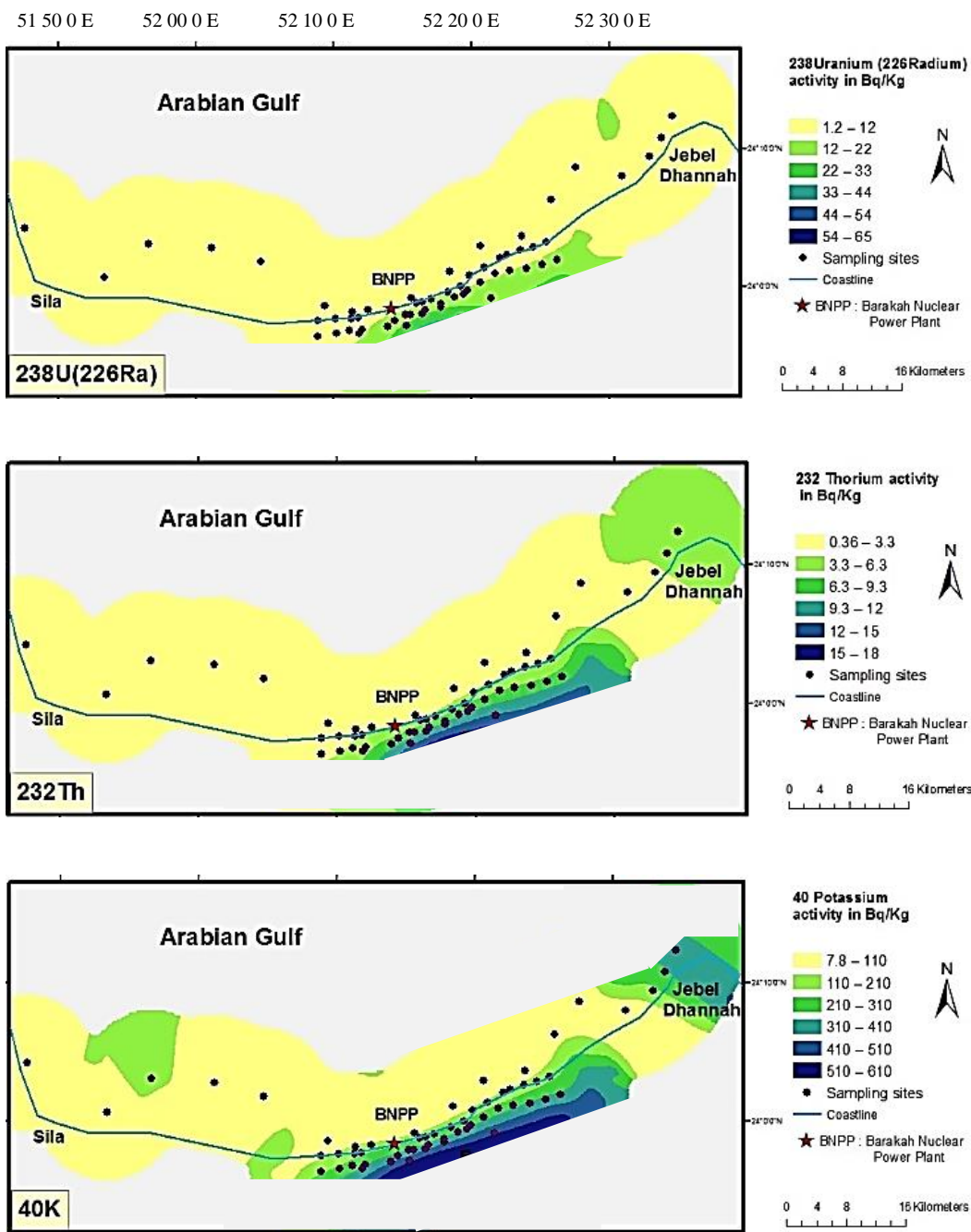


Figure 4.20: Spatial Distribution pattern of radionuclides activities, Rad_{eq} and abs. dose in the studied area

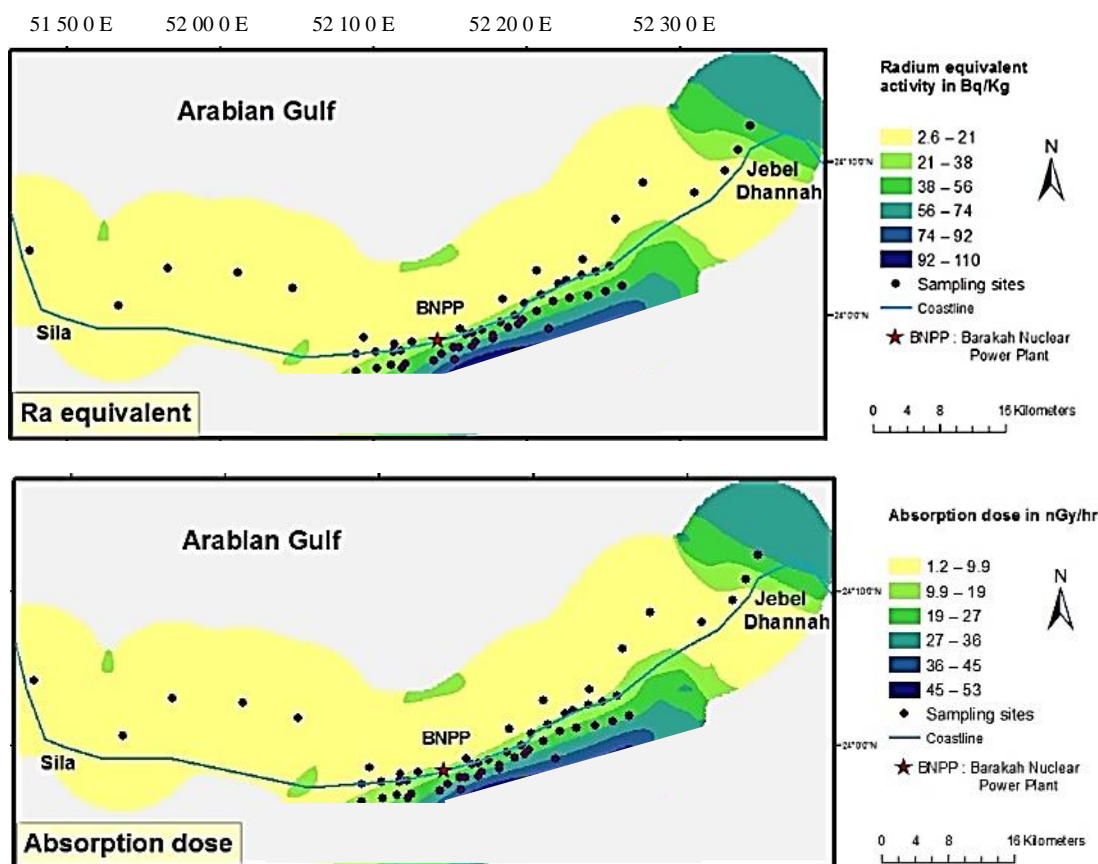


Figure 4.20: Spatial Distribution pattern of radionuclides activities, Rad.eq. and abs. dose in the studied area

4.3.3 Regional and World Average Comparison of Radionuclide Activity Concentrations

Some measured values of radionuclides activities presented from other researchers are given for comparison in Table 4.11. Activity concentrations of radionuclide in soil for Oman, Yemen and Jordan are below the world average except India, which was very high. On the other hand, the estimated activity concentrations of the current study is close with the published data done by (Alali, 2003) on shore sediments in Abu Dhabi. Moreover, the activity concentrations of radionuclide in shore of Chain and Gulf of Aqaba are very close that of UAE, while

beaches of Iran and Turkey shows elevated activity concentrations for all radionuclides. Furthermore, radionuclide activity concentrations in bottom sediments of the current studied area are very close to that of Gulf of Aqaba while the estimated activity concentrations of ^{238}U of Red Sea is higher than the world average.

Table 4.11: International and regional comparison of radionuclide activity concentrations (in Bq/kg)

	References	Location	^{238}U (^{226}Ra)	^{232}Th	^{40}K
soil	This study (soil samples)	UAE	15.68	8.31	349.72
	(Kannan et al., 2002)	India	36-258	352-3872	324-405
	(Saleh , 2012)	Oman	14.4	9.95	158.2
	(Abd El-Mageed et al., 2011)	Yemen	44.4	58.2	822.7
	(Ahmad et al., 1997)	Jordan	9.9	20.1	88.7
shore	This study (shore samples)	UAE	4.43	1.68	106.30
	(Alali, 2003)	UAE	26.38	4.78	219.21
	(Lu & Zhang 2008)	China	7.6-17.2	7.8-25.1	883.4-1313.6
	(Abdi et al., 2009)	Iran	177	117	1085
	(Al-Trabulsy et al., 2011)	Gulf of Aqaba	11.4	22.5	641.1
	(Orgun et al., 2007)	Turkey	290.4	532.0	1160.8
bottom	This study (Bottom sediments)	UAE	1.59	0.32	1.26
	(Ababneh et al., 2010)	Gulf of Aqaba	3.43	0.74	2.83
	(Al-Zahrany et al., 2012)	Red Sea	35.3	0.92	34.34
Worldwide values (UNSCEAR, 2000)		-	33	45	420

4.4 Relationships between Heavy Metals, Rare Earth Elements (REE) and Natural Radioactivity Concentrations

In order to investigate the correlations between heavy metals, REE and natural radionuclides in all studied soil, shore and bottom sediment samples, some statistical analysis including the correlation matrix (Pearson correlation coefficient) and cluster analysis were carried out using SPSS program.

4.4.1 Pearson Correlation Coefficient

Pearson correlation coefficient (Rollinson, 1993) is used to study the correlation (at 95% level) between radionuclides, major oxides, heavy metals, and REE in the studied samples. Table 4.12 and 4.13 represent the correlation matrix between all elements in soil samples. Some major oxides such as Al_2O_3 , FeO and K_2O are highly positively correlated with some heavy metals in the studied soil samples. It is clear from this correlation that, in soil, FeO plays an important role in adsorbing heavy metal elements (Teemofeeva and Golov, 2007). The negative correlation of both Ca and Sr with all heavy metals and major oxides in soil samples indicate evaporitic source of Ca and Sr. This is supported by the mineralogical composition of soil samples that shows the presence of both aragonite and calcite.

Both Co and Mn show significant positive correlation with most of the rest elements except for Ca where the relation is negative. This can be related to that Co and Mn are mainly controlled by the content of continental clay (Fruth and Scherreiks, 1975). Significant positive correlations were found among major oxides and heavy metals (Table 4.12), especially Cu-Zn ($R^2=0.89$), Cu-Co ($R^2=0.93$), Cu-Mn ($R^2=0.75$), Cu-V ($R^2=0.91$), Cu-Cr ($R^2=0.89$), Mn-V ($R^2=0.88$), Al_2O_3 -Cr ($R^2=0.94$) and Al_2O_3 -Cu ($R^2=0.93$).

On the other hand, ^{232}Th shows significantly negative correlation with Ca and positive correlation with SiO_2 and Al_2O_3 (Table 4.13). Table 4.13 also shows significant positive correlation between ^{40}K and SiO_2 ($R^2=0.82$), which may be interpreted as presence of some anorthoclase and microcline minerals as indicated from mineralogical composition of the soil samples and the high measured activity concentration of ^{40}K by gamma analysis in the current study.

Correlations between major oxides (%) and heavy metals (ppm) in shore samples are shown in Table 4.14. The strong positive correlation between Sr - Ca suggests that strontium is associated with Ca in marine biogenic carbonate material. The presence of relatively high Sr concentration indicates the presence of significant amount of aragonite (Fernandez-Bastero et al., 1999). This agree with the biogenic origin of most of the carbonate deposits of the Arabian Gulf (Ellis and Milliman, 1985). Furthermore, this explanation is supported by the mineralogical composition of the shore samples where it shows the presence of aragonite as a major and moderate in many sites as well as the high carbonate content (average of 67.70 %). Significant correlation is found among major oxides and heavy metals (Table 4.14), especially Cu-Zn ($R^2=0.64$), Cu-Co ($R^2=0.79$), Cu-Mn ($R^2=0.91$), Cu-V ($R^2=0.65$), Cu-Cr ($R^2=0.89$), Mn-Cr ($R^2=0.95$), Al_2O_3 -Cr ($R^2=0.95$).

Table 4.15 shows the correlation of ^{238}U , ^{232}Th , ^{40}K (Bq/kg) and major oxides (%) in shore samples. There are negative correlations between each of Ca and Sr with ^{238}U , ^{232}Th , ^{40}K . On the other hand, SiO_2 and Al_2O_3 show positive correlations with ^{238}U , ^{232}Th , ^{40}K . Moreover, all major oxides and heavy metals are negatively correlated with Ca and Sr but positively correlated with SiO_2 and Al_2O_3 . The

previous relations may pointing that uranium and thorium has detrital sources possibly associated with silicate minerals.

Table 4.16 and 4.17 represent the correlation matrix between all elements in bottom sediments. Table 4.16 shows many significant positive correlations between Al_2O_3 , FeO and K_2O with some metals or among heavy metals. These significant positive correlations especially for Mn and Fe with other heavy metals are due to oxidation and reduction process in solutions that are controlled by the activity of free electrons (Sposito, 1983). Both Mn and Fe have different valences and many heavy metals such as Cu, Co, Cr, and Ni are associated with their oxides. Mineralogical shows minerals such as magnesite (Oxide of iron, manganese, niobium, and tantalum). MgO shows negative correlation with most of the elements except Ca and Sr. Magnesium is a major constituent of carbonate minerals such as dolomite $\text{CaMg}(\text{CO}_3)_2$, which is present in bottom sediment samples as revealed by mineralogical composition of the samples. Significant correlation is found among major oxides and heavy metals (Table 4.16), especially Cu-Ni ($R^2=0.81$), Cu-Co ($R^2=0.82$), Cu-FeO ($R^2=0.81$), Cu- K_2O ($R^2=0.81$), Zn-Ni ($R^2=0.92$), Zn-Co ($R^2=0.93$), Zn-Mn ($R^2=0.94$), Zn-FeO ($R^2=0.93$), FeO-Cr ($R^2=0.96$), Al_2O_3 -Cr ($R^2=0.98$), Al_2O_3 -Co ($R^2=0.98$).

Table 4.17 shows significant positive correlation between ^{40}K and SiO_2 ($R^2=0.84$), which is similar to soil samples in addition to a significant negative correlation of ^{40}K with both Sr and Ca. Both ^{232}Th and ^{238}U show significantly negative correlation with Ca and Sr, in addition to significantly positive correlation with SiO_2 and Al_2O_3 . Soil, shore and bottom sediment samples have positive correlations between SiO_2 and ^{232}Th , suggesting a terrigenous source of ^{232}Th . This

result is supported by Al Rashdi and Siad (2015) findings on Abu Dhabi beach sediments.

Using Pearson correlation between the activity concentrations of ^{238}U , ^{232}Th , ^{40}K (Bq/kg) and the ΣREE in soil, shore and bottom sediment samples (Tables 4.18-4.20) indicate that the ^{238}U and ^{232}Th content is significantly positive correlated with the ΣREE content in shore and bottom sediments. On the other hand, soil samples exhibit significantly positive correlation between ^{232}Th and ΣREE while a lower positive correlation between ΣREE and each of ^{238}U and ^{40}K , which is in agreement with the findings reported by Popic et al., 2001 in soil samples in Norway.

Table 4.12: Pearson correlation coefficients between major oxides (%) and heavy metals (ppm) in soil samples (red values indicate significant correlation at 0.01 level)

	Cu	Pb	Zn	Ni	Co	Mn	Cd	V	Cr	As	Mo	Ca	Sr	SiO ₂ %	FeO%	MgO%	Al ₂ O ₃ %	Na ₂ O%	K ₂ O%	ΣREE	
Cu	1.00																				
Pb	0.53	1.00																			
Zn	0.89	0.61	1.00																		
Ni	0.51	0.50	0.59	1.00																	
Co	0.93	0.64	0.90	0.71	1.00																
Mn	0.75	0.65	0.70	0.46	0.83	1.00															
Cd	0.47	0.47	0.53	0.34	0.59	0.82	1.00														
V	0.91	0.53	0.83	0.43	0.89	0.88	0.58	1.00													
Cr	0.89	0.37	0.86	0.54	0.83	0.49	0.24	0.76	1.00												
As	-0.12	0.10	-0.08	0.07	-0.13	-0.03	-0.10	-0.06	-0.06	1.00											
Mo	0.42	0.28	0.36	0.35	0.51	0.66	0.57	0.53	0.26	-0.03	1.00										
Ca	-0.49	-0.48	-0.40	-0.31	-0.57	-0.60	-0.42	-0.56	-0.28	0.50	-0.38	1.00									
Sr	-0.08	0.02	-0.05	-0.03	-0.06	0.05	0.21	-0.04	-0.06	0.08	-0.09	0.24	1.00								
SiO ₂ %	0.27	0.38	0.14	-0.13	0.28	0.39	0.27	0.33	0.07	-0.36	0.13	-0.76	-0.15	1.00							
FeO%	0.95	0.52	0.85	0.44	0.91	0.77	0.49	0.90	0.85	-0.28	0.40	-0.63	-0.07	0.43	1.00						
MgO%	0.48	0.38	0.51	0.47	0.51	0.58	0.46	0.58	0.42	0.41	0.63	-0.06	-0.13	-0.27	0.33	1.00					
Al ₂ O ₃ %	0.93	0.42	0.87	0.36	0.84	0.58	0.34	0.83	0.94	-0.16	0.24	-0.39	-0.07	0.28	0.91	0.33	1.00				
Na ₂ O%	0.18	0.04	0.16	0.50	0.25	0.19	0.15	0.16	0.13	-0.24	0.30	-0.18	-0.15	-0.39	0.16	0.30	0.02	1.00			
K ₂ O%	0.78	0.50	0.83	0.43	0.76	0.59	0.45	0.73	0.72	-0.31	0.24	-0.48	-0.22	0.18	0.78	0.40	0.79	0.36	1.00		
ΣREE	0.88	0.60	0.80	0.312	0.84	0.75	0.52	0.83	0.75	-0.30	0.22	-0.62	0.04	0.55	0.94	0.18	0.88	0.01	0.76	1.00	

Table 4.13: Pearson correlation coefficients between ^{238}U , ^{232}Th , ^{40}K (Bq/kg) and major oxides (%) in soil samples (red values indicate significant correlation at 0.01 level)

	^{238}U	^{232}Th	^{40}K	Ca	Sr	SiO ₂ %	FeO%	MgO%	Al ₂ O ₃ %	Na ₂ O%	K ₂ O%
^{238}U	1.00										
^{232}Th	0.13	1.00									
^{40}K	0.25	0.53	1.00								
Ca	-0.33	-0.62	-0.86	1.00							
Sr	0.27	-0.02	-0.15	0.24	1.00						
SiO ₂ %	0.25	0.57	0.82	-0.76	-0.15	1.00					
FeO%	0.26	0.68	0.42	-0.63	-0.07	0.43	1.00				
MgO%	0.24	-0.17	-0.25	-0.06	-0.13	-0.27	0.33	1.00			
Al ₂ O ₃ %	0.12	0.55	0.25	-0.39	-0.07	0.28	0.91	0.33	1.00		
Na ₂ O%	-0.02	-0.01	-0.11	-0.18	-0.15	-0.39	0.16	0.30	0.02	1.00	
K ₂ O%	0.13	0.47	0.36	-0.48	-0.22	0.18	0.78	0.40	0.79	0.36	1.00

Table 4.14: Pearson correlation coefficients between major oxides (%) and heavy metals (ppm) in shore samples (red values indicate significant correlation at 0.01 level)

	Cu	Pb	Zn	Ni	Co	Mn	Cd	V	Cr	As	Mo	Ca	Sr	SiO ₂ %	FeO%	MgO%	Al ₂ O ₃ %	NA ₂ O%	K ₂ O%	ΣREE	
Cu	1.00																				
Pb	0.58	1.00																			
Zn	0.64	0.67	1.00																		
Ni	0.57	0.37	0.52	1.00																	
Co	0.79	0.44	0.53	0.50	1.00																
Mn	0.91	0.44	0.50	0.64	0.69	1.00															
Cd	0.26	0.24	0.27	0.14	0.24	0.34	1.00														
V	0.65	0.15	0.35	0.31	0.33	0.73	0.27	1.00													
Cr	0.89	0.50	0.45	0.64	0.66	0.95	0.13	0.60	1.00												
As	0.02	-0.10	-0.30	-0.37	-0.12	0.08	0.50	0.21	-0.03	1.00											
Mo	0.48	0.25	0.38	0.15	0.03	0.43	-0.27	0.46	0.45	0.00	1.00										
Ca	-0.75	-0.34	-0.30	-0.41	-0.48	-0.79	-0.32	-0.52	-0.77	-0.38	-0.42	1.00									
Sr	-0.81	-0.46	-0.54	-0.44	-0.64	-0.81	-0.38	-0.56	-0.73	-0.27	-0.48	0.85	1.00								
SiO ₂ %	0.70	0.28	0.13	0.36	0.44	0.78	0.13	0.46	0.82	0.33	0.46	-0.94	-0.78	1.00							
FeO%	0.57	0.36	0.16	0.23	0.42	0.44	-0.37	0.03	0.63	-0.08	0.43	-0.58	0.45	0.68	1.00						
MgO%	0.52	0.30	0.59	0.42	0.60	0.54	0.33	0.55	0.40	0.05	0.18	-0.29	-0.67	0.21	-0.05	1.00					
Al ₂ O ₃ %	0.82	0.50	0.31	0.53	0.56	0.87	0.12	0.51	0.95	0.09	0.40	-0.82	-0.67	0.87	0.70	0.20	1.00				
NA ₂ O%	-0.03	0.07	-0.18	0.05	-0.06	0.08	-0.04	-0.35	0.23	0.00	-0.03	-0.28	-0.07	0.40	0.30	-0.39	0.36	1.00			
K ₂ O%	0.54	0.15	-0.09	0.10	0.34	0.53	-0.17	0.20	0.67	0.19	0.37	-0.75	-0.50	0.87	0.82	-0.13	0.76	.50	1.00		
ΣREE	0.84	0.43	0.38	0.61	0.61	0.92	0.21	0.56	0.94	0.12	0.42	-0.90	-0.80	0.91	0.66	0.34	0.96	0.28	0.71	1.00	

Table 4.15: Pearson correlation coefficients between ^{238}U , ^{232}Th , ^{40}K (Bq/kg) and major oxides (%) in shore samples (red values indicate significant correlation at 0.01 level)

	^{238}U	^{232}Th	^{40}K	Ca	Sr	SiO ₂ %	MgO%	Al ₂ O ₃ %	Na ₂ O%	K ₂ O%
^{238}U	1.00									
^{232}Th	0.72	1.00								
^{40}K	0.60	0.64	1.00							
Ca	-0.72	-0.78	-0.89	1.00						
Sr	-0.61	-0.53	-0.81	0.85	1.00					
SiO ₂ %	0.64	0.77	0.89	-0.94	-0.78	1.00				
FeO%	0.33	0.43	0.58	-0.58	-0.45	0.68				
MgO%	0.30	0.03	0.41	-0.29	-0.67	0.21	1.00			
Al ₂ O ₃ %	0.76	0.81	0.76	-0.82	-0.67	0.87	0.20	1.00		
Na ₂ O%	0.04	0.54	0.32	-0.28	-0.07	0.40	-0.39	0.36	1.00	
K ₂ O%	0.40	0.60	0.75	-0.75	-0.50	0.87	-0.13	0.76	0.50	1.00

Table 4.16: Pearson correlation coefficients between major oxides (%) and heavy metals (ppm) in bottom sediments (red values indicate significant correlation at 0.01 level)

	Cu	Pb	Zn	Ni	Co	Mn	Cd	V	Cr	As	Mo	Ca	Sr	SiO2%	FeO%	MgO%	Al2O3%	Na2O%	K2O%	ΣREE	
Cu	1.00																				
Pb	0.29	1.00																			
Zn	0.75	0.14	1.00																		
Ni	0.81	0.08	0.92	1.00																	
Co	0.82	0.09	0.93	0.98	1.00																
Mn	0.68	-0.07	0.94	0.96	0.94	1.00															
Cd	0.31	-0.41	0.62	0.60	0.57	0.69	1.00														
V	0.78	-0.06	0.78	0.92	0.92	0.85	0.52	1.00													
Cr	0.79	0.00	0.92	0.97	0.98	0.95	0.57	0.92	1.00												
As	0.57	0.16	0.12	0.37	0.34	0.16	0.03	0.53	0.31	1.00											
Mo	0.77	0.28	0.39	0.64	0.59	0.46	0.18	0.68	0.57	0.80	1.00										
Ca	-0.54	-0.56	-0.74	-0.65	-0.68	-0.61	-0.15	-0.50	-0.65	0.01	-0.28	1.00									
Sr	-0.51	-0.55	-0.73	-0.69	-0.69	-0.67	-0.23	-0.47	-0.65	-0.02	-0.31	0.88	1.00								
SiO2%	0.47	0.35	0.74	0.65	0.65	0.69	0.18	0.47	0.68	-0.17	0.20	-0.88	-0.80	1.00							
FeO%	0.81	0.20	0.93	0.96	0.97	0.92	0.46	0.88	0.96	0.31	0.59	-0.78	-0.75	0.78	1.00						
MgO%	-0.11	-0.21	-0.45	-0.22	-0.23	-0.31	-0.14	-0.05	-0.25	0.41	0.15	0.59	0.36	-0.74	-0.37	1.00					
Al2O3%	0.77	0.06	0.91	0.98	0.98	0.94	0.56	0.93	0.98	0.35	0.59	0.68	-0.66	0.68	0.97	-0.27	1.00				
Na2O%	0.47	0.26	0.06	0.24	0.25	0.07	-0.07	0.34	0.17	0.64	0.66	0.11	-0.01	-0.31	0.17	0.61	0.19	1.00			
K2O%	0.81	0.09	0.82	0.93	0.93	0.84	0.59	0.93	0.90	0.55	0.72	-0.53	-0.53	0.44	0.89	-0.05	0.93	0.44	1.00		
ΣREE	0.72	0.02	0.94	0.95	0.95	0.97	0.53	0.86	0.97	0.18	0.47	-0.70	-0.70	0.79	0.97	-0.39	0.96	0.04	0.83	1.00	

Table 4.16: Pearson correlation coefficients between ^{238}U , ^{232}Th , ^{40}K (Bq/kg) and major oxides (%) in bottom sediments (red values indicate significant correlation at 0.01 level)

	^{238}U	^{232}Th	^{40}K	Ca	Sr	SiO ₂ %	MgO%	Al ₂ O ₃ %	Na ₂ O%	K ₂ O%
^{238}U	1.00									
^{232}Th	0.71	1.00								
^{40}K	0.66	0.98	1.00							
Ca	-0.53	-0.74	-0.75	1.00						
Sr	-0.49	-0.71	-0.73	0.88	1.00					
SiO ₂ %	0.64	0.81	0.84	-0.88	-0.80	1.00				
MgO%	-0.19	-0.46	-0.53	0.59	0.36	-0.74	1.00			
Al ₂ O ₃ %	0.75	0.94	0.91	-0.68	-0.66	0.68	-0.27	1.00		
Na ₂ O%	0.01	0.03	-0.08	0.11	-0.01	-0.31	0.61	0.19	1.00	
K ₂ O%	0.59	0.81	0.75	-0.53	-0.53	0.44	-0.05	0.93	0.44	1.00

Table 4.17: Pearson correlation coefficients between the activity concentrations of ^{238}U , ^{232}Th , ^{40}K (Bq/kg) and the REE (in ppm) in soil samples (red values indicate significant correlation at 0.01 level)

	^{238}U	^{232}Th	^{40}K	Rad. eq.	Abs. dose	Σ REE
^{238}U	1.00					
^{232}Th	0.13	1.00				
^{40}K	0.25	0.53	1.00			
Rad. eq.	0.76	0.62	0.76	1.00		
Abs. dose	0.74	0.61	0.79	0.99	1.00	
Σ REE	0.31	0.76	0.51	0.65	0.64	1.00

Table 4.18: Pearson correlation coefficients between the activity concentrations of ^{238}U , ^{232}Th , ^{40}K (Bq/kg) and the REE (in ppm) in shore samples (red values indicate significant correlation at 0.01 level)

	^{238}U	^{232}Th	^{40}K	Rad. eq.	Abs. dose	Σ REE
^{238}U	1.00					
^{232}Th	0.72	1.00				
^{40}K	0.6	0.64	1.00			
Rad. eq.	0.76	0.77	0.96	1.00		
Abs. dose	0.74	0.75	0.97	0.99	1.00	
Σ REE	0.78	0.81	0.82	0.89	0.89	1.00

Table 4.19: Pearson correlation coefficients between the activity concentrations of ^{238}U , ^{232}Th , ^{40}K (Bq/kg) and the REE (in ppm) in bottom sediment samples (red values indicate significant correlation at 0.01 level)

	^{238}U	^{232}Th	^{40}K	Rad. eq.	Abs. dose	Σ REE
^{238}U	1.00					
^{232}Th	0.71	1.00				
^{40}K	0.66	0.98	1.00			
Rad. eq.	0.78	0.98	0.98	1.00		
Abs. dose	0.77	0.98	0.98	1.00	1.00	
Σ REE	0.75	0.97	0.96	0.97	0.97	1.00

4.4.2 Cluster Analysis of Soil, Shore and Bottom Sediment Samples

Cluster analysis is the simplest form of meaningfully grouping of measured variables (David, 1973). Cluster analysis is also define as a multivariate technique extensively using by numerical taxonomists (Sokal and Sneath, 1963). Dendrogram is a method of showing the degree of similarity between multivariate objects. The samples with closest relation will lie near each other (Rock, 1988 and Haan, 2002).

Hierarchical agglomerative cluster analysis is performed using 26 variables; radionuclides, REE, heavy metals, and major oxides (^{238}U , ^{232}Th , ^{40}K , Abs. dose, Ra_{eq} , $\sum \text{REE}$, Cu, Pb, Zn, Ni, Co, Mn, Fe, Cd, V, Cr, As, Mo, Ca, Sr, $\text{SiO}_2\%$, $\text{FeO}\%$, $\text{MgO}\%$, $\text{Al}_2\text{O}_3\%$, $\text{Na}_2\text{O}\%$, $\text{K}_2\text{O}\%$) for each environments (soil, shore and bottom sediments) using Centroid method with Squared Euclidean distances as a measure of similarity. The results is presented as dendrograms (Figures 4.21-4.23) for soil, shore and bottom sediments, respectively. The three dendrograms are almost similar showing that all elements are cluster together except Fe and Sr. In soil dendrogram (Figure 4.21), elements cluster with Sr at linkage distance of 8, then Fe will join the association at linkage distance of 25. While elements cluster with Fe at linkage distance of 2 and 7 in shore (Figure 4.22) and bottom sediments (Figure 4.23), respectively. Finally, Sr linked the association at linkage distance of 25 for both. While

The association of these elements can be explained using XRD analysis results. Quartz and/or aragonite are the main composition for shore and bottom sediments, while for soil it is quartz. Therefore, the elements associations in shore and bottom sediments indicate the dominance of carbonate minerals while the association of soil samples is terrestrial origin.

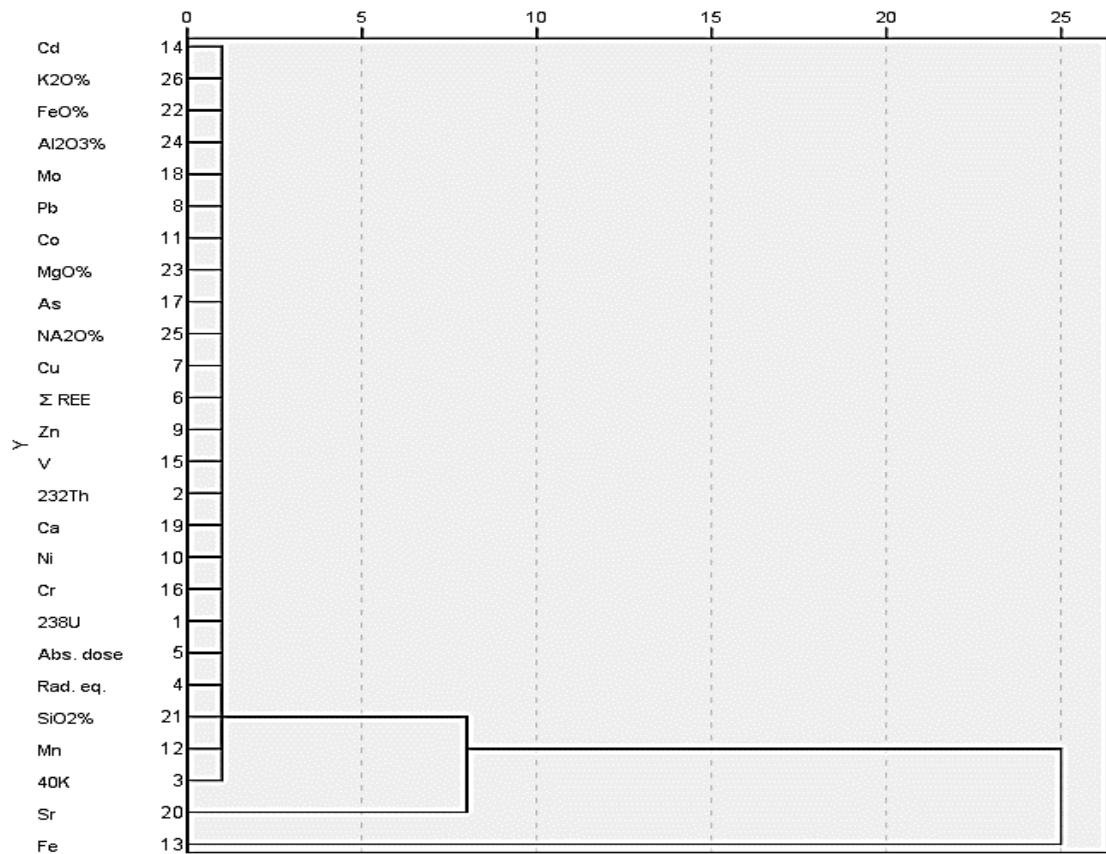


Figure 4.21: Dendrogram for soil samples using centroid method

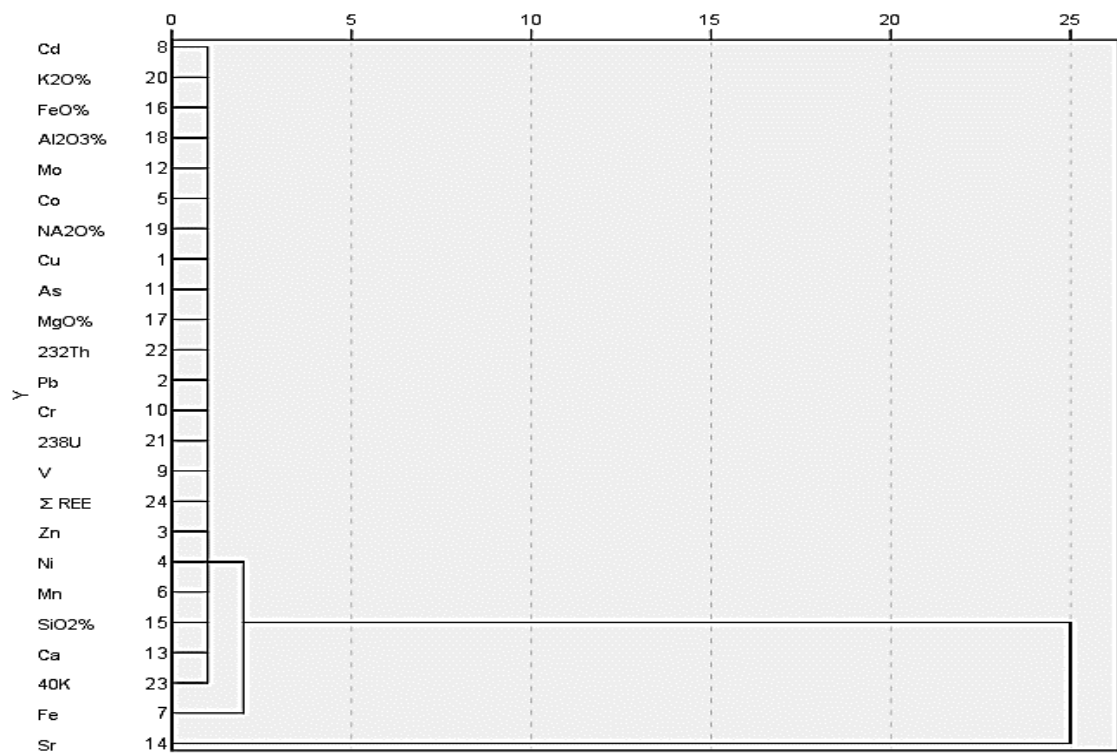


Figure 4.22: Dendrogram for shore samples using centroid method

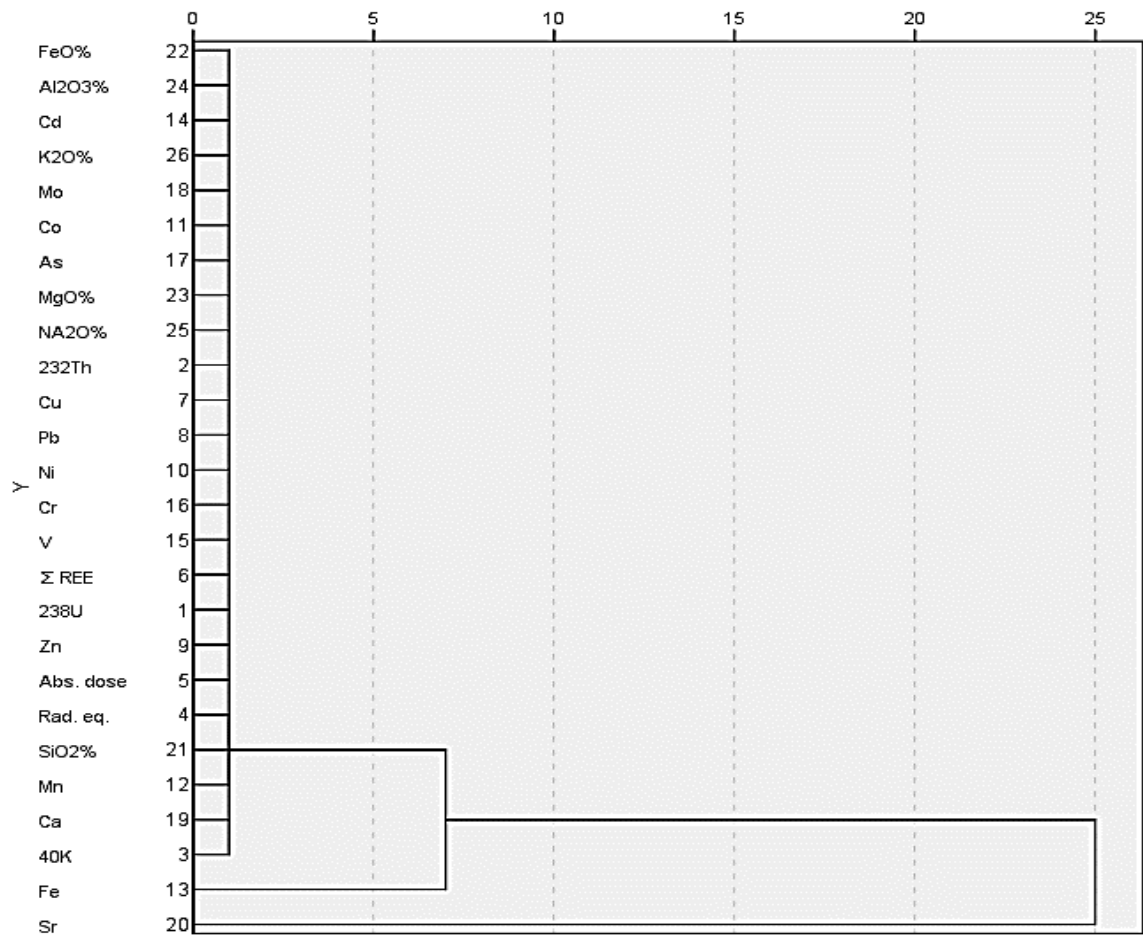


Figure 4.23: Dendrogram for bottom sediment samples using centroid method

Chapter 5: Conclusion and Recommendation

5.1 Concluding Summary

The aim of this study is to examine the heavy metal concentrations and the activity concentrations of gamma-emitting natural radionuclides, in addition to determination of ^{234}U and ^{238}U activity ratio of the area surrounding the nuclear power plant in the UAE, the Barakah Nuclear Power Plant (NPP). Moreover, to establish a documented radiological reference data about Barakah area pre-operation of BNPP to enable the assessment of revealing any radioactive contamination and evaluate any associated environmental impact, after the nuclear power plant commences. The current study will be the first published radiological study focuses on the Barakah NPP site.

Based on the obtained results and discussion, the following main conclusions and recommendations can be drawn out:

- Fifty-eight samples were collected across three areas, Sila, Barakah and Jebel Dhannah, and were grouped in three categories, “soil”, “shore” and “bottom” depending on where the samples were collected from.
- On average, soil samples showed more heavy metal concentrations than the bottom samples, which in turn, were higher than the shore samples. Overall, iron and manganese were present in the highest concentrations, while cadmium was present in the lowest concentrations.
- According to the grain size analysis, most of the samples were mainly composed of medium to course sand. The inverse relationship between

the grain size and the contamination of heavy metals was observed for all metals.

- All heavy metals concentrations were significantly below the UAE soil contamination safe limits. The levels of heavy metals and REE reported in the current study were lower than levels reported in the soil, shore and bottom sediments of countries around the world.
- Enrichment factor calculated for heavy metals showed no to moderate enrichment (As and Cd). While the contamination factor (CF) was $CF < 1$ which indicate low contamination factor. Geoaccumulation results indicate that the studied area was uncontaminated. Furthermore, the pollution load index, > 1 , indicates polluted area.
- The BNPP area was uncontaminated with REE, furthermore, soil, shore and bottom sediment samples show different degree of REE enrichment.
- LREE were more abundant than HREE. Among the REE, Nd was the most abundant element. The chondrite normalized REE patterns in shore, soil and bottom sediments indicated an enrichment of LREE over HREE.
- With exception of La in shore samples, all the REE show no enrichment. Contamination factor for REE $CF < 1$, which indicates a low contamination factor and geoaccumulation results indicate that the studied area was uncontaminated. Moreover, the pollution load index, < 1 , indicates no pollution in the area.
- The spatial distribution of REE was more compact in the south compared to the north, with less severe contaminations in the east and west.

- The natural radioactivity of ^{238}U (^{226}Ra), ^{232}Th and ^{40}K measured suggested that the measured natural concentration activities were below the world average and the anthropogenic radionuclide ^{137}Cs is below the detection limit.
- The $^{234}\text{U}/^{238}\text{U}$ ratio measured by alpha spectrometry show wide range, which reflect that the area was not, closed system with different sources, there was disequilibrium between ^{234}U and ^{238}U , and that can be attributed to the geology of the area.
- The studied relations between major oxides and radionuclides may pointing that uranium and thorium have detrital sources possibly associated with silicate minerals.
- The highest concentrations of heavy metal and REE in addition to natural radioactivity concentrations appeared in same sites (S14, S15 (Soil), B4, B15 (shore) and M17, M18 (bottom)).
- This study is considered as a radiological baseline for the Barakah Nuclear Power Plant area and might be used to evaluate the impact from Barakah Nuclear Power Plant when operation start in 2018.

5.2 Further Work

- Periodic radiological monitoring around the Barakah Nuclear Power Plant is recommended after the operation of the plant.
- Anthropogenic radionuclides such as Pu and Po might be considered in the coming investigations around the area.

References

- Ababneh, Z.Q., Al-Omari, H., Rasheed, M., Al-Najjar, T., & Ababneh, A.M. (2010). Assessment of gamma-emitting radionuclides in sediment cores from the gulf of Aqaba, Red Sea. *Radiation Protection Dosimetry*, 141 (3), 289-298.
- Abbot, R. T. (1976). *Kingdom of the seashell*. Crown publishers, New York, USA. 16-26.
- Abd El-Mageed, A.I., El-Kamel, A.H., Abbady, A., Harb, S., Youssef, A.M.M., & Saleh, I.I. (2011). Assessment of natural and anthropogenic radioactivity levels in rocks and soils in the environments of Juban town in Yemen. *Radiation Physics and Chemistry*, 80 (6), 710-715.
- Abdi, M.R., Hassanzadeh, S., Kamali, M., & Raji, H.R. (2009). ^{238}U , ^{232}Th , ^{40}K and ^{137}Cs activity concentrations along the southern coast of the Caspian Sea, Iran. *Marine Pollution Bulletin*, 58 (5), 658-662.
- Abu-Hilal, A.H. (1987). Distribution of trace elements in near shore surface sediments from the Jordan Gulf of Aqaba (Red Sea). *Marine Pollution Bulletin*, 18, 190–193.
- Abyachi, J. K., & Douabul, A. A. (1986). Trace element geochemical association in the Arabian Gulf. *Mar. Poll. Bull*, 17, 353-356.
- Ahmad, N., Matiullah, Khatebeh, A.J.A.H., Ma'ly, A., & Kenawy, M.A. (1997). Measurement of natural radioactivity in Jordanian sand. *Radiation Measurements*, 28 (6), 341-344.
- Akinlua, A., Olise F., Akomolafe, A., & McCrindle, R. (2016). Rare earth element geochemistry of petroleum source rocks from northwestern Niger Delta. *Marine and Petroleum Geology*, 77, 409-417.
- Al Jundi, J. (2002). Population doses from terrestrial gamma exposure in areas near to old phosphate mine, Russaifa, Jordan. *Radiat. Meas*, 35, 23–28.
- Al Rashdi, M. R. (2004). Geological assessment of the intertidal environment in some area along the Arabian Gulf and Gulf of Oman coastal region, UAE: a comparative study. United Arab Emirates University. http://scholarworks.uaeu.ac.ae/all_theses/571/
- Al Rashdi, S., & Siad, A. (2015). Geochemical classification and characterization of the beach sands of Abu Dhabi, United Arab Emirates: A combination of cluster and discriminant analysis. *Visnyk of Taras Shevchenko National University of Kyiv: Geology*, 4 (71), 30-36.

- Al Rashdi, S., Arabi, A. A., Howari, F. M., & Siad, A. (2015). Distribution of heavy metals in the coastal area of Abu Dhabi in the United Arab Emirates. *Marine Pollution Bulletin*, 97 (1-2), 494–498.
- Al-Abdali, F., Massoud, M. S., & Al-Ghadban, A. N. (1996). Bottom sediments of the Arabian Gulf-III. Trace metal contents as indicators of pollution and implications for the effect and fate of the Kuwait oil slick. *Environmental Pollution*, 93 (3), 285–301.
- Alali, Y. (2003). Natural radioactivity measurement in beach sand for UAE coastal areas. Master thesis, UAEU. http://scholarworks.uaeu.ac.ae/all_theses/671/
- Al-Arfaj, A. A., & Alam, I. A. (1993). Chemical characterization of sediments from the Gulf area after the 1991 oil spill. *Marine Pollution Bulletin*, 27, 97–101.
- Ali, U., Malik, R.N., & Syed, J.H. (2014). Mass burden and estimated flux of heavy metals in Pakistan coast: sedimentary pollution and eco-toxicological concerns. *Environmental Science and Pollution Research*, 22, 4316–4326.
- Ali, Y.A., Beltagy, A.I., & Lotfy, M. (1987). Grain size analysis, areal distribution of sediments and environment of deposition of tidal and bottom sediments from Ghardaqa region, Red Sea area. *Bulletin Institute Oceanography & Fisheries*, 13 (2), 147-167
- Alshamsi, D.M., Murad, A.A., Aldahan, A., & Hou, X. (2013). Uranium isotopes in carbonate aquifers of arid region setting. *Journal of Radioanalytical and Nuclear Chemistry*, 298 (3), 1899-1905.
- Alsharhan, A.S., & Kendall, C.G. (2002). Holocene carbonates/evaporites of Abu Dhabi, and their Jurassic ancient analogs. *Sabkha Ecosystems*, 187-202.
- Alsharhan, A.S., & Kendall, C.G. (2003). Holocene Coastal Carbonates and Evaporites of the Southern Arabian Gulf and Their Ancient Analogues. *Earth Sci. Rev.*, 61 (3-4), 191–243.
- Alsharhan, A.S., Rizk, Z. A., Nairn, A.E.M., Bakhit, D.W., & Alhajari, S. A. (Eds.). (2001). *Hydrogeology of an Arid Region: The Arabian Gulf and Adjoining Areas*: Elsevier B.V., 173-177.
- Alsharhan, A.S, & El-Sammak, A.A. (2004). Grain-size analysis and characterization of sedimentary environment of the United Arab Emirates Coastal Area. *Journal of Coastal Research*, 20, 464-477.
- Al-Sulaiti, H., Nasir, T., Al Mugren, K.S., Alkhomashi, N., Al-Dahan, N., Al-Dosari, M., Bradley, D.A., & Habib, A. (2012). Determination of the natural radioactivity levels in north west of Dukhan, Qatar using high-

- resolution gamma-ray spectrometry. *Applied Radiation and Isotopes*, 70 (7), 1344-1350.
- Al-Trabulsi, H.A., Khater, A.E.M., & Habbani, F.I. (2011). Radioactivity levels and radiological hazard indices at the Saudi coastline of the Gulf of Aqaba. *Radiation Physics and Chemistry*, 80 (3), 343-348.
- Al-Zahrany, A.A., Farouk, M.A., & Al-Yousef A.A. (2012). Distribution of naturally occurring radioactivity and ^{137}Cs in the marine sediment of Farasan Island, southern Red Sea, Saudi Arabia. *Radiation Protection Dosimetry*, 152 (1-3), 135-139.
- Amaral, E.J., & Prayor, W.A. (1977). Depositional environment of the St. Peter Sandstone Deducted by Textural Analysis: *Journal of sedimentary research*, 47 (1), 32-52.
- Anagnostakis, M., Hinis, E., & Simopoulos, S. (2002). ^{238}U and its daughter products in Greek surface soils, in *The Natural Radiation Environment VII: Seventh International Symposium on the natural radiation environment*, Rhodes, Greece, 175-186.
- Andersen, M., Erel, Y., & Bourdon., B. (2009). Experimental evidence for ^{234}U – ^{238}U fractionation during granite weathering with implications for $^{234}\text{U}/^{238}\text{U}$ in natural waters. *Geochimica et Cosmochimica Acta*, 73, 4124–4141.
- Antonina, A., Shazili, M., Kamaruzzaman, Y., Ong, C., Rosnan, Y., & Sharifah, N. (2013). Geochemistry of the Rare Earth Elements (REE) Distribution in Terengganu Coastal Waters: A Study Case from Redang Island Marine Sediment. *Open Journal of Marine Science*, 3, 154-159.
- Arnedo, M.A., Tejera, A., Rubiano, J.G., Alonso, H., Gil, J.M., Rodríguez, R., & Martel, P. (2013). Natural radioactivity measurements of beach sands in gran Canaria, Canary Islands Spain. *Radiation Protection Dosimetry*, 156 (1), 75-86.
- Baeza, A. Del Rio, M., Jimenez, A., Miro, C., & Paniagua, J. (1995). Influence of geology and soil particle size on the surface area/volume activity ratio for natural radionuclides. *J. Radioanal. Nucl. Chem.*, 189 (2), 289-99.
- Baiulescu, G.E., Dumitrescu, P., & Zurgravescu, G. (1991). *Sampling*. Ellis Horwood. England, 66-67.
- Bajoga, A.D, Alazemi, N., Regan, P.H., & Bradley, D.A. (2015). Radioactive investigation of NORM samples from Southern Kuwait soil using high-resolution gamma-ray spectroscopy. *Radiation Physics and Chemistry*, 116, 305-311.

- Basaham, A. S., & El-Sayed, M. A. (1998). Distribution and Phase Association of Some Major and Trace Elements in the Arabian Gulf Sediments. *Estuarine, Coastal and Shelf Science*, 46 (2), 185–194.
- Beretka, J., & Mathew, P. (1985). Natural radioactivity of Australian building materials, industrial wastes and by-products. *Health. Phys.*, 48, 87-95.
- Birch, G. (2003). A Scheme for Assessing Human Impacts on Coastal Aquatic Environments Using sediments.in: Woodcoffe, C. D., Furness, R. A. (Eds.), *Coastal GIS (2003)*. Wollongong University Papers in Center for Maritime Policy, Australia, 14, 55-57.
- Bosch, D. T., Dance, S. P., Moolenbeek, R. G., & Oliver, P. G. (1995). *Seashells of Eastern Arabian*. Motivate publishing. Emirates printing press, Dubai, UAE, 1-296.
- Bowen, H.J. (1979). *Environmental Chemistry of the Elements*. Academic Press, London, UK, 23-24.
- Bradl, H. (2002). *Heavy Metals in the Environment: Origin, Interaction and Remediation Volume 6*. Academic Press, London, UK, 50-55.
- Bristow, C. (1999). Aeolian and Sabkha sediments in the Miocene Shuweihat Formation, Emirate of Abu Dhabi, United Arab Emirates; in whybrow and Hill, fossil vertebrates of Arabia. *International conference of the Fossil vertebrates of Arabia, Jebel Dhannah*, 50–60.
- Caetano, M., Falcao, M., Vale, C., & Bebianno, M.J. (1997). Tidal flushing of ammonium, iron and manganese from inter-tidal sediment pore waters. *Marine Chemistry*, 58, 203–211.
- Chakraborty, P., Zhao, J., & Chakrabarti, C.L. (2009). Copper and nickel speciation in mine effluents by combination of two independent techniques. *Analytica Chimica Acta*, 636, 70–76.
- Chau, N., Dulinski, M., Jodlowski, P., Nowak, J., Rozanski, K., Sleziak, M., & Wachniew, P. (2011). Natural radioactivity in groundwater—a review. *Isotopes in environmental and health studies*, 47 (4), 415-437.
- Chen, K., Yang, C., & Jiao, J. (2013). Rare Earth Elements Geochemistry and Provenance Discrimination of Sediments in Tolo Harbour, Hong Kong. *Journal Marine Georesources & Geotechnology*, 15, 51-57.
- Cheng, H., Edwards, R.L., Hoff, J., Gallup, C.D., Richards, D.A., & Asmerom, Y. (2000). The half-lives of uranium-234 and thorium-230. *Chemical Geology*, 169 (1-2), 17-33.

- Cheng, Q., Wang, R., & Huang, W. (2015). Assessment of heavy metal contamination in the sediments from the Yellow River Wetland National Nature Reserve the Sanmenxia section, China. *Environmental Science and Pollution Research*, 22, 8586–8593.
- David, J. (1973). *Statistical and cluster analysis in geology*. Wiley, New York, USA, 550-551.
- De Mora, S., Fowler, S. W., Wyse, E., & Azemard, S. (2004). Distribution of Heavy Metals in Marine Bivalves, Fish and Coastal Sediments in the Gulf and Gulf of Oman. *Marine Pollution Bulletin*, 49 (5-6), 410–424.
- Dresel, E., Evans, J. C., Farmer, O. T., (2002). Investigation of Isotopic Signatures for Sources of water Contamination at the Hanford. Site Prepared for the U.S. Department of Energy under Contract DE-AC06-76RL01830.http://www.pnl.gov/main/publications/external/technical_reports/pnnl-13763.pdf
- Dubin, A. (2004). Geochemistry of rare earth elements in the ocean. *Lithology and Mineral Resources*, 39, 289-307.
- EAD. (2012). Environment Agency-Abu Dhabi. Abu Dhabi Emirate Soil survey. WWW.ead.ae.
- Eissa, H., Medhat, M., Said, S., & Elmaghraby, E., (2010). Radiation dose estimation of sand samples collected from different Egyptian beaches. *Radiation Protection Dosimetry*, 147 (4), 533-40.
- El Assaly, F.M. (1981). Methods of calibrating a gamma spectrometer for qualitative and quantitative analysis of low-level radioactivity in geological and environmental samples (IAEA-SM-252/44). Proceedings on an international symposium in methods of low level counting and spectrometry organized by IAEA, Berlin, 41-58.
- El Tokhi, M., Amin, B., & Alaabed, S. (2015a). Distribution of Heavy Metals in the Bottom Sediments of the Arabian Gulf, United Arab Emirates. *Acta Physica Polonica A*, 128, 103–107.
- El Tokhi, M., Amin, B., & Alaabed, S. (2015b). Geochemical behavior of elements of marine sediments of the Abu Dhabi area, United Arab Emirates. *Third International Conference on Engineering Geophysics*, 3, 340-343.
- El Tokhi, M., Amin, B., & Alaabed, S. (2016). Trace Metals Contamination of Bottom Sediments of Abu Dhabi Area, UAE. *Acta Physica Polonica A* 130, 138–141.

- Ellis, J., & Milliman, I. (1985). Calcium carbonate suspended in Arabian Gulf and Red Sea waters: biogenic and detrital, not chemogenic. *Sedimentary petrology*, 55, 805-816.
- El-Sammak, A. (2001). Heavy metal pollution in bottom sediment, Dubai, United Arab Emirates. *Bull. Environ. Contam. Toxicol*, 67, 295-302.
- EML. Environmental Measurements Laboratory. (1979). Dept. of Energy (USA), HASL-300, 28th edition, 98-99.
- Farid, M.E., Abd El-Mageed, A.I., Saleh, E.E., Mansour, M., & Mohammed, A.K. (2013). Assessment of natural radioactivity and the associated hazards in some local cement types used in Yemen. *Radiation Protection and Environment*, 36, 27-31.
- Faure, G., & Mensing, T. (2005). *Isotopes: Principles and Applications* 3rd Edition. John Wiley and Sons, New Jersey, USA, 502-503.
- Fernandez-Bastero, S., Alejo, I., Nombela, M., Garcia-Gil, S., Francés, G., Rubio, B., Pérez-Arlucea, M., Jiménez, R., Rey, D., Bernabeu, A., Pazos, O., Gago duport, L., Vilas, F., & Santos, A. (1999). Chemical factors controlling the steady-state distribution of mixed carbonate-siliciclastic sediments in Bayona Bay (northwest Spain). *Boletín del Instituto Español de Oceanografía*, 15, 289-302.
- Folk, R.L. (1966). A Review of grain-size parameters. *Sedimentology*, 6, 73-93.
- Folk, R.L., Ward, M.C. (1957). A study in the significance of grain size parameters. *Journal of Sedimentary Petrology*, 27, 3-26.
- Fowler, S.W., Readman, J., Oregioni, B., Villeneuve, J., & McKay, K. (1993). Petroleum hydrocarbons and trace metals in near shore Gulf sediments and biota before and after the 1991 Gulf war: An assessment of temporal and spatial trends. *Marine Pollution Bulletin*, 27, 171-182.
- Freije, A. (2015). Heavy metal, trace element and petroleum hydrocarbon pollution in the Arabian Gulf: Review. *Journal of the Association of Arab Universities for Basic and Applied Sciences*, 17, 90-100.
- Friend, P.F. (1999). Rivers of the Lower Baynunah Formation, Emirate of Abu Dhabi. In: Whybrow, P.J., & Hill, A. (Eds). *Fossil Vertebrates of Arabia*. Yale University Press, 39-49.
- Fruth, L., & Scherreiks, R. (1975). Facies and geochemical correlations in the upper Hauptdolom it (Norian) of the eastern lechtaler Alps. *Sedimentary Geology*, 13 (1), 27-45.

- Fu, x., Wanga, J., Zengb, Y., Tana, F., & He, J. (2011). Geochemistry and origin of rare earth elements (REEs) in the Shengli River oil shale, northern Tibet, China. *Chemie der Erde Geochemistry*, 71, 21–30.
- Gao, X., & Chen, C. (2012). Heavy metal pollution status in surface sediments of the coastal Bohai Bay. *Water Research*, 46, 1901–1911.
- Graham, E., Anthony, K., & Robert, A. (2002). Quaternary Development of the United Arab Emirates Coast: New Evidence from Marawah Island, Abu Dhabi. *GeoArabia*, 7, Gulf PetroLink, Bahrain.
- Haan, C. (2002). *Statistical methods in hydrology*. Iowa State Press, USA, 313-314.
- Hansen, WL. (1971). High-purity germanium crystal growing. *Nuclear Instruments and Methods*, 94 (2), 377-380.
- Haskin, A., Frey, A., Schmitt, A., & Smith, H. (1966). Meteoritic, solar and terrestrial rare earth distributions. In: Ahrens H., Press F., Runcorn K., Urey C. (Eds.), *Physics and chemistry of the earth*. Pergamon Press, Oxford, UK, 169-321.
- Holden, N.E. (1990). Total half-lives for selected nuclides. *Pure and Applied Chemistry*, 62 (5) 941-958.
- Horowitz, A. J. (1987). The relation of stream sediment surface area, grain size and composition to trace element chemistry. *Applied geochemistry*, 2, 437-451.
- Hu, Y., Liu, X., & Bai, J. (2013). Assessing heavy metal pollution in the surface soils of a region that had undergone three decades of intense industrialization and urbanization. *Environmental Science and Pollution Research*, 20, 6150–6159.
- Huber, N.D. (2007). Nuclear Gulf Cooperation Council, Energy publisher. <http://www.dailyestimate.com/article.asp?id = 10724>.
- Hunting Geology and Geophysics. (1979). Report on a mineral survey of UAE, AlAin Area. Ministry of Petroleum and Mineral Resources, Abu Dhabi, 9, 1-22.
- IAEA. (1989). *Measurement of radionuclides in food and environmental samples*. Vienna, Austria.
- IEA. (2013). International Energy Agency. 2013 Key World Energy Statistics. www.iea.org.

- Jallad, K.N. (2014). Radioactive characterization of sand samples from Failaka Island in Kuwait. *Journal of Radioanalytical and Nuclear Chemistry*, 303 (1), 733-741.
- Jamali, F., Aghda, F., & Aliyari, A. (2006). Evaluation of seismic sources for hazard assessment in the Fujairah Emirate (UAE). IAEG2006, paper number 305.
- Juma, A.H. (1995). Heavy Mineral and Metals content of Coastal Sediments between Dibba and Kalba, Eastern Coast. United Arab Emirates University.
- Kampf, J., & Sadrinasab, M. (2006). The circulation of the Persian Gulf: a numerical study. *Ocean Science*, 2, 27-41.
- Kannan, V., Rajan, M.P, Iyengar, M.A.R., & Ramesh, R. (2002). Distribution of natural and anthropogenic radionuclides in soil and beach sand samples of Kalpakkam (India) using hyper pure germanium (HPGe) gamma ray spectrometry. *Applied Radiation and Isotopes*, 57 (1), 109-119.
- Kasper-Zubillaga, J., Acevedo-Vargas, B., Bermea, O., & Zamora, G. (2008). Rare earth elements of the Alrar Desert dune and coastal sands, Northwestern Mexico. *Chemie der Erde.*, 68, 45-59.
- Keshavarzi, B., Mokhtarzadeh, Z., & Moore, F. (2015). Heavy metals and polycyclic aromatic hydrocarbons in surface sediments of Karoon River, Khuzestan Province, Iran. *Environmental Science and Pollution Research*, 22, 19077-19092.
- Keyser, R., & Twomey, T. (2008). False Positive Probability as a Function of Background for Short Data Collection Times in a Germanium Detector Portal Monitor. *Proceedings of the 2008 INNEM Annual Meeting*, 22-25.
- Land, L.S., Mack, L.E., Milliken, K.L., & Lynch, F.L. (1997). Burial diagenesis of argillaceous sediments, south Texas Gulf of Mexico sedimentary basin: A reexamination. *Geological Society of America Bulletin.*, 109, 2-15.
- Liaghat, S., Hosseini, M., & Zarasvandi, A. (2003). Determination of the origin and mass change geochemistry during bauxitization process at the Hangam deposit, SW Iran. *Geochem. J.*, 37, 627-637.
- Lijzen, J.P., Baars, A.J., & Otte, P.F. (2001). Technical evaluation of the Intervention Values for Soil/sediment and Groundwater. Human and ecotoxicological risk assessment and derivation of risk limits for soil, aquatic sediment and groundwater. National Institute of Public Health and the Environment, 1-147.

- Lokier, S.W. (2013). Coastal Sabkha Preservation in the Arabian Gulf. *Geoheritage*, 5 (1), 11-22
- Lu, X., & Zhang, X. (2008). Measurement of natural radioactivity in beach sands from Rizhao bathing beach, China. *Radiation Protection Dosimetry*, 130 (3), 385-388.
- Malik, R.N., Jadoon, W.A., & Husain, S.Z. (2009). Metal contamination of surface soils of industrial city Sialkot, Pakistan: a multivariate and GIS approach. *Environmental Geochemistry and Health*, 32, 179–191.
- McCave, I. N. (1984). Size spectra and aggregation of suspended particles in the deep ocean. *Deep Sea Research*, 31, 329-352.
- Ministry of Energy, Petroleum and Minerals sector. (2006). Initial National Communication to the United Nations Framework Convention on Climate Change. <http://unfccc.int/resource/docs/natc/arenc1/.pdf>.
- Moriarty, F. (1975). *Pollutants and Animals: A factual perspective*. George Allen and Unwin Ltd., London, UK, 15-16.
- Mujahid, S., Rahim, A., Hussain, S., & Farooq, M. (2008). Measurements of Natural Radioactivity and Radon Exhalation Rates from Different Brands of Cement Used in Pakistan. *Radiation Protection Dosimetry*, 130, 206-212.
- Muller, G. (1979). Heavy Metals in the Sediment of the Rhine-Changes seity. *Umsch Wiss Tech*, 79, 778–783.
- Murad, A.A., Alshamsi, D.M., A., Hou, X., AlShidi, F., AlKendi, R., & Aldahan, A. (2014). Radioactivity in groundwater along the borders of Oman and UAE. *Journal of Radioanalytical and Nuclear Chemistry*, 299 (3), 1653-1660.
- Naidu, K., Reddy, N., Sekhar, R., Rao, G., & Krishna, M. (2013). REE geochemistry of monazites from coastal sands between Bhimunipatnam and Konada, Andhra Pradesh, East coast of India. *Current Science*, 110-118.
- NEA-OECD. (1979). Nuclear Energy Agency. Exposure to Radiation from Natural Radioactivity in Building Materials. Report by NEA Group of Experts. OECD, Paris. France.
- Nenadović, S., Nenadović, M., Kljajević, L., Vukanac, I., Poznanović, M., Mihajlović-Radosavljević, A., & Pavlović, V. (2012). Vertical distribution of natural radionuclides in soil: Assessment of external exposure of

population in cultivated and undisturbed areas. *Science of the Total Environment*, 429, 309-316.

- NNDC (National Nuclear Data Center) (2011). Brookhaven National Laboratory, "Nuclear Decay Data(NuDat)". Decay Radiation Data, NuDat 2.5, [Http://www.nndc.bnl.gov/nudat2/](http://www.nndc.bnl.gov/nudat2/).
- Orgun, Y., Altinsoy, N., Sahin, S.Y., Güngör, Y., Gültekin, A.H., Karahan, G., & Karacik, Z. (2007). Natural and anthropogenic radionuclides in rocks and beach sands from Ezine region (Canakkale), Western Anatolia, Turkey. *Applied Radiation and Isotopes*, 65 (6), 739-47.
- Paces, J., Ludwig, k., Peterman, Z., & Neymark, L. (2001). $^{234}\text{U}/^{238}\text{U}$ evidence for local recharge and patterns of groundwater flow in the vicinity of Yucca Mountain, Nevada, USA. *Applied Geochemistry*, 17, 751-779.
- Parizanganeh, A. (2008). Grain size effect on trace metals in contaminated sediments along the Iranian Coast of the Caspian Sea. In: *Proceedings of Taal 2007: The 12th World Lake Conference*. 329–336.
- Pekey, H., Karakas, D., Ayberk, S., Tolum, L., & Bakoglu. M. (2004). Ecological risk assessment using trace elements from surface sediments of Izmir Bay (Northeastern Marmara Sea) Turkey. *Marine Pollution Bulletin*, 48, 946-953.
- Popic, J., Salbu, B., Strand, T., & Skipperud, L. (2001). Assessment of radionuclide and metal contamination in a thorium rich area in Norway. *Journal of Environment Monitoring*, 13 (6), 1730-1738.
- Powers, R.W., Ramirez, L.F., Redmond, C.D., & Elberg Jr, E.L. (1966). *Geology of the Arabian Peninsula; sedimentary geology of Saudi Arabia*. USA Government Printing Office. Washington, USA, 44-48.
- Pradhan, J.K., & Kumar, S. (2014). Informal e-waste recycling: environmental risk assessment of heavy metal contamination in Mandoli industrial area, Delhi, India. *Environmental Science and Pollution Research*, 21, 7913–7928.
- Prager, E. J., Southard, J. B., & Vivoni Gallart, E. R. (1996). Experiments on the entrainment threshold of well sorted and poorly sorted carbonate sands. *Sedimentology*, 43, 33-40.
- Prudincio, M., Gouveia, M., & Braga, S. (1995). REE Distribution in present-day and surface environments of Basaltic (Central Portugal). *Clay Minerals*, 30, 239-248.

- Purser, B.H., & Seibold, E. (1973). The principal environmental factors influencing Holocene sedimentation and diagenesis. In: Purser, B.H. (Ed.), *The Persian Gulf—Holocene Carbonate Sedimentation and Diagenesis in a Shallow Epicontinental Sea*. Springer, New York, USA, 1–9.
- Raj, S.M., & Jayaprakash, M. (2007). Distribution and enrichment of trace metals in marine sediments of Bay of Bengal, off Ennore, south-east coast of India. *Environmental Geology*, 56, 207–217.
- Reeves, G. M., Sims, I., & Cripps, J. C. (2006). *Clay Materials Used in Construction*. Geological Society of London. Engineering Geology Special Publications, London, UK, 520- 525.
- Reynolds, R. M. (1993). Physical oceanography of the Gulf, Strait of Hormuz, and the Gulf of Oman Results from the Mt Mitchell expedition. *Marine Pollution Bulletin*, 27, 35–59.
- Riotte, J., & Chabaux, F. (1999). ($^{234}\text{U}/^{238}\text{U}$) activity ratios in freshwaters as tracers of hydrological processes: the Strengbach watershed (Vosges, France). *Geochimica et Cosmochimica Acta*, 63, 1263–1275.
- Rock, N. (1988). *Numerical geology, lecture notes in earth sciences*. New York: Springer-Verlag. New York, USA, 426-427.
- Rollinson, H.R. (1993). *Using Geochemical Data*. Taylor & Francis Ltd.
- Fruth, L. Scherreiks, R. (1975). Facies and geochemical correlations in the upper Hauptdolom it (Norian) of the eastern lechtaler Alps. *Sediment Geology*, 13 (1), 27-45.
- Rosholt, J.N. (1959). Natural radioactive disequilibrium of the Uran serie. *US Geology Survey Bulletin*, 1084-1089.
- Rubio, B., Nombela, M., & Vilas, F. (2000). Geochemistry of major and trace elements in sediments of the Ria de Vigo (NW Spain): an assessment of metal pollution *Marine Pollution Bulletin*, 40, 968-980.
- Saad, H.R., & Al-Azmi, D. (2002). Radioactivity concentrations in sediments and their correlation to the coastal structure in Kuwait. *Applied Radiation and Isotopes*, 56 (6), 991-997.
- Sahu, B.K. (1964). Depositional mechanisms from the size analysis of clastic sediments. *Journal of Sedimentary Research*, 34 (1), 73– 83.
- Saif-Uddin, S., Ghadban, A.N., Aba, A., & Behbehani, M. (2012). Concentration of selected radionuclides in seawater from Kuwait. *Marine Pollution Bulletin*, 64 (6), 1261-1264.

- Saleh, I.H. (2012). Radioactivity of ^{238}U , ^{232}Th , ^{40}K , and ^{137}Cs and assessment of depleted uranium in soil of the Musandam Peninsula, Sultanate of Oman. *Turkish Journal of Engineering and Environmental Sciences*, 36 (3), 236-248.
- Saleh, Y.S., & Marie, M.S. (2014). Assessment of metal contamination in water, sediment, and tissues of *Arius thalassinus* fish from the Red Sea coast of Yemen and the potential human risk assessment. *Environmental Science and Pollution Research*, 22, 5481–5490.
- Schnetger, B., Brumsack, J., Schale, H., Hinrichs, J., & Dittert, L. (1999). Geochemical characteristics of deep-sea sediments from the Arabian Sea: a high-resolution study. *Deep Sea Research*, 47, 2735-2768.
- Scoullou, M., Botsou, F., & Zeri, C. (2014). Linking Environmental Magnetism to Geochemical Studies and Management of Trace Metals. Examples from Fluvial, Estuarine and Marine Systems. *Minerals*, 4, 716–745.
- Sheppard, C., Price, A., & Roberts, C. (1992). Marine ecology of the Arabian region: Patterns and processes in extreme tropical environments. Academic Press, London, UK, 359-367.
- Sholkovitz, E.R. (1988). Rare earth elements in the sediments of the North Atlantic Ocean, Amazon Delta, and East China Sea: reinterpretation of terrigenous input patterns to the oceans. *The American Journal of Science*, 288, 236–281.
- Shriadah, M.A. (1998a). Heavy metals in mangrove sediments of the United Arab Emirates Shoreline (Arabian Gulf). *Water, Air and Soil Pollution*, 116, 523-534.
- Shriadah, M.A. (1998b). Impact of an oil spill on the marine environment of the United Arab Emirates Along the Gulf of Oman. *Marine Pollution Bulletin*, 36 (11), 879–879.
- Shriadah, M.A. (1999). Oil contamination along oil tanker routes of the United Arab Emirates (The Arabina Gulf and Gulf of Oman). *Bulletin of Environmental Contamination and Toxicology*, 63, 203–210.
- Sokal, R., & Sneath, P. (1963). *Principals of numerical taxonomy*. London and San Francisco: Freeman, UK, 358-359.
- Sposito, G. (1983). In *Applied Enviromental Geochemistry*. Academic Press, London, UK, 123-127.
- Steve, M., Richard, E., Jason, M., Andrew, F., & Leon, L. (2012). Engineering geological characterisation of the Barzaman Formation, with reference to

- coastal Dubai, UAE. *Bulletin of Engineering Geology and Environment*, 71 (1), 1-19.
- Sultan, K., & Shazili, M. (2009). Rare Earth Elements in Tropical Surface Water, Soil and Sediments of the Ter engganu River Basin, Malaysia. *Journal of Rare Earths*, 27, (6), 1072-1078.
- Sutherland, R. (2000). Bed sediment associated trace metals in an urban stream, Oahu, Hawaii. *Environmental Geology*, 39, 611-27.
- Tari, M., Moussavi Zarandi, S.A., Mohammadi, K., & Zare, M.R. (2013). The measurement of gamma-emitting radionuclides in beach sand cores of coastal regions of Ramsar, Iran using HPGe detectors. *Marine Pollution Bulletin*, 74 (1), 425-434.
- Taylor S.R., & McLennan S.M. (1985). *The continental crust: its composition and evolution*. Blackwell, Oxford, UK, 311- 312.
- Taylor S.R., & McLennan S.M. (1995). The geochemical evolution of continental crust. *Reviews of Geophysics*, 33, 1-64.
- Tchounwou, P.B., Yedjou, C.G., Patlolla, A.K., & Sutton, D.J. (2012). Heavy Metals Toxicity and the Environment. *EXS*, 101, 133–164.
- Teemofeeva, Y., & Golov, V. (2007). Sorption of Heavy metal by iron-manganese nodules in soils of Primorskii Region. *European Journal of Soil Science*, 12, 1308-1315.
- Thurber, D.L. (1962). Anomalous U^{234}/U^{238} in nature. *Journal of Geophysical Research*, 67 (11), 2381-2395.
- Tokarev, I., Zubkov, A., Rumynin, V., Polyakov, V., Kuznetsov, V., & Maksimov, F. (2005). Origin of high $^{234}U/^{238}U$ ratio in post-permafrost aquifers. In: Merkel BJ, Hasche-Berger A (eds) *Uranium in the Environment, mining impact and consequences*, Springer, New York. 874-856.
- Tomlinson, D.L., Wilson, J.G., Harris, C.R., & Jeffrey, D.W. (1980). Problems in the assessment of heavy-metal levels in estuaries and the formation of a pollution index. *Helgolander Meeresuntersuchungen*, 33 (1-4), 566–575.
- Tranchida, G., Oliveri, E., Angelone, M., Bellanca, A., Censi, P., D'Elia, M., Neri, R., Placenti, F., Sprovieri, M., & Mazzola, S. (2011). Distribution of rare earth elements in marine sediments from the Strait of Sicily (western Mediterranean Sea): Evidence of phosphogypsum waste contamination. *Marine pollution bulletin*, 26, 182-191.

- Turekian, K.K., & Wedepohl, K.H. (1961). Distribution of the Elements in Some Major Units of the Earth's Crust. *Geological Society of America Bulletin*, 172-175.
- Udden, J.A. (1914). Mechanical composition of clastic sediments. *Geological Society of America Bulletin*, 25 (1), 655–744.
- UNSCEAR (United Nations Scientific Committee on the Effect of Atomic Radiation) (1993). Report to the general assembly .Annex B: Exposures from man-made sources of radiation.
- UNSCEAR (United Nations Scientific Committee on the Effect of Atomic Radiation) (2000). Report to the General Assembly. Annex B: Exposures from Natural Radiation Sources.
- Velea, T., Gherghe, L., Predica, V., & Krebs, R. (2008). Heavy metal contamination in the vicinity of an industrial area near Bucharest. *Environmental Science and Pollution Research*, 16, 27–32.
- Wang, L., & Liang, T. (2015). Geochemical fractions of rare earth elements in soil around a mine tailing in Baotou, China. *Scientific Reports*, 5, 124-129.
- WHO (World Health Organization). (2011). Guidelines for drinking water quality, fourth edition. WHO library cataloguing-in-publication data.
- Whybrow, P. J. (1989). New stratotype; The Baynunah Formation (Late Miocene), United Arab Emirates: Lithology and palaeontology. *Newsletters on Stratigraphy*, 21, 1–9.
- Whybrow, P.J., Friend, P.F., Ditchfield, F., & Bristow, C. (1999). Local stratigraphy of the Neogene Outcrops of the Western Coastal Region of the Emirate of Abu Dhabi. In: *InProceedings of the International Conference on the Fossil Vertebrates of Arabia*, 65–70
- Whybrow, P.J., & Hill, A. (1999). *Fossil Vertebrates of Arabia*, Yale University Press, 50-60.
- WNA (World Nuclear Association). (2017). www.world-nuclear.org.
- Xu, G., Liu, J., & Pei, S. (2015). Geochemical background and ecological risk of heavy metals in surface sediments from the west Zhoushan Fishing Ground of East China Sea. *Environmental Science and Pollution Research*, 22, 20283–20294.
- Xu, Z., Lim, D., Choi, J., Yang, S., & Jung, H. (2009). Rare earth elements in bottom sediments of major rivers around the Yellow Sea: implications for sediment provenance. *Geo-Marine Letters*, 29 (5), 291-300.

- Yang, S., Jung, H., Choi, M., & Li, C. (2002). The rare earth element compositions of the Changjiang (Yangtze) and Huanghe (Yellow) river sediments. *Earth and Planetary Science Letters*, 201, 407-419.
- Yohannes, Y.B., Ikenaka, Y., & Saengtienchai, A. (2013). Occurrence, distribution, and ecological risk assessment of DDTs and heavy metals in surface sediments from Lake Awassa-Ethiopian Rift Valley Lake. *Environmental Science and Pollution Research*, 20, 8663–8671.
- Yuan, Y., Wei, H., Zhao, L., & Jiang, W. (2008). Observations of sediment resuspension and settling off the mouth of Jiaozhou Bay, Yellow Sea. *Continental Shelf Research*, 28, 2630–2643.
- Zaremotlagh, S., & A. Hezarkhani, A. (2016). A geochemical modeling to predict the different concentrations of REE and their hidden patterns using several supervised learning methods: Choghart iron deposit, bafq, Iran. *Journal of Geochemical exploration*, 165, 35-48.
- Zhou, L., Yang, B., & Xue, N. (2013). Ecological risks and potential sources of heavy metals in agricultural soils from Huanghuai Plain, China. *Environmental Science and Pollution Research*, 21, 1360–1369.
- Zielinski, R.A., Simmons, K.R., & Orem, W.H. (2000). Use of ^{234}U and ^{238}U isotopes to identify fertiliser-derived U in the Florida Everglades. *Applied Geochemistry*, 12, 369-383.
- Zvab Rozic, P., Dolenc, T., & Bazdaric, B. (2012). Major, minor and trace element content derived from aquacultural activity of marine sediments (Central Adriatic, Croatia). *Environmental Science and Pollution Research*, 19, 2708–2721.

List of Publications

- 1- Paper titles “Distribution of Heavy Metals Around the Barakah Nuclear Power Plant in the United Arab Emirates” was published in ESPR journal in August 2017, V24, pp19835-19851.